Time and Space Variation of Strong Motions Parameters for Subduction Interface Earthquakes

Jesus Vladimir Pina Valdes

Communauté UNIVERSITÉ Grenoble Alpes

THÈSE

Pour obtenir le grade de

DOCTEUR DE LA COMMUNAUTE UNIVERSITE GRENOBLE ALPES

Spécialité : **Sciences de la Terre et de l'Univers et de l'Environnement (CESTUE)**

Arrêté ministériel : 25 mai 2016

Présentée par

Jesús PIÑA-VALDÉS

Thèse dirigée par **Fabrice COTTON, Professeur, GFZ**, et codirigée par **Anne SOCQUET, Enseignant-chercheur, UGA**

préparée au sein du **Laboratoire Institut des Sciences de la Terre** dans **l'École Doctorale Terre, Univers, Environnement**

Variations Temporelle et spatiales du Paramètres du movement fort du terrain de séismes de subduction

Time and Space Variation of Strong Motions Parameters for Subduction Interface Earthquakes

Thèse soutenue publiquement le **25 septembre 2017**, devant le jury composé de :

Monsieur Philippe GUÉGUEN
Directeur de Recherche, IFSTTAR - ISTerre, Président du Jury
Monsieur Pascal BERNARD
Physicien CNAP, IPGP Institut de Physique du Globe de Paris, Rapporteur
Monsieur Fabian BONILLA
Directeur de Recherche, IFSTTAR - Université Paris Est, Département GERS Laboratoire Séismes et Vibrations, Rapporteur
Monsieur Adrian RODRIGUEZ-MAREK
Professeur, Virginia Tech Institute - Department of Civil and Environmental Engineering, Examinateur
Monsieur Fabrice COTTON
PR2, GFZ German Research Centre for Geosciences, Directeur de thèse
Madame Anne SOCQUET
Physicien CNAP, UGA - Université de Grenoble Alpes, Directeur de thèse

Résumé

Les mouvements forts du sol générés par les séismes peuvent être reliés aux caractéristiques de la source sismique (chute de contrainte, vitesse de rupture, etc.), et aux conditions frictionnelles des failles. Ces caractéristiques sont généralement étudiées via l'analyse des enregistrements accélérométriques des grands séismes à basses fréquences (≤ 1 Hz). L'amélioration des réseaux accélérométriques a permis l'enregistrement de nombreux séismes de magnitudes faibles et modérées (Mw ≤ 6,0). Ces enregistrements contiennent des informations dans la bande de hautes fréquences (1 Hz - 50 Hz), qui ne peuvent pas être exploitées avec les méthodes sismologiques classiques.

Pour exploiter ces données de mouvements forts des séismes de faible intensité dans l'objectif d'étudier étudier les conditions frictionnelles de l'interface de subduction, nous explorons deux méthodes pour comparer le contenu fréquentiel des séismes: la première basée sur les rapports spectraux et la deuxième basée sur les équations de prédiction du mouvement du terrain (GMPE). Ces méthodes ont été utilisées pour étudier la variabilité spatiale et temporelle du contenu fréquentiel des séismes rompant l'interface de subduction au nord du Chili et au Japon. Leurs avantages et limitations respectifs ont été analysés. Ces comparaisons méthodologiques nous ont a permis de confronter et de valider les résultats, et ainsi de proposer une nouvelle méthodologie fiable basée sur l'analyse des résidus de GMPE pour analyser le contenu fréquentiel des séismes.

L'analyse des résultats obtenus a montré une dépendance avec la profondeur du contenu en fréquence des séismes de l'interface de subduction, concordant avec les observations de grandes ruptures de subduction [Lay et al., 2012]. En même temps, des variations du contenu fréquentiel des séismes ont été détectées le long de la fosse de subduction, ce qui nous a conduit à décrire une segmentation latérale de

l'interface de subduction. Cette segmentation a été comparée avec la distribution spatiale de la sismicité, à la géométrie de l'interface de subduction et à ses conditions de glissement. Finalement, avant le séisme d’Iquique de 2014 (Mw 8.1) au nord du Chili, nous avons détecté une évolution temporelle du contenu en fréquence des séismes associée à l’occurrence d'un glissement lent précurseur au choc principal.

Abstract

The strong ground motions generated by earthquakes can be related to the characteristics of the earthquakes source (stress drop, rupture velocity etc..), and therefore to the frictional conditions of the faults. These characteristics are usually studied by analyzing the low frequency band (≤ 1Hz) of the strong motion records of large earthquakes. The improvement of strong motion networks has generated large datasets of records of moderate and low magnitude earthquakes (Mw ≤ 6.0). These records contain information in the high frequency band (1 Hz – 50 Hz), which cannot be exploited using classical seismological methods.

In order exploit the strong motion records of low magnitude earthquakes to study the subduction interface's frictional conditions, we explore two methods for comparing the earthquakes frequency content: the first one based on spectral ratios, and the second one based on Ground Motion Prediction Equations (GMPEs). These methods have been used to investigate the spatial and temporal variability of the frequency content of subduction interface earthquakes in North Chile and Japan. Their respective benefits and limitations have been analyzed. These methodological comparisons allowed us to cross compare and validate the results, and to propose a new, reliable methodology based on the analysis of GMPEs residuals to compare the earthquakes frequency content.

The analysis of the results showed a depth dependency of the frequency content of subduction earthquakes in agreement with the one derived from large megathrust ruptures [*Lay et al.*, 2012]. Additionally, variations of the earthquake frequency content along trench have been detected, which may drive to a lateral segmentation of the subduction interface. This segmentation has been compared to the spatial distribution of the seismicity, the geometry of the subduction interface and its slippage conditions. Finally, before the occurrence of 2014 Iquique Earthquake Mw 8.1 in North Chile, a temporal evolution of the frequency content of the foreshocks has been detected, associated to a precursory slow slip of the subduction interface.

Table of Contents

Introduction

Strong ground motions correspond to strong ground-shakings perceptible at the surface in the near field of an earthquake. They are generated by high frequency waves (0.1-50 Hz) radiated from the seismic source. Due to the destructive effects of the ground motions, their study has became a fundamental part of seismic hazard assessments [e.g. *Atkinson and Boore*, 2003; *Scherbaum et al.*, 2004; *Zhao et al.*, 2007; *Arango et al.*, 2012; *Kale and Akkar*, 2013] as well as studies for infrastructure safety improvement and slopes stability evaluation.

In the last decades the development of strong motion sensors, the growth of ground motions networks and the improvement of computer storage systems have generated a huge quantity of strong motion records of high quality around the world [e.g. *Aoi et al.*, 2004; *Okada et al.*, 2004; *Kumar et al.*, 2012; *Dawood et al.*, 2016]. This is an essential source of information, mainly used for seismological engineering purposes, such as the development of tools and models to improve seismic hazard analysis [e.g. *Youngs et al.*, 1997; *Ambraseys et al.*, 2004; *Zhao et al.*, 2006; *Haendel et al.*, 2014; *Abrahamson et al.*, 2016; *Montalva et al.*, 2017]. However, this type of data has also provided valuable information of high frequency seismic waves that have allowed the seismologist community to improve the knowledge of seismic sources and rupture processes [e.g. *Hanks*, 1979; *Hartzell and Heaton*, 1983; *Lay et al.*, 2012].

Since seismic hazard is mainly controlled by high strong ground motion amplitudes, engineering seismology focuses on the analysis of large magnitude earthquake ground motions. Also, the seismological community has used mainly the low frequency band (<1Hz) of ground motion records for the study of rupture velocities and slip distributions of large earthquake ruptures [e.g. *Peyrat et al.*, 2010; *Ide et al.*, 2011; *Kurahashi and Irikura*, 2011].

Earthquakes of low and moderate magnitudes have small ruptures sizes, short rupture durations, limited slip and release relatively low amounts of energy. They do not generate destructive waves. Due to their characteristics, those earthquakes are usually modeled as punctual sources of seismic waves. Additionally, due to the fact that their signal in the low frequency band is not energetic enough, it is not possible to use classical seismological methods to study their rupture areas. This means that so far, a large volume of strong ground motion records have been left out of the interest of the seismological and the engineering seismological communities too.

The improvement of strong motion networks combined to the high number of moderate and low magnitude earthquakes, and their distribution along large seismogenic faults, open a great opportunity for developing new methods to study the high frequency waves radiated by seismic sources. This large volume of information may allow the identification of medium and small-scale features on faults rupture and their temporal variations. These data may also give the opportunity to analyze the factors that control the slip behavior during the interseismic period, such as fault roughness variabilities or fluid migrations. Their study, may lead to a better understanding of the parameters that control the earthquake cycle and give more information about earthquakes nucleation processes.

Interesting areas that meet valuable conditions to investigate the variation of strong ground motions, are the Continental Active Margins (CAM). This kind of subduction boundaries produce a substantial part of the seismic activity of the world, their lateral extension generate large and continuous fault planes (the subduction interfaces), generate earthquakes of large magnitude and an important number of earthquakes of low and moderate magnitude. As a significant portion of the population is settled near this type of subduction margins (e.g. Japan, East coast of South America, New Zealand), there is a need to provide robust and reliable strong ground motion models to improve seismic hazard assessments. These needs result in the deployment of an important number of strong ground motion stations, which have generated a large volume of subduction interface earthquakes records. These large datasets configure an auspicious scenario for the development, application and testing of new methodologies to extract information of the interface seismogenic zone from the strong ground motion of the interface subduction earthquakes. Particularly, these new data are useful to improve the resolution of the characterization of interface subduction frictional environment, traditionally inferred from geodetic and seismological observation of large megathrust ruptures [*Lay et al.*, 2012].

The slip frictional behavior of the subduction interface, as well the factors that control it, are still not well understood. Geodetic observations, the slip distribution associated

with large megatrhust ruptures and also the spatial distribution of the seismicity suggests that the frictional properties of the subduction interface vary laterally [e.g. *Ruff,* 1992; *Kawasaki et al.*, 2001; *Moreno et al.*, 2012; *Chlieh et al.*, 2014]. Several characteristic and parameters of the subduction interface vary also laterally, the most obvious variations being the geometry and orientation of the subduction trench respect to the plate convergence. Moreover, features and conditions of converging plates such as the subduction of oceanic ridges and seamounts, type of sediments, subduction angle of the lower plate, convergence velocity, characteristics of the accretionary prism, pore pressure, temperature gradient, roughness, etc., can vary along the subduction trench and also along down-dip, and their variation may impact on the frictional behavior of the subduction interface as well on the seismic coupling, on the size asperities, on coseismic rupture length and also on the strong ground motion generation [e.g. Lallemand and Le Pichon, 1987; Byrne et al., 1988; Scholz, 1988; Hyndman and Wang, 1993; Hyndman et al., 1995; Tanioka et al., 1997; Lay and Bilek, 2007; Kaneko et al., 2010; Heuret et al., 2011a; Scholz and Campos, 2012; Kurahashi and Irikura, 2011]

Recent studies have detected the effects of down-dip and along trench of variation of the frictional properties in the interseismic coupling of the subduction interface, using geodetic observation [e.g. *Béjar-Pizarro et al.*, 2010; *Loveless and Meade*, 2010; *Métois et al.*, 2016], and teleseismic data of large megathrust ruptures have revealed that this variability may affect also the wave radiation patterns [*Lay et al.*, 2012]. However, the high frequency records have not been exploited so far despite of the large volume of ground motion records of subduction interface earthquakes. In this context, this work aims at exploring new methodologies to analyze the high frequency waves contained in strong ground motion records of subduction interface seismicity, in order to obtain new information that allows improving the knowledge of the subduction interface seismogenic zone. Our final goal is to document slip frictional behavior, subduction segmentations, as well as the transient processes observed during the seismic cycle and the nucleation of large megathrust earthquakes.

With this aim, three main questions have been raised:

1 - How can the strong ground motion be used to improve the knowledge of the subduction interface and the seismic cycle?

To face this question, we have analyzed the earthquake frequency content, since the variation of high frequency content may impact strong ground motions [e.g. Boore, 1983 ; Irikura, 1986 ; Rathje et al., 1998; Rathje et al., 2004]. Moreover they are

dependent on the frictional condition of the subduction interface [*Lay et al.*, 2012]. Therefore coherent variation in the frequency content may be related to the frictional condition of the subduction interface.

To detect and describe properly the variability of frequency content radiated by earthquakes of low and moderate moment magnitude, tools and methods extensively used in engineering seismology have been used. Their limitations and sensibility with scaling effects, geometrical spreading and path attenuation in high the frequency range (> 1 Hz), have been evaluated and discussed.

2 - Can recorded ground motions bring light about the variability of frictional properties of subduction interface along dip and along strike?

To answer this question, we have searched coherent variations in the frequency content radiated by earthquakes of low and moderate moment magnitude. Then, the consistency between the detected ground motions variations detected with parameters often used as proxy of the subduction interface frictional properties has been evaluated. In this context, parameters that present well known spatial variabilities such as the spatial distribution of the seismicity, topographical markers, interseismic deformation, subduction slab geometries and gravity anomalies, have been considered to understand regional dependencies of strong ground motions..

3- Are the strong ground motion sensitive to the transient processes observed on the subduction interface during the seismic cycle?

Answering this question is a sensitive point since temporal evolution of ground motion may reveal (if detectable) important informations about the nucleation process of megathrust earthquakes.

To answer to this question, we have searched transient variations of the frequency content radiated by earthquakes of low and moderate moment magnitudes, before and after the occurrence of large megathrust earthquakes, and over regions that have shown transient slip behavior during the interseismic period.

In this works we have used the ground motions records of two strong motion network installed in Chile and Japan. The first strong ground motion dataset corresponds to records of the CX-network installed in the northern part of the Chile subduction, between -17° and -24° of latitude. This network is working since 2007 and has now 21 strong motion stations installed at homogeneous rock sites, far away of the urban

concentrations, ensuring reliable records of high quality. During the period analyzed, the network has recorded the strong ground motions of earthquakes associated to two mayor seismic crisis (2007 Tocopilla earthquake Mw 7.8 and 2014 Iquique Mw 8.1).

The second strong ground motion database used in this study has been built using the records of the KiK-network [*Dawood et al.*, 2016], which is working since 1998 with more than 650 strong ground motion stations along Japan. Its stations are located far of the urban influence, with documented site conditions, which guarantee records of high quality. During the time window studied, this network provides strong motion records of more than 700 interface subduction earthquakes, including data associated to the seismic crisis of 2011 Tohoku-Oki earthquake Mw 9.0.

Chapter 1: Factors controlling the Seismicity on the Subduction Interface

1.1 Subduction Zones in Continental Active Margins

Subductions occur in the convergent boundaries of tectonic plates, when one plate is underthrusted beneath another one of less density, and sinks into the Earth's mantle. This process is generated by the interaction of factors such as the gravity and convective flows in the asthenosphere [e.g. *Wilson*, 1993; *Stern*, 2002]. Most of the subduction zones are located in Continental Active Margins (CAM), where the continental plate rides over the subducted oceanic slab (Figure 1.1). Subduction zones generate large earthquake activity that is classified into four types of seismicity: outer rise, intraplate, intraslab and interface. The outer rise seismicity takes place in the in the shallow part of the oceanic plate, beyond the subduction trench. The crustal seismicity is located in the shallow part of the continental plate and in the accretionary prism. The intraslab seismicity occurs at depth, on the oceanic plate that is already subducted. Finally, the interface seismicity is generated in the contact between both plates.

The largest subduction earthquakes, such as 1960 Mw 9.5 Valdivia earthquake, 1964 Mw 9.2 Alaska, 2004 Mw 9.3 Sumatra earthquake, 2010 Mw 8.8 Maule earthquake, or 2011 Mw 9.0 Tohoku earthquake, are hosted at the contact between both plates that is called subduction interface and allows the slippage of both plates [e.g. Hoechner et al., 2008 ; Delouis et al., 2010 ; Simons et al., 2011].

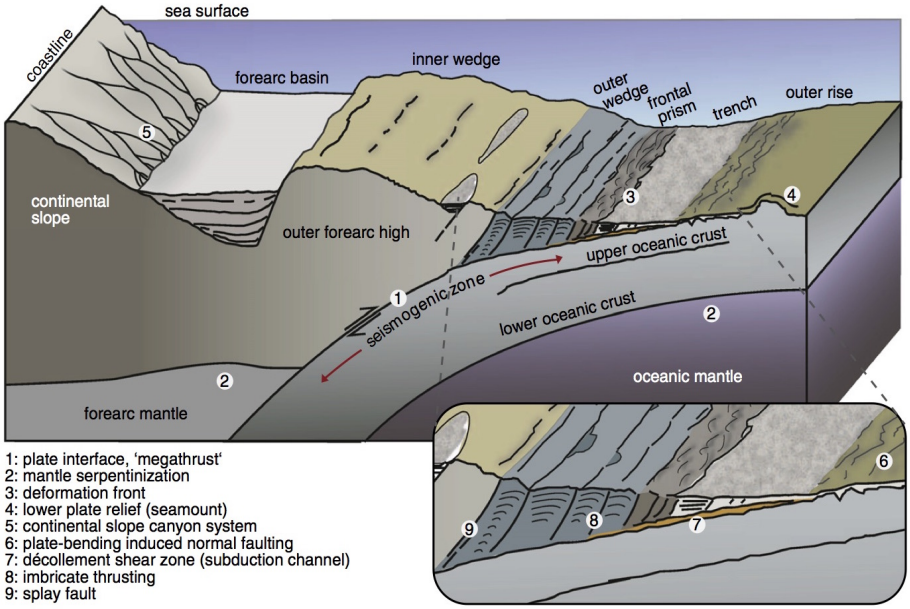

Figure 1.1: Schematic 3D view of a generic CAM subduction zone (after *Kopp* [2013]).

The rheological behavior of the subduction interface is controlled by parameters such rock type, temperature, slip velocity, geometry, pressure. The condition of these parameters at shallow depths and their regional variability, generate variations of the frictional properties that control the slip behavior of the subduction interface. This implies that the slippage of the upper portion of subduction interface is not homogenous neither continuous in terms of time and spatial distribution, varying from fully locked zones that only slip during an earthquake, to regions dominated by constant aseismic slip. This generates complex interactions between these two kinds of slip behaviors that seem to impact factors such as epicenters locations, earthquakes time recurrence, moment magnitude, area of rupture, rupture propagation velocity, coseismic slip distribution, wave frequency content [e.g. Kanamori, 1977 ; Aki, 1984 ; Scholz, 1998 ; Oleskevich et al., 1999 ; Heuret et al., 2012 ; Lay et al., 2012 ; Loveless and Meade, 2016]. Most of the data used to develop these models are the seismological observations that mainly provide informations on the seismic behavior, and from geological observations that provide informations on persistent features at geological time scale. Recent advances in spatial geodesy have provided reliable information on the occurrence of transient process of very low velocity and long time duration, which can vary from hours to decades, allowing improve the models of the interface slip behavior between earthquakes and the nucleation earthquake processes [Kanamori and Brodsky, 2004 ; Ozawa et al., 2012 ; Béjar-Pizarro et al., 2013 ; Ozawa, 2014 ; Lay, 2015 ; Métois et al., 2016 ; Ruiz et al., 2014 ; Schurr et al., 2014 ; Socquet et al., 2017].

This chapter presents a revision of most accepted physical models that describe the seismic ruptures mechanisms of the subduction interface and its frictional behavior that is controlled by the interaction between aseismic and seismic slip, as well as the relevant theories and observations that support these models.

1.2 Slip Mechanics of the subduction interface

The slip of the subduction interface usually accommodates most of the horizontal motion of the plates in CAM subduction zones. This generates an inverse slip motion on the subduction interface, which rake is mainly controlled by the direction of the plates convergence. An important part of this accommodation it is generated by fast subduction interface earthquakes, the rest of the motion being accommodated by slow slippage that do not produce seismicity [Kanamori and Brodsky, 2004].

The earthquakes are generated by a sudden slippage on a pre-existent fault or plate interface. They correspond mainly to a frictional phenomenon where the role of the fragile fracture propagation plays a secondary role [*Scholz*, 1998]. They have been explained in late 60's by the Stick-Slip frictional mechanism observed in rock samples experiments [*Brace and Byerlee*, 1966; *Byerlee*, 1970]. This model can be applied to explain the subduction interface earthquakes, assuming that regions of the subduction interface stay locked between earthquakes while the subducted slabs sinks. This increases the shear stress on the locked surface until it reaches a critical shear stress level that triggers a sudden fast slippage of the locked region, generating and abrupt shear stress drop on it.

In the other hand, the aseismic slip is generated by creep behavior, which produce continuous and stable slow ductile sliding. It is observed in deeper regions, where the materials reach the crystal plasticity due to the conditions of pressure and temperature. Such aseismic slip is also observed at shallow depths, where the materials are poorly consolidated, generating creep by cataclastic flows [*Sibson*, 1977; *Ruff and Kanamori*, 1983].

Both slip mechanisms coexist on the subduction interface. Meanwhile creep behavior can be observed on the shallow interface (less than 10 km depth) and deeper than 60 km depth, the stick-slip mechanism is normally observed between 10 and 60 km depths in a region denominated seismogenic zone [*Tichelaar and Ruff*, 1993; *Scholz*, 1998]. This makes that the slip of the subduction interface can occur at relatively constant rates of the order of millimeters per year in stable aseismic sliding fashion,

as well as by short and violent seismic episodes at fast sliding rates of the order meters per second [*Kanamori and Brodsky*, 2004].

1.3 Rate and State friction law

Laboratory experiments of friction in rock samples during the 70's modeled the earthquakes as a spring-and-slider system. In the early 80's, the formulation of friction law has been derived, that explains both slip mechanisms described above [*Rice*, 1983; *Ruina*, 1983].

This model characterized the friction with two coefficients: the static friction coefficient (μ_s) and the dynamic friction coefficient (μ_d). In the standard stick-slip behavior, the shear stress on the contact plane must exceed μ_s to initiate the slip, and once the slip started, the slip strength falls to μ_d . The experiments showed that μ_s depends on the history of the sliding surface and increases with the log of the time where the surface remains static [*Dieterich*, 1972]. Its variability is conditioned by parameters such as the rock type and the temperature [*Scholz*, 1998]. Additionally, it was observed that μ_d in the case of steady-state sliding depends on the slip velocity [*Scholz et al.*, 1972]. If the slip velocity varies, the system evolves to a new steady-state friction (μ_d) after covering a critical slip distance that is necessary to reach the sliding steady-state friction (Figure 1.2). All these observations have been derived into the Rate and State friction law, which considers that the friction coefficient (μ) depends on the slip velocity (v) and a state variable (θ). Thus the shear stress is defined as:

$$\tau = \sigma\mu(v,\theta) = \sigma\left[\mu_0 + a * \ln\left(\frac{v}{v_o}\right) + b * \ln\left(\frac{v_o\theta}{D_c}\right)\right] \qquad (1.1)$$

Where σ is the effective normal stress, v_o is a velocity-normalizing constant, μ_0 is the steady-state friction at $v = v_o$, D_c is the critical slip distance, a and b are constants that are defined by the material properties, and θ is a state variable.

To describe the evolution of the state variable θ with time, two models derived from empirical observations have been proposed. The first one is the aging law [*Dieterich*, 1981]:

$$\frac{d\theta}{dt}=1-\frac{\theta v}{D_c} \tag{1.2}$$

And the second one is the slip law [*Ruina*, 1983]:

$$\frac{d\theta}{dt}=\frac{-v\theta}{D_c}\ln\left(\frac{v\theta}{D_c}\right) \tag{1.3}$$

In the steady-state sliding conditions, both models indicate that the variable reaches a constant value $\theta_{ss}=D_c/v$. Replacing this on equation 1.1, the stress shear in the steady-state conditions becomes:

$$\tau=\sigma\mu(v,\theta)=\sigma\left[\mu_0+(a-b)*\ln\left(\frac{v}{v_o}\right)\right] \tag{1.4}$$

The frictional stability depends on the critical slip distance and the combined parameter $(a-b)$, defined as the velocity dependence of steady-state friction by:

$$(a-b)=\frac{\partial\mu^{ss}}{\partial\ln(v)} \tag{1.5}$$

A positive value of the parameter $(a-b)$ means that friction increases with the slip velocity, and is known as velocity-strengthening behavior. This generates stable behavior where the slip occurs aseismically, earthquakes cannot be nucleated and its propagation will produce a negative stress drop, which will rapidly terminate it [*Scholz*, 1998].

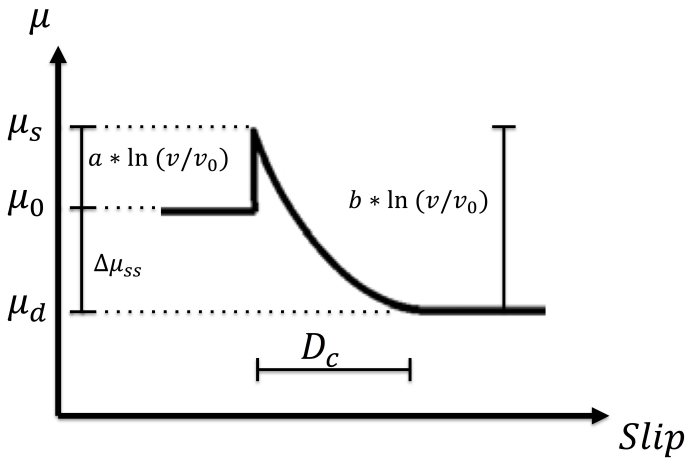

Figure 1.2: Schematic illustration of the evolution of friction according to the slip during a change of slip velocity.

A negative value of the parameter $(a-b)$ means that friction decreases with the slip velocity, and is known as velocity-weakening behavior. The conditions of the system will be controlled by the effective normal stress and its relation with the critical effective normal stress (σ_c). Thus if , $\sigma > \sigma_c$ sliding will be unstable under a quasi-static load. In the opposite case, if $\sigma < \sigma_c$ the regime be conditionally stable. This mean that the sliding will be stable under quasi-static loading but can become unstable under dynamic loading if the velocity increment exceeds a certain level (Figure 1.3). As a consequence, earthquakes can only be nucleated in unstable regime but may propagate within conditionally stable regions.

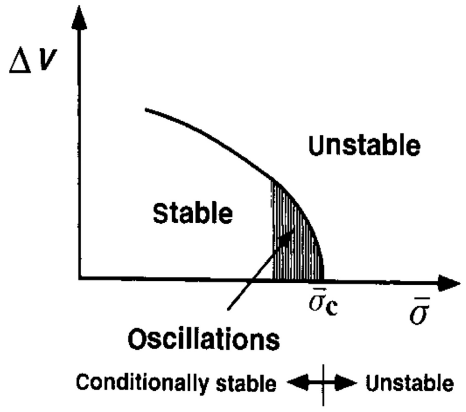

Figure 1.3: Stable and unstable domains depend on the relation between the effective normal stress, the critical effective normal stress and the velocity change generated by dynamic loading (after *Scholz*, [1998]).

1.4 Interaction of slip mechanisms on the subduction interface.

The complex nature of the subduction process and the heterogeneity of the contact between both plates generate large variations in the conditions that control the frictional behavior of the subduction interface [*Tichelaar and Ruff,* 1993; *Scholz*, 1998; *Oleskevich et al.*, 1999; *Kopp*, 2013]. This suggests that slip of the subduction interface is conditioned by complex interactions between the regions that present continuous aseismic slip, regions that show transient slip and regions that only slip when an earthquake occurs [*Aki,* 1979, 1984]. This is supported by geodetic and seismological observation [*Ito et al.*, 2007; *Béjar-Pizarro et al.*, 2010; *Ozawa*, 2014; *Loveless and Meade*, 2016; *Socquet et al.*, 2017], which suggest that the subduction interface is characterized by an heterogeneous distribution of regions controlled by

the three different friction stability regimes (stable, unstable and conditionally stable) that accommodate the slippage of the plates [e.g. *Pacheco et al.*, 1993; *Scholz*, 1998; *Lay et al.*, 2012].

The stable regions are characterized by a steady slippage, they are thought to be uncoupled during the interseismic period, which means that both plates slip freely in an aseismic regime (creep). They show a velocity-strengthening behavior and do not accumulate strain. Unstable areas only slip during seismic episodes. They are said to be coupled, which means that they remain locked most of the time until their sudden rupture into an earthquake (stick-slip). They are also called asperities, and show a velocity-weakening behavior. Elastic strain is accumulated while they are locked, which is released during seismic ruptures that radiate elastic waves. Finally, the conditionally stable areas behave as stable regions in the time span between earthquakes and eventually can slip at high velocity during the earthquakes.

The interactions between the seismic and aseismic slip on the subduction interface is the base of the loading/unloading tectonic process and generate relatively regular seismicity. During the sinking of the oceanic plate, the aseismic slip of stable subduction interface areas generates a steady strain increase on unstable regions (asperities) meanwhile they stay locked. This increases steadily the shear stress on the asperities until the static shear stress strength is reached. Then, a sudden rupture begins generating a high velocity slip, that may eventually propagate over nearby conditionally stable regions. Once the rupture propagation stops, the slip on the asperity is arrested and it turns back to locked, meanwhile on the stable and conditionally stables zones around the rupture the slip slows down progressively until it reaches a stable slip velocity, resuming the load process.

1.5 Seismogenic zone and segmentation of the subduction interface

The velocity dependence of steady-state friction $(a-b)$, which is a material property, is the main parameter that controls the frictional stability of the faults. Its value is highly dependent on temperature. It adopts negative values at low temperatures and increase to positive values at temperatures above about 350°C, which correspond to the temperature where quartz initiate its crystal plasticity. In the same way, poorly consolidated sediments and cataclasites show positive values of $(a-b)$ parameter, but at elevated pressure and temperature as the material

becomes lithified, its value decrease [*Scholz*, 1998]. These observations suggest a high dependency of the frictional stability of the subduction interface on depth, making more plausible the aseismic slip at shallow depths and deeper than isotherm 350°C, while the conditions for unstable and conditionally stable regimes are favored in between (Figure 1.4). Indeed, the seismicity of the subduction interface is distributed in a narrow band generally located between 5 and 60 km depths, that seems to be strongly constrained by the thermal and structural conditions [*Tichelaar and Ruff,* 1993; *Hyndman and Wang*, 1993; *Hyndman et al.*, 1995; *Oleskevich et al.*, 1999]. This region is denominated seismogenic zone.

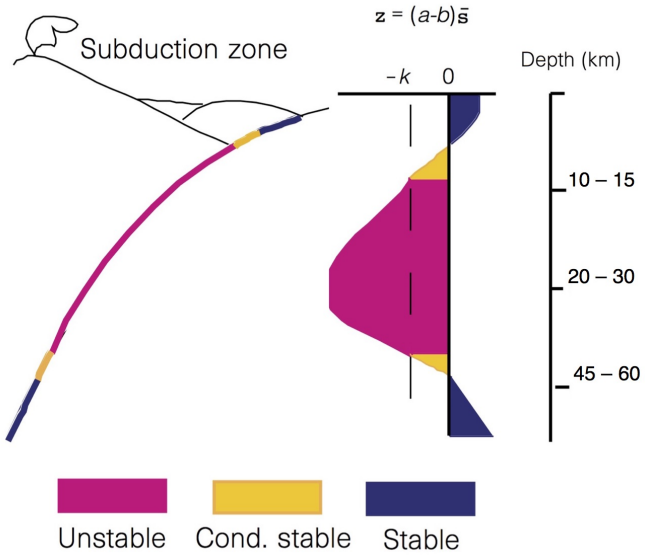

Figure 1.4: Synoptic model of the subduction interface frictional stability with depth (modified from *Scholz* [1998]).

Theoretical thermal models locate the upper boundary of the seismogenic zone between 2 and 10 km of depth [*Oleskevich et al.*, 1999; *Hyndman et al.*, 1997]. At these depths, an accretionary prism commonly overlies the subduction interface, which makes that the interface is in contact with unconsolidated sediments rich in fluids. These characteristics generate appropriate conditions for anelastic deformation of sediments and suggest that velocity-strengthening behavior most likely dominates the slip at very shallow depths. Despite of this, if large seismic ruptures are nucleated at relatively shallow depths, they may propagate towards to the trench as a result of the conditionally stable behavior [*Scholz*, 1998; *Hu and Wang*, 2008]. Even when the shallow portion of the subduction interface is most likely under stable sliding, tsunami earthquakes ruptures that show large slip and anomalous weak high seismic frequency radiation [*Kanamori*, 1972] have been observed near to the trench. Additionally, low moment earthquakes at shallow depths

of subduction interface show similar scaling characteristics to the large tsunami earthquakes [*Bilek and Lay,* 2002]

In the central portion of the seismogenic subduction zone between 15 and 40 km depths, the thermal and pressure conditions suggest that this zone should be most likely controlled by velocity-weakening behavior. This is supported by the large seismic activity observed in this portion of the interface. However, geodetic observations have showed that velocity-strengthening behavior can also exist at these depths [e.g. *Béjar-Pizarro et al.*, 2010; *Loveless and Meade*, 2010; *Métois et al.*, 2012; *Métois et al.*, 2013; *Métois et al.*, 2016]. This zone hosts large megathrust ruptures that usually break almost the whole seismogenic zone (Shallow, central and deeper regions, between 5 and 55 km depth). Recent observations of the large ruptures of 2010 Mw 8.8 Maule and 2011 Mw 9.0 Tohoku-Oki earthquakes have evidenced differences in seismic radiation as a function of depth. In addition, slip inversions show that the coseismic slip is mostly concentrated in the central and shallow portion of the seismogenic zone [*Lay et al.*, 2012]

The deeper boundary of the seismogenic zone seems to be controlled by thermal and structural condition, depending on the particular characteristic of the subduction zone. As explained before, the transition between unstable and stable slip is located around the isotherm 350° [*Scholz*, 1988; *Hyndman and Wang*, 1993] . In fast and young subduction zones where this isotherm is located at high depths, the transition from velocity-weakening to velocity-strengthening behavior seems to be controlled by the Moho depth and the contact with the serpentinized mantle [*Hyndman et al.*, 1997; *Peacock and Hyndman*, 1999]. Even when the seismic activity in some regions suggests a relatively abrupt transition from unstable to stable slip regimes at depths between 45 and 60 km [*Tichelaar and Ruff*, 1993], interface seismicity of low magnitude is still observable deeper this limits. Recent observations have shown that there can be a transitional region where slow slip events and low frequency events occur [e.g. *Ito et al.*, 2007], although this is not observable in all subduction zones. Hence, the transition from seismogenic to aseismic sliding can be either abrupt or gradual, and is influenced by age, temperature and geometry of the subducting plate.

The variations with depth of rupture properties along the subduction seismogenic zone, such as the coseismic slip distribution and the earthquake frequency radiation, have driven to the proposition of a conceptual model by *Lay et al.* [2012], which consider four different rupture domains along dip (labeled from A to D) (Figure 1.5).

The domain A corresponds to the shallowest portion of the subduction interface. It goes from the trench down to around 15 km depth. This domain presents aseismic

deformation but also can experiment large coseismic displacements during tsunami earthquakes. Since some tsunami earthquakes seem to be nucleated in the deeper part of this region and propagate towards the trench, this region is most likely controlled by a conditionally stable regime and may host some small asperities of unstable behavior in its deeper part.

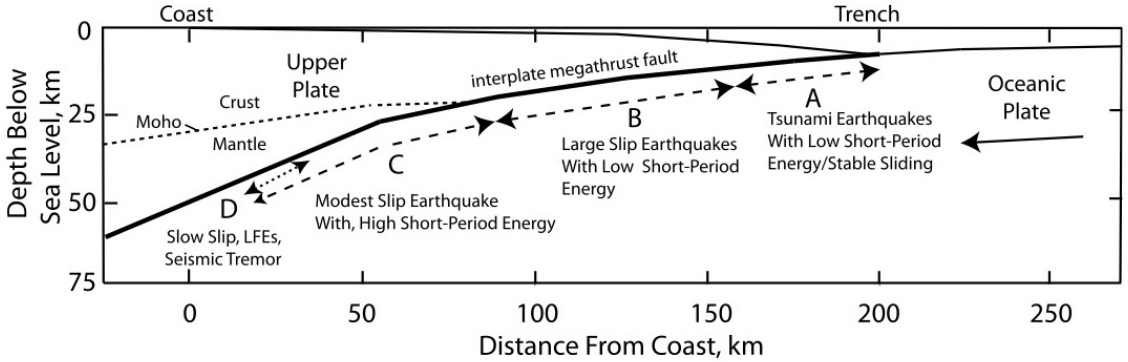

Figure 1.5: Schematic cross-section of rupture domains along dip for the subduction seismogenic zone, derived from the characteristics of the subduction interface seismic ruptures at different depths, scaled for the subduction zone off the northeast coast of Honshu where the great 2011 Tohoku earthquake occurred (after *Lay et al.* [2012]).

The domain B corresponds to the zone from 15 to 35 km depth approximately. It breaks during great earthquakes, and the rupture is characterized by a large slip and a modest amount of high frequency radiations. This suggests that this domain is most likely populated by large and homogeneous asperities of unstable behavior.

The domain C corresponds to region from 35 to 55 km depth approximately. It can host earthquakes of large magnitude, but tends to slip moderately and to radiate a relatively high amount of high frequency energy. This suggests that this domain must be mostly populated by asperities of unstable behavior from small to medium size, surrounded by conditionally stable areas that allow the breakage of several asperities during the large ruptures.

Finally, the domain D corresponds to a down-dip transitional region where the slip regime varies gradually from conditionally stable and unstable to stable aseismic slip behavior. This domain is not observed in all subduction zones. Its presence is indicated by the occurrence of slow slip events, low frequency earthquakes and tectonic tremors, which suggest that this zone is most likely dominated by stable aseismic slip with the presence of sparse isolated small asperities.

This detailed characterization of the seismic behavior along the seismogenic zone of subduction interface, have also driven to the proposition of most elaborated models of the sliding heterogeneity of the subduction interface (Figure 1.6), where systematic depth variations in the extension of seismic versus conditionally stable/aseismic sliding define the properties of the domains of the seismogenic zone [*Lay et al.*, 2012].

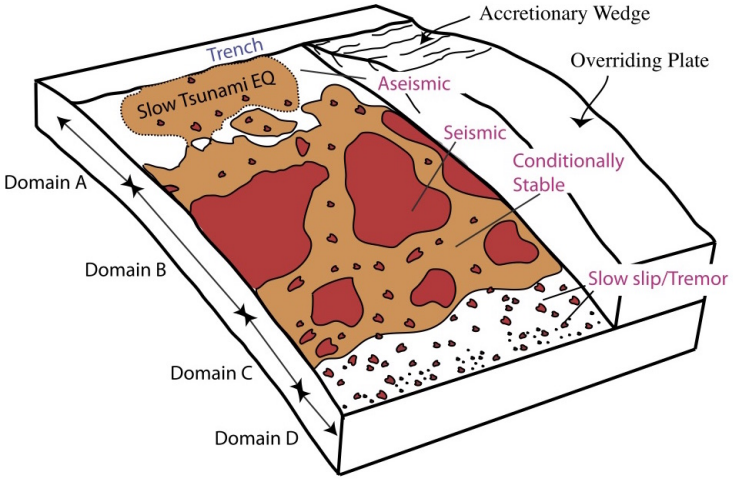

Figure 1.6: Schematic model of the frictional environment for seismogenic subduction interface (after *Lay* [2015]).

The down-dip sliding heterogeneity of the subduction interface seems to be relatively well solved and successfully explains the location, along-dip rupture extension and variations of high-frequency radiation in large megathrust ruptures. However, the megathrust ruptures also present lateral restrictions for its propagation, which can be related to the lateral heterogeneity of the subduction interface. This introduces complexities into the rupture process, which may prevent not all the accumulated strain be released during a single rupture [*Konca et al.*, 2008; *Béjar-Pizarro et al.*, 2010; *Perfettini et al.*, 2010].

The lateral extension of successive subduction earthquakes suggests that some barriers seem to be permanent features of the seismogenic zone, while others may act sporadically during certain ruptures [*Ando*, 1975]. The nature of the barriers is not clear. Geophysical and bathymetric observations have shown that geological structures of the upper and/or bottom plates such oceanic ridges, seamounts, and fault zones, can interrupt the lateral sliding homogeneity of the seismogenic zone along the trench, and may act as barriers for the rupture propagation [*Ruegg et al.*, 1996; *Cummins et al.*, 2002; *Collot et al.*, 2004; *Melnick et al.*, 2009; *Béjar-Pizarro et al.*, 2010; *Yomogida et al.*, 2011; *Métois et al.*, 2013]. However, the effects of those

features of the subduction interface in the slip regime are still a matter of discussion, because they can act as strongly coupled asperities [e.g. *Abercrombie et al.*, 2001] or as barriers [e.g. *Kodaira et al.*, 2002].

1.6 The Seismic Cycle on CAM and transient deformation of the continental crust.

The seismic cycle is a consequence of the cyclic nature of loading/unloading tectonic process. It is based on the evolution of the strain, stress and slip velocities in the asperities and surrounding regions between two consecutive seismic ruptures of relatively similar characteristics. 4 different phases can be identified in a complete cycle.

The interseismic period, or load phase, is the longer phase of the cycle, that can reach durations beyond 1000 years depending on the velocity convergence [*McCaffrey*, 2007]. During this period the regions of the seismogenic interface that show velocity-weakening behavior stay locked, while the regions dominated by velocity-strengthening behavior slip freely. This generates an accumulation of elastic strain in the upper crust, which produces elastic deformation in the continental crust, that experiments a subsidence offshore towards the trench and onshore uplift [*Béjar-Pizarro et al.*, 2013]

The preseismic or nucleation phase is the least known phase due to the lack of information and the few observations of it. However, observations preceding the recent megathrust ruptures of 2011 Mw 9.0 Tohoku-Oki and 2014 Mw 8.1 Iquique have shown evidences of long nucleation processes. They have been preceded by an intense foreshock activity, and increases of the background seismicity rate in the months before the mainshock [Kato et al., 2012, 2016, Bouchon et al., 2013; Ruiz et al., 2014; Schurr et al., 2014; Bouchon et al., 2016; Marsan et al., 2017]. At the same time, cGPS time series show transient slow slip lasting from days to months and years, previously to occurrence rupture [*Ruegg et al.*, 2001; *Ruiz et al.*, 2014; *Socquet et al.*, 2017; *Mavrommatis et al.*, 2014; *Yokota and Koketsu*, 2015]

The coseismic phase corresponds to the main unloading phase. The unstable regions break generating high velocity slip that propagates the rupture across the unstable areas and potentially into the conditionally stable regions around the main asperity. This makes that the elastic strain accumulated during the interseismic phase

be released violently, which generates the subsidence of the onshore continental crust and the fast uplift of the ocean floor towards the trench (Figure 1.7).

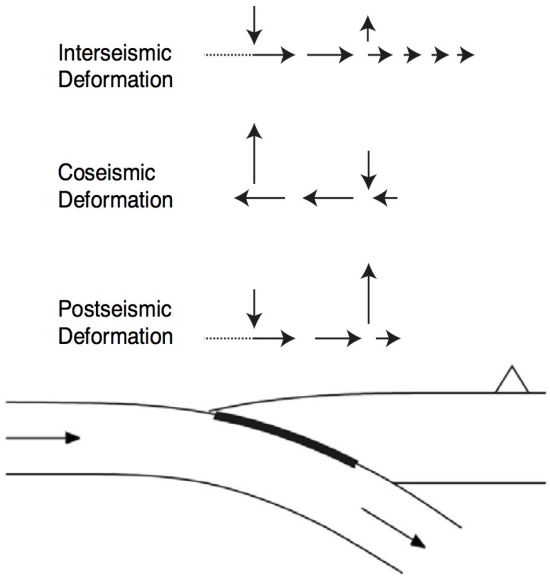

Figure 1.7: Deformation of the continental crust during in the interseismic, coseismic and postseismic phases. The arrows show the sense of the deformation at each phase (modified from *Wang* [2007]).

Finally, the postseismic phase corresponds to the relaxation of the change of stress generated by the coseismic rupture. Part of this relaxation is generated by afterslip that can be observed in the deeper portion of the interface, where is most likely dominated by stable and conditionally stable slip behavior, but also at seismogenic depths in metastable areas with brittle creep behavior that generate aftershock activity [*Perfettini et al.*, 2005]. Afterslip can last from a few days to several months after the megathrust rupture [*Bürgmann et al.*, 2001]. Another component of the postseismic relaxation is generated by the asthenosphere viscoelastic relaxation, which can last up to several decades after the rupture [*Wang*, 2007] and affects wide areas extending over several thousand km [*Moreno et al.*, 2011; *Trubienko et al.*, 2013; *Klein et al.*, 2016]. Poro-elastic rebound is another post-seismic relaxation mechanism that is generated by the changes in the pore pressure induced by the modification of the stress field after the rupture [*Jonsson et al.*, 2003], and that is mostly seen within geometrical complexities of crustal faults. It is not a dominant mechanism in subduction zones.

Chapter 2: Earthquakes Ground Motions

2.1 Introduction

Earthquake strong ground motions correspond to ground shakings radiated from a seismic source in the frequency band from 0.1 to 50 Hz. During an earthquake, these seismic waves are radiated from the earthquake source while the rupture and the slip are propagating along the fault plane. Two kind of waves are radiated, P waves, which produce the compression and dilation of the medium in the direction of propagation, and S waves, that generate orthogonal shear deformation to the direction of propagation [e.g. *Kanamori*, 1986; *Udías,* 1991; *Aki,* 1993; *Kanamori and Brodsky*, 2004]. These waves travel trough the crust and along its surface. During their paths they are attenuated and amplified [e.g. *Jackson and Anderson*, 1970; *Sanchez-Sesma*, 1987; *Aki*, 1993; *Bonilla et al.*, 1997].

The strong earthquake ground motions are usually measured by strong motion instruments, which record the acceleration of the ground at high frequency rates in the near field. Since strong ground motions have a high destructive potential, they are the focus of the engineering seismology community. A huge amount of work has been performed by this community to develop ground-motion prediction models [e.g. *Atkinson and Boore*, 2003; *Ambraseys et al.*, 2004; *Aoi et al.*, 2004; *Scherbaum et al.*, 2004; *Zhao et al.*, 2006, 2007; *Arango et al.*, 2012; *Kumar et al.*, 2012; *Kale and Akkar*, 2013; *Abrahamson et al.*, 2016].

Mathematical formulations of the theory of generation and propagation of elastic waves, have explained the effects of the attenuation of seismic waves during their propagation in continuous medium. At the same time kinematics and dynamics models of the source rupture have been developed in order to explain the relation between waves generation and the earthquake source slip history [e.g. *Madariaga*, 1976; *Udías*, 1991; *Madariaga and Ruiz*, 2016]. These development, the

characterization of earthquakes scaling laws and the characterization of the site amplification waves in the upper layers of the crust, have allowed the development of empirical models that allows to predict strong ground motions at the surface of the crust [e.g. *Joyner and Boore*, 1988; *Youngs et al.*, 1995, 1997; *Zhao et al.*, 2006; *Strasser et al.*, 2009; *Edwards and Fäh,* 2014; *Abrahamson et al.*, 2016; *Montalva et al.*, 2017]

2.2 Seismic waves radiation.

Seismic waves are generated by the fault motion. Since both sides of the fault do not return to their initial position this is a non-elastic displacement. Thus a fault displacement can be represented by a dislocation generated by a shearing motion. This motion is initiated when the elastic strain accumulation in the vicinity of the fault overcomes the static frictional stress. The sliding motion initiate at a point (the earthquake hypocenter), and a slip front expands outward over the fault, separating regions that are slipping from regions that have not yet slipped (Figure 2.1 - right). Thus, the expansion of the rupture and the slip can be seen as functions of space and time that generate a source time function, which control the waveform signal [*Lay and Wallace*, 1995; *Udías et al.*, 2014]

This can be better understood considering a single point of the rupture plane and assuming its displacement as a ramp function, its derivative (velocity) is boxcar shaped and the second derivative (acceleration) is showing two large pulses, one at the beginning of the slip and other at the end (Figure 2.1 - left). The displacement of this point generates a single pulse, proportional to the derivative of the slip, which is called the particle velocity that depends on the frictional constitutive law [*Lay and Wallace*, 1995; *Aki and Richards*, 2002; *Stein and Wysession*, 2009]. As the rupture spreads with propagation velocity, other points of the plane start to slip and stop at different times, generating individual pulses until the rupture ends. The simple superposition of those pulses generates the source waveform. Thus the epicenter location and the direction of propagation of the rupture, as well variations of rupture velocity, variability in the slip velocity and the slip distribution, will impact the source time function and the wave frequency content.

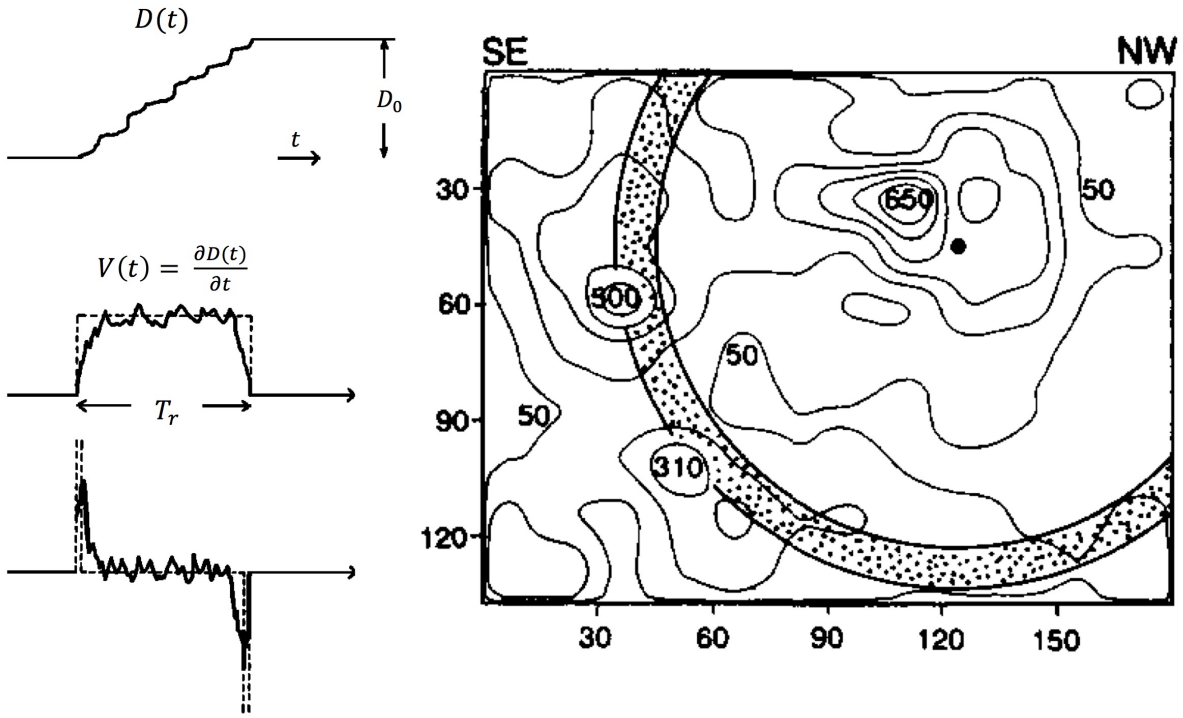

Figure 2.1: *Left* - Schematic diagram of dislocation and its time derivatives at a given point on a fault (after *Aki* [1967]). *Right* – Slip distribution (cm) for the Michoacan Earthquake Mw=8.1 (after *Heaton* [1990]). The black dot shows the hypocenter location and the shaded region represent the propagation of the rupture. The slip of each area of the rupture plane begins once the rupture front pass over them

2.3 Earthquake strong ground motion at the surface of the crust.

The earthquakes strong ground motions are usually measured by instrument installed at the Earth surface or at very shallow depths. The waves travel from the earthquake source along the crust and its surface. Along their paths, they are refracted and reflected. Part of their energy is dispersed. This means that the motion recorded at the surface in a given site, is the result of the convolution of various factors that can be described by:

$$u(t)=s(t)*D(t)*P(t)*St(t) \qquad (2.1)$$

Where $u(t)$ is the motion at the surface, $s(t)$ represent the slip time function, F_s represent the effects of the rupture propagation, $P(t)$ represent the effects of Earth structure and $St(t)$ represent particular effects of the site.

The time radiation dependency of the pulses from the source and its amplitudes are highly dependent on the magnitude. Since, the initiation of the slip at each point of the source is controlled by the rupture propagation, Doppler-like consequences are expected in the waveforms (Figure 2.2). This means that if the rupture front is propagated towards the site where the motions are recorded, part of the seismic energy from the fault arrives in a single large pulse of motion (velocity or displacement). This wave pulse represents the cumulative effect of the seismic radiation from the moving dislocation. This effect is called directivity [*Naeim,* 2001; *Stein and Wysession*, 2009].

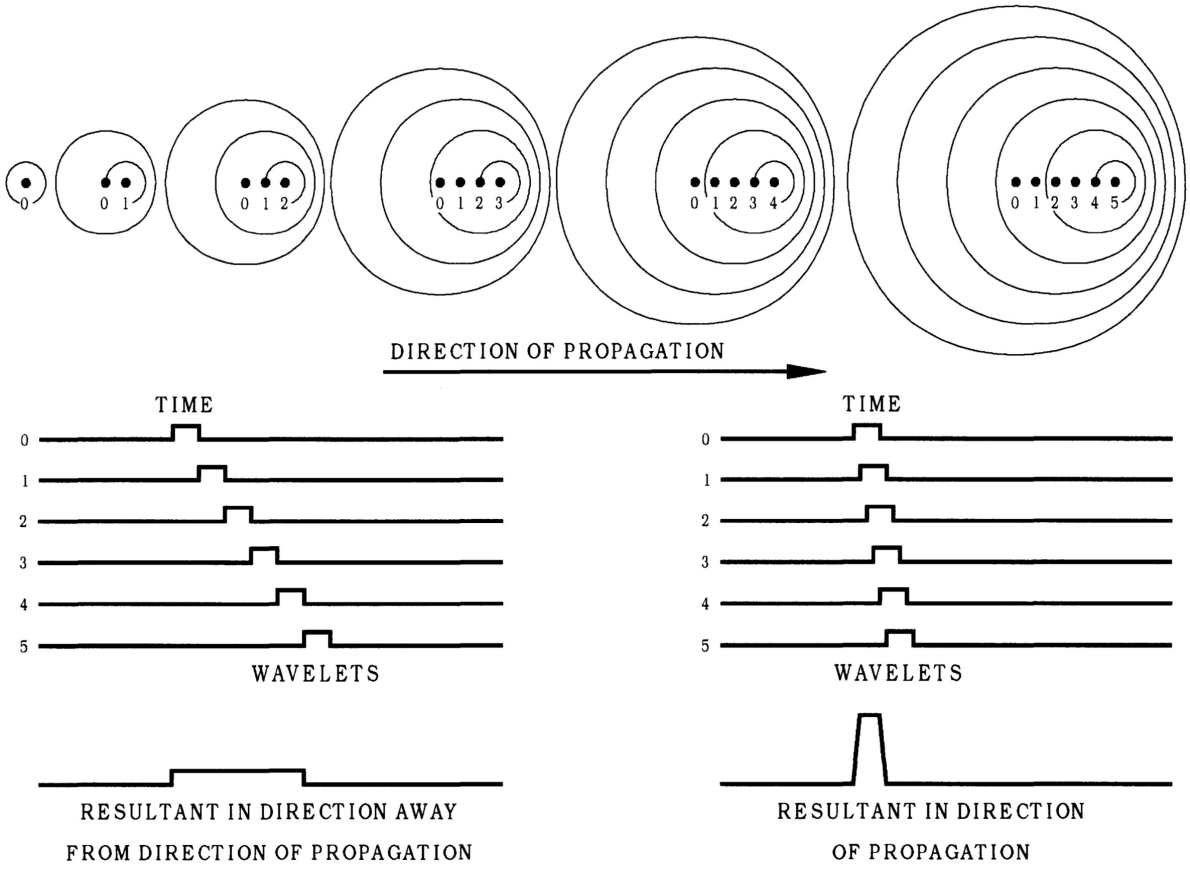

Figure 2.2: *Top* – Effects of the rupture front propagation velocity on the wave pattern radiation. *Bottom* – Effect of rupture front propagation on ground motion experienced at a site located behind and in front of the propagation rupture (after *Naeim* [2001])

The seismic waves are progressively damped as they travel because of the non-elastic properties of the rocks and soils of the earth crust. At the same time, the different layers and structures of the crust reflect and refract the waves radiated from

the earthquake source: these effects affect the ground motion, which are represented in the term S_p of equation (2.1).

The shallow conditions of the site where the instruments measure the strong ground motions have a high impact on ground-motions. Soft soils and topographic condition have showed to have a huge impact on strong ground motion records [*Sanchez-Sesma*, 1987; *Aki*, 1993; *Bouchon et al.*, 1996]. These effects are represented by the $St(t)$ term of equation 2.1.

For engineering purposes it is useful to quantify these strong ground motions. In this sense, ground-motions can be characterized by several parameters. The most direct is the Peak Ground Acceleration (PGA) that corresponds to the maximum acceleration of the ground recorded during an earthquake. It is the simplest parameter that allows comparing the intensity of ground motions of different records. Other useful parameters corresponds to the time duration of the strong motion signal and the ground motion frequency content, which correspond to a family of parameters analyzed in the frequency domain through Fourier spectra [*Naeim,* 2001].

The combination of these three parameters describes the properties of ground motions, which may impact buildings. However, the earthquake engineering community is using another tool (acceleration response spectra) to characterize the effects of ground-motions on structures.

The acceleration response spectra represent the envelopes of peak acceleration responses of single-degree-of-freedom (SDOF) oscillators at different periods. Thus, the acceleration response spectrum of a ground motion is a relationship between the natural period of vibration of a SDOF oscillator and the maximum absolute acceleration that it experiences under the ground shaking. Hence, the construction of a response spectrum involves the analysis of many different SDOF systems. The value of each point on the spectrum is the peak response of a single degree of freedom system at a given period (Figure 2.3).

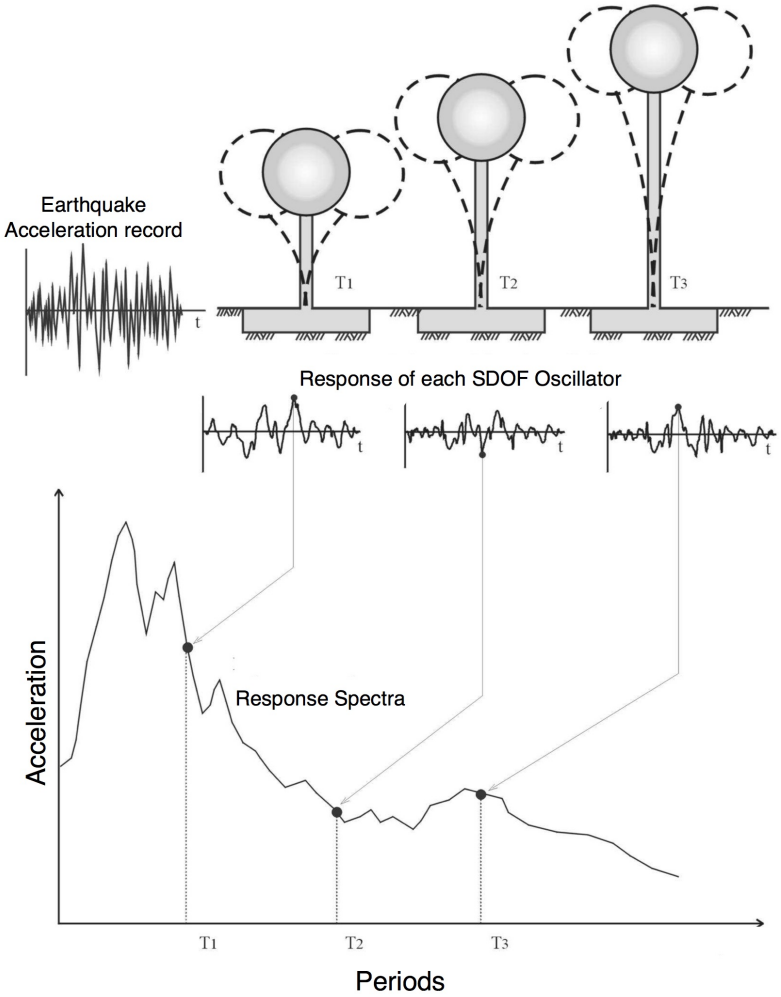

Figure 2.3: Schematic representation of the construction of the acceleration response spectra from a strong motion record.

2.4 Strong ground motion prediction

The prediction of the strong ground motion generated by earthquakes at a particular site is an important aspect of the mitigation of seismic hazard. Since earthquake ground motions are influenced by factors as magnitude, distance from the source, local site conditions, regional geological conditions, propagation path of the waves, earthquake source conditions, mechanism of faulting, the problem of predicting strong ground motions is not a simple issue. Moreover the different factors contributing to ground motions are not easy of separate. To address this issue Ground Motion Prediction Equation (GMPE), have been developed to describe the

log-normal statistical properties of strong ground motions [*Campbell,* 1981; *Joyner and Boore*, 1988].

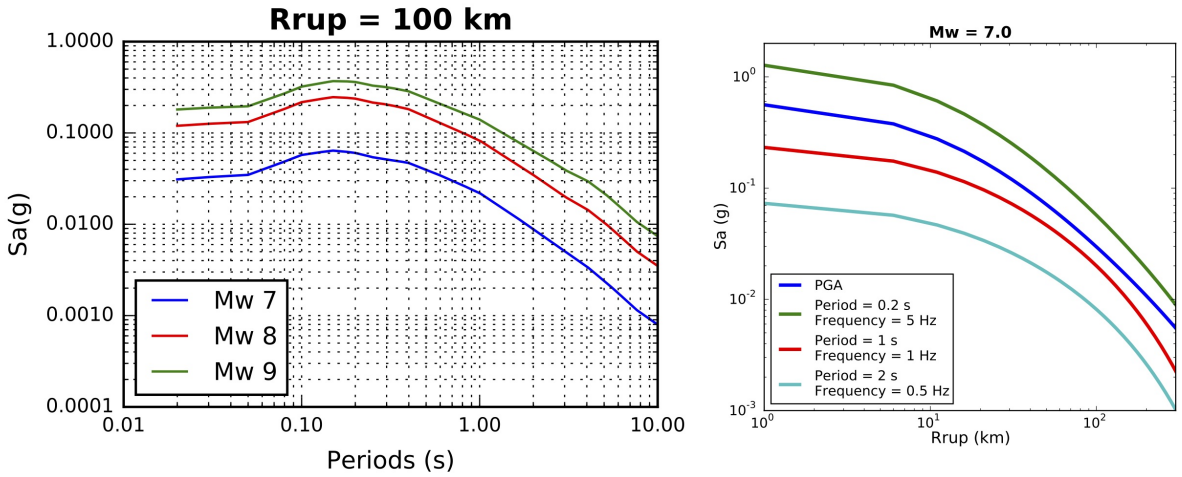

Figure 2.4: *Left* – Horizontal acceleration response spectra at a distance of 100 km from the source for earthquakes of Mw 7, 8 and 9, obtained with the GMPE model of *Abrahamson et al.* [2016]. *Right* – Variation of the horizontal acceleration with respect to the distance source for PGA and SDOF oscillators with periods of 0.2, 1.0, and 2 s obtained with the GMPE model of *Abrahamson et al.* [2016].

GMPEs provide a statistical estimation of the expected ground motion (acceleration response spectra and theirs standard deviation) due to a given earthquake scenario (Figure 2.4). The goal of these models is the engineering estimation of the response of simple structures to the ground-shaking [*Edwards and Fäh,* 2014]. The form of a GMPEs usually correspond to:

$$\log(Y) = f_{source}(M) + f_{path}(R, M) + f_{site}(V_{s30}, ...) + \sigma \qquad (2.2)$$

where Y correspond to the predicted mean of the ground motion, f_{source} is a function of the earthquake source that considers the effects of scaling with the magnitude (M) of the ground motions. The term f_{path} corresponds to a function that takes into account the attenuation generated by the path between the source and the site, which normally depends on the distance site to source (R) and the earthquake magnitude. The term f_{site} is a function that considers the local effects at the recording site. This term is usually characterized by the average of the share-wave velocity in the upper 30 m of the site (V_{s30}) . Finally, σ is a term that represents the variability of the ground motion that corresponds to the standard deviation of the model.

The form presented below, correspond to the most simple representation that explain ground motions. More complex models can incorporate more parameters such a term to model the differences of source conditions with depth or a term to evaluate the decay behind magmatic arcs [e.g. *Zhao et al.*, 2006; *Abrahamson et al.*, 2016]. However, very complex models may increase the uncertainty of the predictions if the input metadata is limited [*Edwards and Fäh,* 2014].

The functional forms associated to GMPEs can vary from one author to another. The users have to be aware that these functional forms are based on simplifications of the physical processes associated to the scaling properties and attenuations of the ground motions.

The term f_{source} related to the source describe the effect of the earthquake size (magnitude) but also the variation of the corner frequency with the magnitude, additionally it can include a term related to the focal mechanism that considers the variability of ground motion by type of faulting [e.g. *Youngs et al.*, 1997; *Naeim*, 2001; *Zhao et al.*, 2006; *Edwards and Fäh,* 2014; *Abrahamson et al.*, 2016]. The f_{path} term that model the effects of the wave path on ground motion, usually consider the geometric decay as magnitude dependent. In some GMPEs, this terms also considers a particular term for the anelastic decay. Finally, the term f_{site} that model the effects of the site is highly model-dependent. (V_{s30}) is usually used to classify site conditions [*Zhao et al.*, 2006; *Edwards and Fäh,* 2014; *Abrahamson et al.*, 2016].

Chapter 3: Methodology

3.1 Scientific hypothesis and approaches followed during the PhD

As discussed in previous chapters, the variation of parameters such as pressure, fluids and temperature along the subduction interface, generate heterogeneities of the frictional behavior on it (Scholz, 1998). This induces variations of the roughness along the interface, which impacts the frequency content of the seismic waves released during the rupture [*Lay and Wallace*, 1995; *Aki and Richards*, 2002; *Stein and Wysession*, 2009]. Recent observations related to megathrust earthquakes have showed that the deep portion of the ruptures generates more high frequency than the shallow part. It has also been showed that the shallow part generate largest slips than the deeper part of the rupture [*Koper et al.*, 2011; *Kurahashi and Irikura*, 2011; *Koper et al.*, 2012; *Hooper et al.*, 2012]. The extension along-dip of the megathrust ruptures added to the variability of the frequency content and slip, have driven to the proposition of depth dependent frictional environment models [*Lay et al.*, 2012], which suggest that the shallow portion of the subduction interface is mainly controlled by velocity-strengthening and conditionally stable behavior, meanwhile the subduction interface at intermediate depths is most likely controlled by large and homogeneous patches under velocity-weakening behavior surrounded by small regions of conditionally stable behavior. The size of these large patches decreases with depth, which increases the heterogeneity of the frictional conditions and consequently the increase of the roughness of the deeper portion Figure 1.6).

Recent observations on regions where megathrust earthquakes have occurred, suggest that large and homogeneous asperities that brake during the megathrust earthquakes seem to be locked during the interseismic period, but can show transient slip associated to the nucleation process, days to month before the rupture [*Loveless and Meade*, 2010; *Kato et al.*, 2012; *Ruiz et al.*, 2014; *Schurr et al.*, 2014;

Kato et al., 2016; *Métois et al.*, 2016; *Bouchon et al.*, 2016; *Socquet et al.*, 2017; *Marsan et al.*, 2017]. In the other hand, the deeper portion of subduction interface can exhibit larger transients slips during the interseismic period that may impact the rupture nucleation [*Kato et al.*, 2012; *Mavrommatis et al.*, 2014; *Yokota and Koketsu*, 2015]. These deep transients slips may be related to transient changes of the subduction interface that trigger changes from conditionally stable to unstable behavior in the deeper portion of the subduction interface. These changes could impact in the roughness of the interface. In the other hand, the transient behavior associated to nucleation process may be related also with transient changes of the friction too.

The roughness, the frictional behavior, the coseismic slip amplitude and the extension of along-dip of megathrust ruptures then seem to be correlated and they may impact earthquakes high frequency contents [e.g. *Scholz*, 1998; *Stein and Wysession*, 2009; *Lay et al.*, 2012]. The earthquake source frequency content can then be seen as a proxy of the frictional properties of the subduction interface. Since strong ground motions are controlled by high frequency waves, they may be used to improve the characterization the frictional behavior of the subduction interface, which may help to understand the lateral extension of megathrust ruptures, the transient slip behavior observed in the interseismic periods and the nucleation process of the megathrust ruptures.

For this purpose, we propose to investigate the variability of strong ground motions high frequency contents generated by subduction interface earthquakes, from low to large moment magnitudes. The correlation between the strong ground motion variability with parameters that control the frictional environment models, such as depth, should confirm the *Lay et al.* [2012] model derived of large megathrust ruptures. This method may also be useful to identify lateral variations of the frictional conditions of the subduction interface. The transient variability of the strong ground motion may also be related to observed transient slip behavior and nucleation's processes.

With this general aim, two methods are proposed for the comparison of strong ground motion records: the first method allows to analyze directly the acceleration frequency content of earthquakes using the spectral ratio of earthquakes pairs. The second method analyzes source frequency contents using an indirect method and residuals to Ground Motion Predictive Equations.

3.2 Direct comparison of Earthquake Frequency Content: Spectral Ratio Method

The spectral ratio technique consist to the computation of ratio between the Fourier spectra of two different signals. This allows to compare the amplitudes of both signals in the whole frequency range. This technique has been largely used in engineering seismology: most of its applications are related to the characterization of site effects [e.g. *Konno and Ohmachi,* 1998; *Bozorgnia and Campbell,* 2004; *Zhao et al.*, 2006].

The acceleration spectra, which is obtained from the surface ground motion records, shows the amplitudes of the Fourier series terms that describe the acceleration record. The spectral ratio, which correspond to the ratio between two acceleration spectrum, allow compares the amplitudes of the Fourier series terms of both records in whole frequency band. Thus the spectral ratio is defined at each frequency f, as:

$$SR(f)=\frac{F_A(f)}{F_B(f)} \tag{3.1}$$

where F_A and F_B are the acceleration Fourier spectra of earthquakes A and B respectively.

It is well know that the ground acceleration frequency content is affected by scaling effects, directivity, site effects, geometrical spreading attenuation and path attenuation [*Aki*, 1967; *Brune,* 1970; *Aki*, 1972; *Aki*, 1993], which makes difficult the direct comparison of the spectra of two different records. Considering this, the acceleration spectra of an earthquake record at a given site, can be seen as a convolution of those factors:

$$F=F_s*S_D*S_p*S_{St} \tag{3.2}$$

where F is the acceleration spectra of the record, F_s is the source spectra that depends on the rupture properties and the earthquake magnitude, S_D correspond to the directivity, S_p correspond to the path from the source to the site, S_{st} and represent effects of the site conditions where the acceleration waveform was recorded.

This consideration have allowed to use the spectral ratios to compare the frequency contents of acceleration records of a couple of shallow and deep earthquakes in Japan [*Lay et al.*, 2012], showing that the deep earthquakes can present amplitudes at high frequency of 10 times higher than shallow earthquakes (Figure 3.1).

In this approach, the authors have computed the spectral ratios using the ground acceleration records larger than 300 seconds from two different earthquakes of similar magnitudes. The acceleration spectral ratios were computed over the three record components (north-south, east-west and up-down). In order to cancel the site effects, they have computed the spectral ratios at each station, then the spectral ratios obtained from each component have been averaged at each station and smoothed, to get one spectral ratio per station. Finally, the spectral ratios of all stations were averaged in three groups geographically defined assuming that path attenuation variations are low within each group (Figure 3.1).

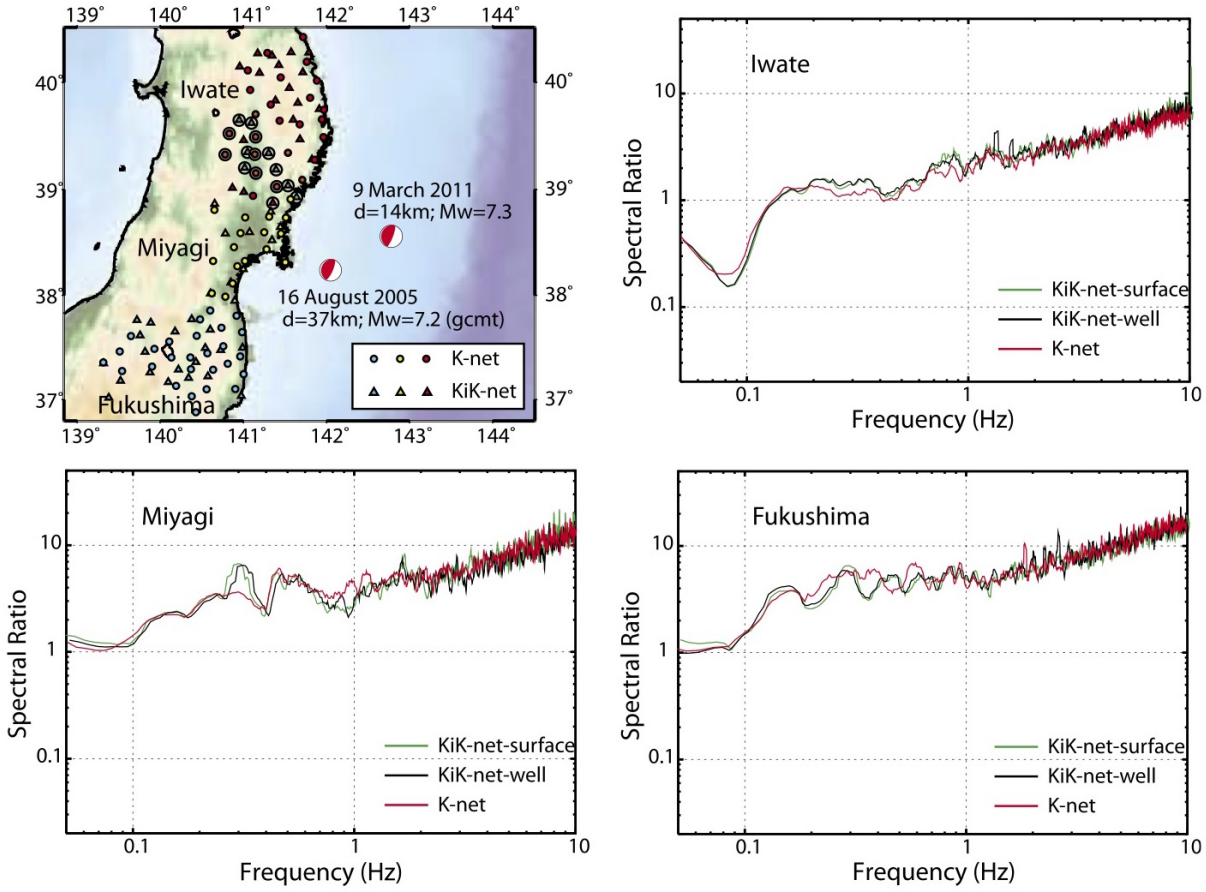

Figure 3.1: Spectral ratio between deep and shallow earthquakes in Japan [*Lay et al.*, 2012]

This methodology generates a large scatter of the resulting ratios due to the inclusion of the vertical component and the late application of the smoothing. For this reason, we have modified this methodology, computing the spectral ratios at each station using only the horizontal acceleration spectra of each station obtained from the smoothed spectra of each horizontal component of the records (equation 4.6 of Chapter 4) Thus we obtain only one smoothed spectral ratio by station. Finally, the horizontal spectral ratios of the different stations are averaged by geometric mean. The modifications introduced in the method proposed by *Lay et al.* [2012], were successfully tested reproducing their results using the same dataset (Figure 3.2), additionally we have verified the stability of the spectral ratios obtained with this modification by getting a lower standard deviation of the obtained spectral ratios.

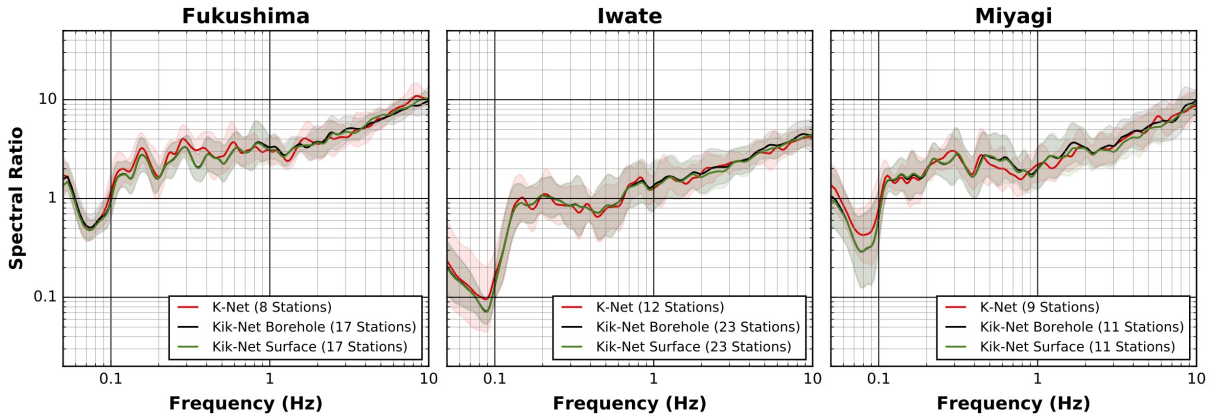

Figure 3.2: Reproduction of the results of *Lay et al.* [2012] using the modified spectral ratio method. Shaded bands represent the standard deviation of the horizontal spectral ratios. Note that the scatter of the spectral ratios originally presented is noticeable reduced.

3.2.1 Detection of temporal variability of frequency contents and limitations of spectral ratio method

The application of this method is reduced to the comparison of the frequency content of pairs of earthquakes. Its scope can then be extended applying it systematically over several pairs of earthquakes. For this, an automatized search over earthquake catalogs has been implemented in order to generate a library of spectral ratios. This search must be constrained by defining the accepted difference of magnitudes and distance between epicenters of the earthquake couple. Limiting these differences is necessary to guarantee low distortions derived form scaling and attenuation effects. Thus the spectral ratios obtained can be grouped in couples that meet specific

requirements and re-averaged in order to get the spectral ratios representatives of each group.

The most interesting application of this method is the possibility to analyze the time variability of the earthquake frequency contents in regions of high seismicity rate. This can be done through the definition of time windows, thus the earthquakes couples can be grouped by the different combinations of time windows. This application may be useful to identify variation of the frictional properties of the subduction interface in time and the identification of nucleation phases of megathrust earthquakes.

These spectral ratio methods must be applied carefully. Due to the constrain of the maximum distance between earthquakes couples, this method is not able to detect regional variability of spectral ratios, and the average of them over large regions may mask regional dependencies, so its use is limited to small areas.

3.3 Indirect comparison of Earthquake Frequency Content: GMPE residuals method

As discussed above, the main problem for the comparison of earthquake acceleration frequency contents is the fact this frequency content depend on scaling effects and wave attenuations. This problem can be addressed analyzing GMPEs residuals.

The GMPEs are able to model the magnitude scaling, geometrical spreading attenuation, path attenuation, and site amplification to predict earthquakes response spectra at a given distance to the source [*Edwards and Fäh*, 2014]. In this sense, it is possible to characterize those effects in a given region through a GMPEs that shows a good fit with the observed ground motions. Thus, differences between the observed and predicted ground motions are generated by variations of factors that can not be captured by the GMPE: path attenuation variations, source scaling variations, stress-drops variations or site effects [*Strasser et al.*, 2009].

The total error describing the differences between observations and GMPEs predictions can be separated in two independent and normally distributed terms that allow to disaggregate the source and path-site prediction misfits [*Abrahamson and Youngs*, 1992]. The first one is denominated between-event term. It correspond to the ground motion variations generated by the variability of source rupture conditions

and cannot be captured by a simple source parameter like the magnitude. The second one is called within-event term, and correspond to the ground motion variations generated by a random variability of propagations conditions between site and source, such as the travel path of the seismic waves or site conditions that cannot be captured by parameters such distance to the source or site classification [*Youngs et al.*, 1995; *Strasser et al.*, 2009; *Al Atik et al.*, 2010].

Consequently, the Between-event residual represents the average shift of the observed ground motions of an individual earthquake, respectively to the median predicted by the GMPE model. In the other hand, the within-event residual, is the misfit between an individual observation from the earthquake-specific median prediction, which is defined as the median prediction of GMPE model plus the between-event residual of the earthquake (Figure 3.3).

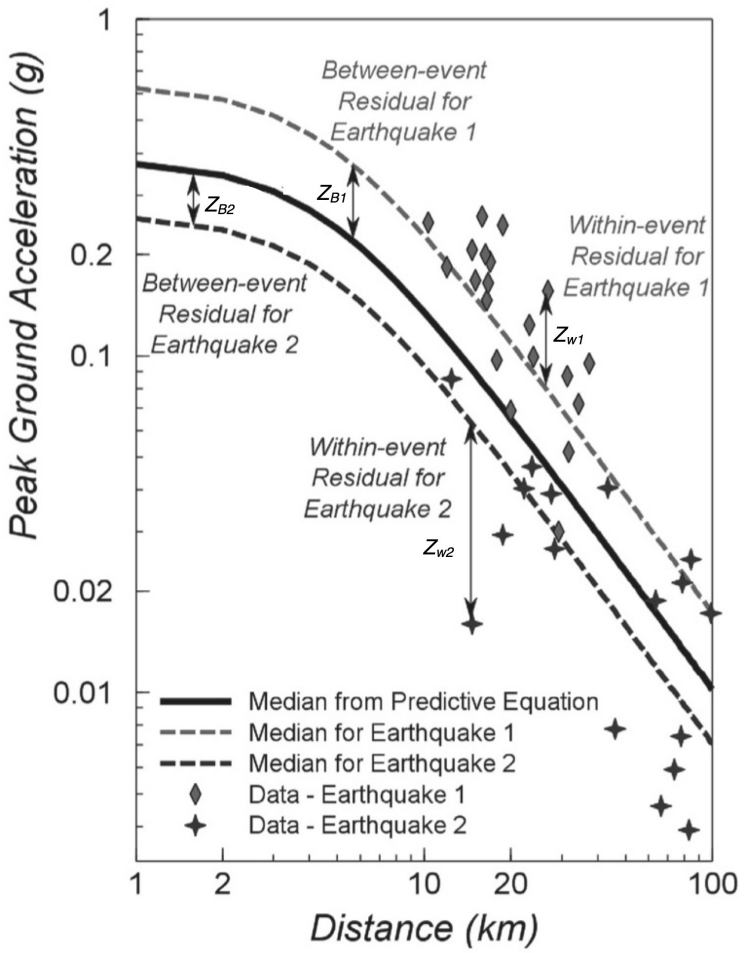

Figure 3.3: Between-event residual (Z_B) and within-event residual (Z_w) of ground motion variability (after *Strasser et al.* [2009])

For a given station, the GMPEs residuals can be computed over all oscillator periods of the response spectra of one specific earthquake. Nevertheless its disaggregation in between-event and within-event residuals is performed combining all the stations records of a given earthquake. This means that the between-event and within-event residuals are characteristic of each specific oscillator period of a given earthquake. This allows to characterize and compare the earthquakes by their between-event residuals at a specific oscillator periods.

This methods allows to compare the frequency content of earthquakes dataset of different magnitudes and locations, analyzing the variability of the between-event residuals. Therefore, coherent spatial distributions of between-event residuals, as well its dependency on parameters characterizing the frictional conditions of the subduction interface, may reveal features that affect the acceleration frequency contents of the strong ground motion.

To use this GMPE approach for the comparison of the earthquake frequency content it is necessary to work with a reliable seismic catalog and a high quality strong ground motion database. This high quality dataset is necessary to validate a GMPE as a model able to capture first order source and propagation effects (“backbone” model).

The GMPEs require as input, specific information of the site and the rupture source. Most of this information is directly provided by the seismic catalog, but usually, part of the information required by the use of GMPEs such as the site to source distance, is not provided. For moderate and low moment magnitude earthquakes, this lack of information can be supplied using the strong motion stations location, the hypocentral location, focal mechanism and source dimensions scaling laws [*Montalva et al.*; *Haendel et al.*, 2014; *Dawood et al.*, 2016]. However, for large magnitude earthquakes it is preferable to estimate distance source to site from the available inversion models. Additionally, it is necessary to classify the seismicity according to the fault mechanisms and the associated tectonic environment.

It is also important to work with a reliable and homogenously processed strong motion database issued from a well-characterized network. For this purpose, the guidelines and recommendations of the COSMOS strong motion record workshop are appropriate [*Boore and Bommer*, 2005].

For the GMPEs selection, it is recommendable to evaluate the fit of GMPEs using a local ground motion database. , The fit of the GMPEs models must to be evaluated comparing the dispersion of the total, between-event and within-event residuals of

the database, with the residual dispersion of the model for long and short periods as well for the Peak Ground Acceleration (PGA).

Chapter 4: Spatio-temporal variations of ground motion in northern Chile before and after the 2014 M_W 8.1 Iquique megathrust event

Paper submitted to Bulletin of Seismological Society of America

Current state: Under revision

Authors: Jesús Piña-Valdés, Fabrice Cotton, Anne Socquet, Sebastian Specht

4.1 Abstract

In order to evaluate the spatio-temporal variations of ground motions in northern Chile we have built a high-quality rock seismic acceleration database and an interface earthquakes catalog. Two GMPE models for subduction zones have been tested and validated for the area. They were then used as backbone models to describe the time-space variations of earthquakes frequency content (Fourier and response spectra). Consistently with previous studies of large subduction earthquakes, moderate interface earthquakes in Northern Chile show an increase of the high-frequency energy released with depth. A regional variability of earthquake frequency content is also observed, which may be related to a lateral segmentation of the mechanical properties of the subduction interface. Finally, interface earthquakes show a temporal evolution of their frequency content in the earthquake sequence associated to the 2014 Iquique Mw 8.1 megathrust earthquake. Surprisingly, the change does not occur with the main shock, but is associated with an 8-month slow slip preceding the megathrust.

4.2 Introduction

A key issue of seismic hazard assessment and engineering seismology is the capability to perform predictions of ground-motions (e.g. peak ground acceleration and response spectra) that can be generated by an earthquake at a specific site. With this aim, Ground Motion Prediction Equations (GMPEs) have been developed in order to describe seismic response spectra of an earthquake. These models are generally parameterized for magnitude, fault type, distance (e.g. to the rupture plane) and site conditions (e.g. soil type). The models are presented in terms of a median and a standard deviation [e.g. *Strasser et al.*, 2009; *Al Atik et al.*, 2010; *Haendel et al.*, 2014]. Several models have been derived for subduction zones [*Youngs et al.*, 1995, 1997; *Zhao et al.*, 2006; *Abrahamson et al.*, 2016]. Because of the lack of data, most of these models have been developed using global databases which are mixing data from a couple of densely instrumented subduction zones (e.g. Japan, Alaska, Cascadia, Chile, Mexico). The development of subduction ground-motion models is then facing three main scientific challenges.

The first challenge is related to the regional variations of ground-motions. Indeed, subduction zones are highly diverse in terms of mechanical behavior and geometry of the subduction interface [*Kanamori*, 1986; *Astiz et al.*, 1988; *Tichelaar and Ruff,* 1993; *Heuret et al.*, 2011] It is therefore necessary to evaluate regional variations of ground-motions, and test the robustness of global models for application to a given region.

The second challenge is related to the impact of interface earthquake depths on ground-shaking. Recent observations of seismological data from megathrust earthquakes have shown that the slip properties and spectral content of waves generated by major subduction events are highly depth dependent [e.g. Lay et al., 2012]. These new observations challenge the ability of GMPEs to take into account the impact of depth on ground-motions of interface earthquakes of moderate Mw, which are excluded from past subduction GMPE models. Such moderate earthquakes (Mw<5) have a limited impact on seismic hazard assessment, which is mainly controlled by large earthquakes. They may however provide key information on the regional variations of the subduction interface properties and associated segmentation.

The third challenge relates to the impact of the processes at stake on the subduction interface during a seismic cycle on the generated ground motions. Recent major subduction earthquakes have also shown long (several years) preparation phases

[Bouchon et al., 2013; Schurr et al., 2014] and postseismic phases [Ozawa et al., 2012; Mavrommatis et al., 2015; Yokota and Koketsu, 2015; Cesca et al., 2016; Kato et al., 2016]. Variations of the frictional properties of the plate interface are likely associated with these pre- and postseismic phases, and may cause ground motion temporal variations. However, these ground-motion time-dependencies have not yet been analyzed.

The northern Chile subduction (Figure 4.1 - a) provides a good case study to analyze regional, depth, and time dependencies of ground motions. The high convergence rate of 65 to 70 mm/yr between the Nazca and South American plates [Argus et al., 2011], generates observed seismicity associated with the interface plate convergence, This zone can be seen as a mature seismic gap between -23°S and -18°S of latitude, as it has experienced only partial ruptures since the 1877 Mw 8.8 megathrust earthquake [Lomnitz, 2004]. In 2007, the Mw 7.7 Tocopilla earthquake broke the deeper portion of subduction interface at the southern part of the gap [Delouis et al., 2009; Béjar-Pizarro et al., 2010; Motagh et al., 2010; Peyrat et al., 2010]. In 2014, the Mw 8.1 Iquique earthquake partially ruptured an approximately 150 km-long portion of the subduction interface centered at 20°S of latitude [Ruiz et al., 2014; Schurr et al., 2014; Gusman et al., 2015], with a coseismic moment release less than half of the moment deficit estimated in the area [Béjar-Pizarro et al., 2013; Métois et al., 2013; Hayes et al., 2014; Métois et al., 2016].

Since this region is identified as a high seismic hazard region, an important effort of seismological and geodetic monitoring has been performed since 2006 by several international agencies. In particular, twenty-one permanent multiparameter stations (including broadband seismometer, accelerometer, and GPS) have been installed in the frame of the Integrated Plate boundary Observatory Chile (IPOC) on relatively homogeneous rock geotechnical conditions. This network has provided a substantial seismic catalog and associated high-quality rock-site conditions strong-motion records, which are suitable to test GMPE’s models and also characterize the spatial and time-variations of the earthquakes ground-motion in this area. Thus given this dataset, relevant GMPEs can be testes for their applicability to ground motion estimates for the region.

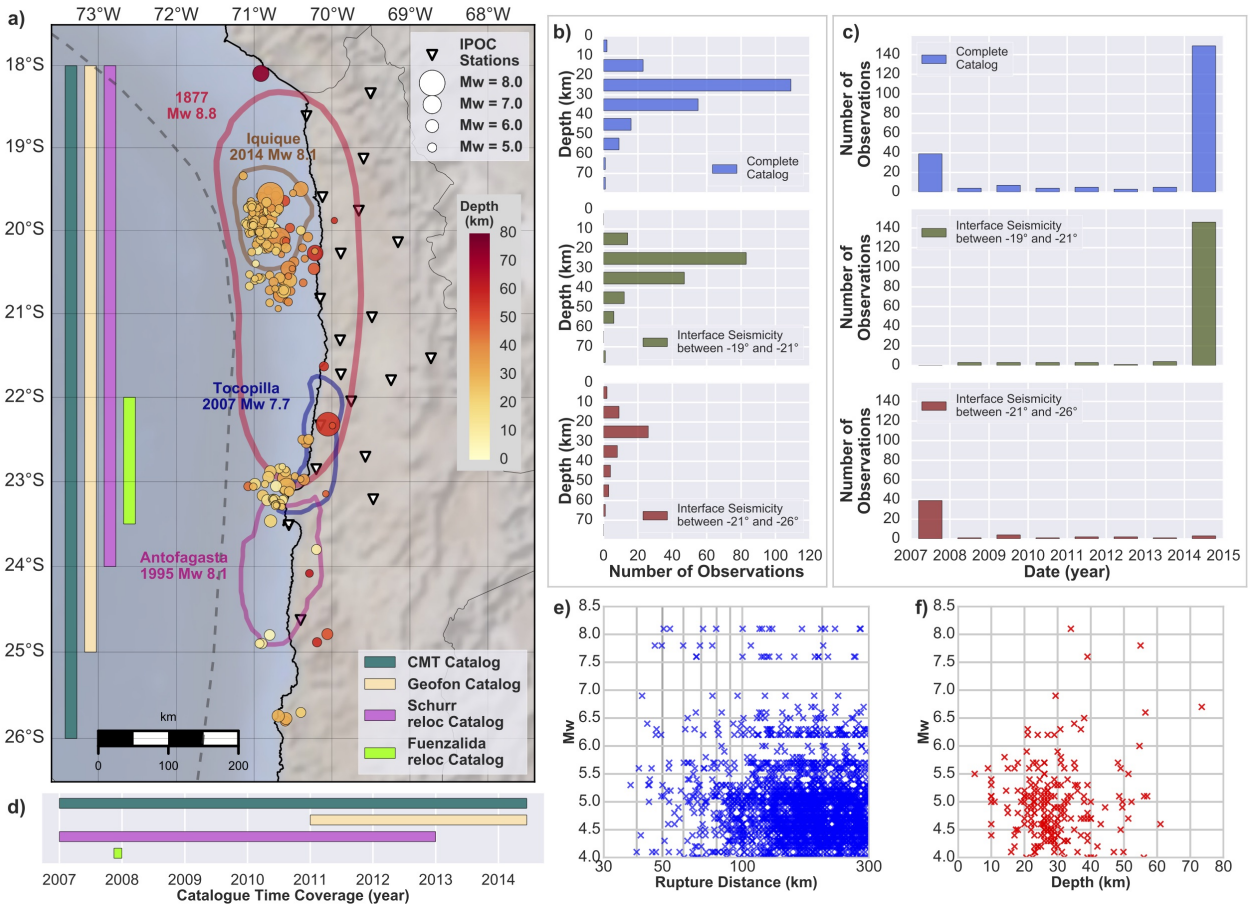

Figure 4.1: a) Spatial distribution of the interface seismicity, the circles indicate the epicenter location, the fill indicate the depth and the size indicates the magnitude. Contours of recent megathrust earthquakes ruptures are shown. Inverted triangles show the distribution of IPOC multiparameter stations. Observed seismicity is concentrated in two clusters: the first one is centered at latitude -20° and the second one at -23°. The vertical bars on the left of the map indicate the latitudinal coverage of the catalogs included in the compilation used in this study. b) Histograms of seismicity depth distribution and c) Histograms of seismicity temporal distribution, for whole catalog (upper), Northern cluster (middle) and Southern cluster (bottom). Most of the seismic activity occurs between 10 and 60 km depth. North cluster is mostly composed by the foreshock and aftershock sequences of Iquique earthquake 2014 (Mw 8.1), and the southern cluster by the aftershock sequence of Tocopilla earthquake 2007 (Mw 7.7). d) Time coverage of the different catalogs. e) and f) Distribution of Mw as a function of rupture distance and depth, respectively.

4.3 Interface Earthquake Catalog

Having a reliable earthquake catalog is a critical point to analyze ground motions. Building a good catalog with a limited level of unknowns can potentially reduce the uncertainty of the ground motion predicted by the GMPEs. Indeed, earthquake catalogs provide most of the key parameters necessary to apply the GMPEs, such as event location and magnitude. In addition, information about fault plane orientation derived from earthquakes focal mechanisms allow to discriminate the style of faulting, a key information to evaluate whether the event occurred on the subduction interface or within the subducted slab.

To compile a seismic catalog of interface seismicity appropriate for our purpose, we have searched events with Mw ≥ 4.0 between January 2007 and June 2014, within the region between 18°-26°S and 69°-72°W of latitude-longitude range. We only considered events with a maximum depth of 90 km and with available focal mechanism solutions (FMS). Our catalog is a compilation of four different catalogs characterized by different accuracies and precisions of the hypocenter location, and different coverage in time and space (Figure 4.1 - a and b). We selected data associated to each earthquake from the most accurate catalog. The four databases below are sorted from most to the least accurate:

1. High-resolution relocated catalog of the Tocopilla 2007 seismic event [Fuenzalida et al., 2013]: magnitude, hypocentral location and focal mechanism of 31 aftershocks, following the Mw 7.7 November 14th, 2007 Tocopilla earthquake. The catalog includes earthquakes located between 21° and 24°S, within 45 days after the mainshock.

2. Relocated catalog of North Chile [Schurr et al., 2012]: magnitude and hypocentral location of 106 earthquakes from January 2007 to December 2012, within 18°-25°S and 69°-72°W, estimated from records of IPOC permanent stations.

3. Geofon data center (GFZ) catalog (automatic estimates): catalog (automatic estimates): magnitude, hypocentral location and focal mechanism of 245 earthquakes from January 2011 to June 2014 within 18°-25°S and 69°-72°W, estimated from records of IPOC permanent stations .

4. Global Centroid Moment Tensor (CMT): magnitude, hypocentral location and focal mechanism of 89 earthquakes from January 2007 to June 2014, within 18°-26°S and 69°-72°W .

The seismicity in the obtained catalog has been classified as either interface or intraplate earthquakes based on focal mechanism solutions, using the Angular Classification with Expectation-Maximization (ACE) cluster analysis [Specht et al., 2017], resulting in 216 identified interface earthquakes. We checked that this data-driven cluster analysis gave consistent classification results with the classical expert classification based on earthquake location and focal mechanisms used by Bastías and Montalva [2016]. Additionally, 112 earthquakes that are not included in the catalog of Bastías and Montalva [2016] were identified, which correspond mainly to earthquake of Mw between 4 and 5 that are not included in the their work.

In the studied time period, the interface seismicity occurred in two main clusters (Figure 4.1 - a). The cluster located south of the gap (~23°S of latitude) is related to the 2007 Mw 7.7 Tocopilla earthquake. The cluster located between 19°S and 21°S of latitude is related to the seismic event of the 2014 Mw 8.1 Iquique earthquake, and contains most of the seismicity included in our catalog. Both of them show depths between 10 and 60 km (Figure 4.1 - c), and are highly concentrated in the years 2007 and 2014 respectively (Figure 4.1 - d).

4.4 Acceleration database and data processing

Multiple strong-motion databases are available in Chile [Arango et al., 2011; Bastías and Montalva, 2016]. We have however chosen to use only the IPOC data in order to use homogeneous rock site data to characterize the spatio-temporal variations of earthquakes frequency content, and also perform GMPE testing using an independent dataset.

The processing of the acceleration dataset has been performed following the guidelines and recommendations of the COSMOS strong motion record workshop [Boore and Bommer, 2005]. We used horizontal acceleration records of interface events with a sampling frequency of 100 Hz. Records were cut 100 s before and 300 s after the reported event time. The raw data were deconvolved before applying a standard correction procedure. First, a baseline correction was performed by detrending and demeaning the acceleration time series in order to remove the

instrument offset. Then, the records were manually picked to define the beginning and the end of the relevant seismic signal. Finally, the signal was tapered and zeros were padded at the beginning and the end of the waveform following Akkar et al. [2014].

The acceleration response spectra have been calculated over the north-south and east-west components, at 5% spectral damping ratio, using the method proposed by Nigam and Jennings [1969] The horizontal acceleration response spectrum was then obtained by calculating the geometric mean of the response spectra of both horizontal components for each oscillator of fundamental period T , as:

$$Sa_{hor}(T)=\sqrt{Sa_{NS}(T)*Sa_{EW}(T)} \qquad (4.1)$$

where Sa_{NS} and Sa_{EW} correspond to the acceleration response spectra of the North-South and East-West acceleration components, and Sa_{hor} corresponds to the horizontal response spectra.

4.5 Evaluation of Ground Motion Predictive Equations

We have tested two GMPEs for subduction environments: the model of Abrahamson et al. [2016] which is a current GMPE model that has been calibrated with a worldwide database, and the model of Montalva et al. [2017] that has been calibrated with a local ground motion database of earthquakes of Mw higher than 5, exclusively occurring on the Chilean subduction zone between -34° and -17° of latitude, including the records of the IPOC stations .

Since we have no rupture plane models for the events, we estimate the rupture plane distance (Rrup), which is defined as the minimum distance between the rupture plane and a given site, by estimating the position and orientation of a rupture plane from the hypocentral depths and the dip and strike given by the focal mechanisms. Because focal mechanisms have two nodal planes, we selected the nodal plane that is (near) parallel to the subduction interface as the rupture plane. As generally there is no information about the hypocenter position relative to the rupture plane, we assumed the hypocenters to be located at the center of the rupture planes and its geometry has been defined by the scaling relations of rupture source proposed by Strasser et al. [2010]. Finally, a grid was defined on each rupture plane, to search the minimum distance between the nodes of the grid and the station site. When the

minimum is localized, a refined grid is defined around the location of the minimum and the process is repeated again until no significant variations are observed [Haendel et al., 2014; Bastías and Montalva, 2016] The result of this procedure is summarized in Figure 4.1 - e that shows the magnitude-rupture distance distribution from 40 to 300 km for the whole range of magnitudes of the catalog.

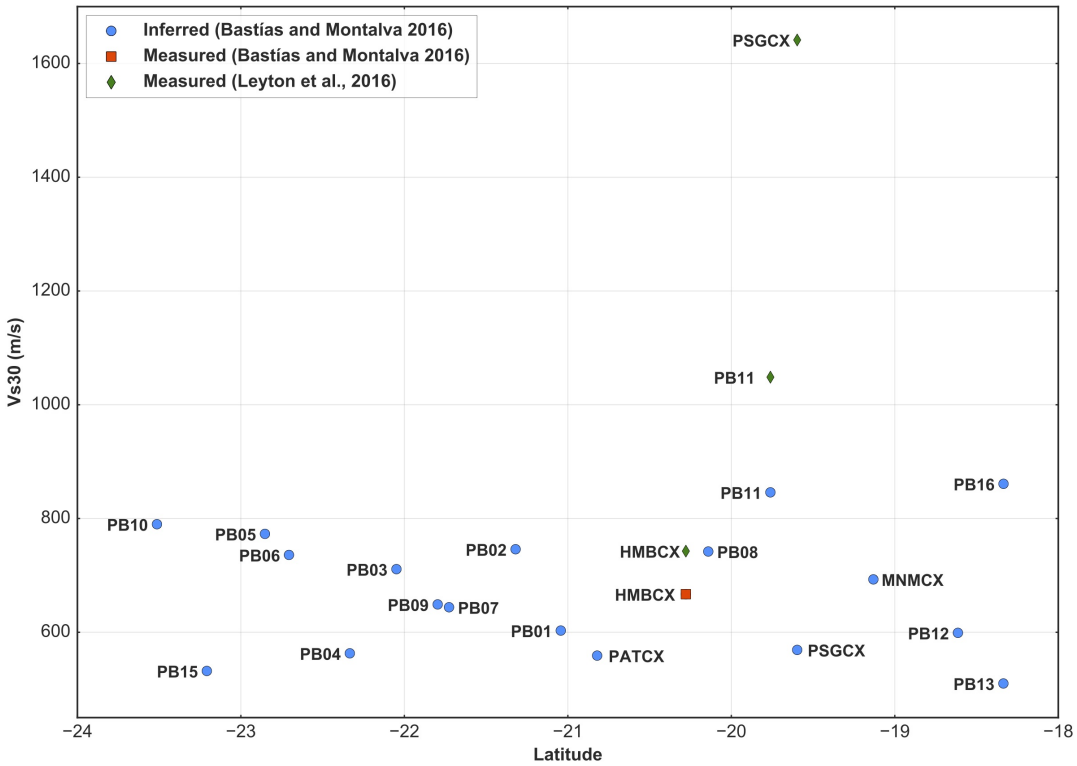

Figure 4.2: Average of the top 30 meters shear wave velocities (Vs30) of the CX-network stations with respect to the latitude. The square and circles indicate the measured and inferred Vs30 values respectively, taken from Bastías and Montalva [2016]. Diamonds show the measured values taken from Leyton et al. [2017]. Note that the station PB13 has been replaced by the station PB16 (located near to the original site). This new station shows an inferred Vs30 69% higher than the PB13 site.

Both selected GMPE's models require the Vs30 value to estimate indirectly the site effects on ground motions. There is no specific geotechnical information for the whole IPOC Network. Such lack of information has been supplied in previous works using proxy-based estimation on the predominant frequencies and the topographical slope [e.g. Bastías and Montalva, 2016]. These inferred values are however lower than measured Vs30 values obtained recently at the stations HMBX, PSGX and PB11 by Leyton et al. [2017] (Figure 4.2) Additionally, stations PB16 and the station PB13 (separated by a distance no larger than 500 m) show significant differences of their inferred Vs30 values. Such discrepancies between inferred and measured values

confirm that a solid characterization of IPOC site conditions would lead to a significant improvement of the network.

Considering the discrepancy between inferred and measured values of Vs30, the homogeneity of geotechnical conditions of sites and the consistence between the theirs geotechnical description and the measured values, a conservative value of Vs30 of 850 m/s has been adopted for all stations of the network, similar to the value Haendel et al. [2014]. This assumption will be tested later in the paper by the computation of site-specific stations terms and their comparisons with inferred Vs30.

Using this information and the data of the earthquake catalog, we have calculated the predicted acceleration response spectra for each station-earthquake pair, for Peak Ground Acceleration (PGA) and three different oscillator periods (0.1 s, 0.8 s, 1.33 s). The respective values of the GMPEs were then compared to the observed horizontal accelerations response spectra for the given oscillator periods to compute the total normalized residuals as:

$$Z_T{}^{ij}(T) = \frac{\log\left[Sa_{obs}{}^{ij}(T)\right] - \log\left[Sa_{pred}{}^{ij}(T)\right]}{\sigma(T)} \qquad (4.2)$$

where $Z_T{}^{ij}(T)$ is the residual at site j for event i with oscillator period T, $Sa_{obs}{}^{ij}(T)$ and $Sa_{pred}{}^{ij}(T)$ correspond to the observed and predicted acceleration response spectra at site j for event i with oscillator period T respectively, and $\sigma(T)$ is the total standard deviation of the model for oscillator period T. These residuals have been calculated only for the records with a rupture plane distance lower than 300 km, to stay in the distance validity range of the GMPEs. Additionally, in order to avoid bias, the records of the stations PB11 and PB15 have been removed, where possible site effects have been reported (D. Bindi and F. Leyton personal communications).

The total residual described above can be separated into between-event and within-event residuals. The first term represents the random effects between events that are not covered by the predictive model and reflects the variation of source factors, such as the stress drop or the slip variability in space and time, that can not be captured by the magnitude and the depth of the source. The within-event residual, represents the variation of ground motion at a given distance to the source that comes from the azimuthal variation in the source, the path, and site effects derived from the complexity of the crustal structure, that are not captured by the distance to the source

or the site classification [Abrahamson and Youngs, 1992; Strasser et al., 2009; Al Atik et al., 2010]

The normalized between-event residual of an earthquake i, is given by:

$$Z_B{}^{i}(T) = \frac{\tau(T) * \sum_{j=1}^{n} \left[\log\left[Sa_{obs}{}^{ij}(T) \right] - \log\left[Sa_{pred}{}^{ij}(T) \right] \right]}{n * \tau(T)^2 + \phi(T)^2} \qquad (4.3)$$

where n is the number of records of the event i, $\tau(T)$ and $\phi(T)$ are the standard deviations of the between-event and the within-event residuals of the model for oscillator period T. In order to reduce the bias, we consider only those between-event residuals of the events that have more than 4 records with distances to the rupture lower than 300 km.

Consequently, the normalized within-event residuals, for the record j of earthquake i, is defined as:

$$Z_W{}^{ij}(T) = \frac{\log\left[Sa_{obs}{}^{ij}(T) \right] - \log\left[Sa_{pred}{}^{ij}(T) \right] - Z_B{}^{i}(T) * \tau(T)}{\phi(T)} \qquad (4.4)$$

To evaluate the fit of the models to the database, we have first plotted histograms of the distribution of the total, between-event and within-event residuals with respect to the model's median for the PGA and the three oscillator periods considered (0.1 s, 0.8 s, 1.33 s, Figure 4.3). The difference between the standard deviation of Abrahamson et al. [2016]) GMPE model and the standard deviation of the residual database, as well as the difference between the median of the model and the median of the residual, suggest that the model does not capture the whole variation of strong motions and underestimates their values for medium (0.8 s) and large (1.33 s) oscillator periods. On the other hand, the similar values between standard deviation in the Montalva et al., [2017] GMPE model and the standard deviation of the residual database, show that this model describes well the variation for the all oscillator periods tested. However the difference between the median of the model and the median of the residual indicates that the model overestimates the ground motion for low oscillator periods (PGA and 0.1 s).

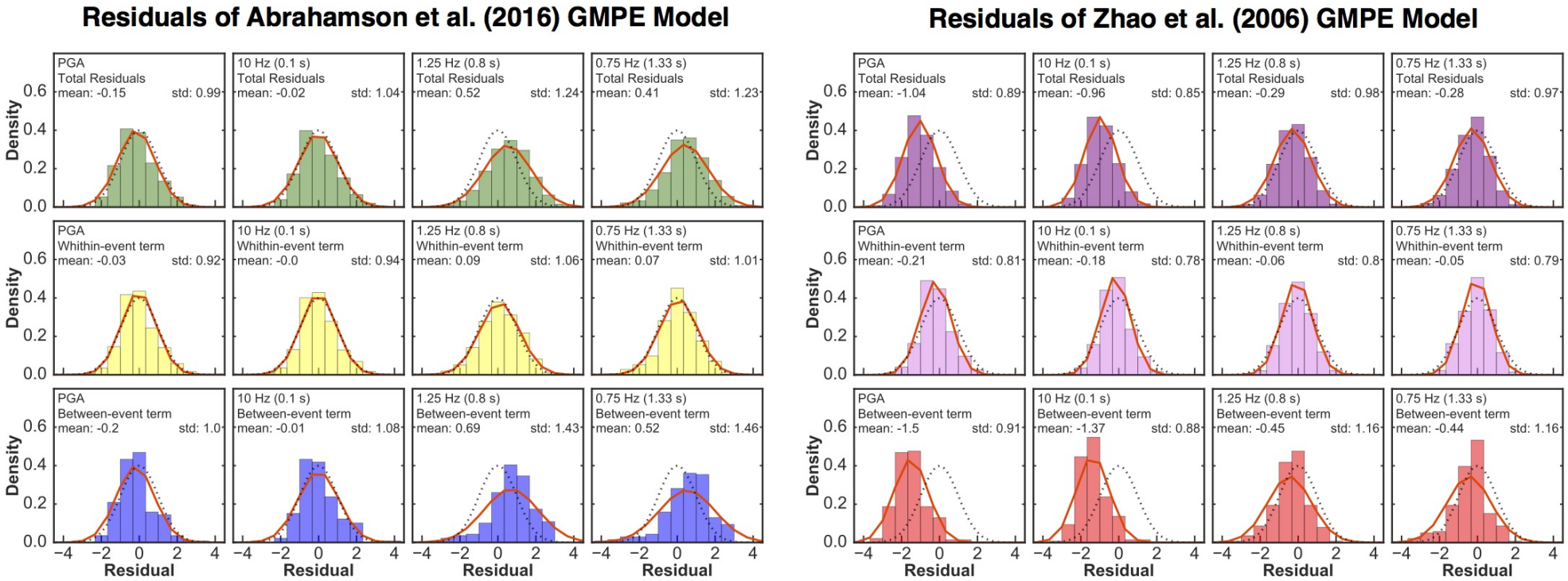

Figure 4.3: Residual histograms with respect to Abrahamson et al. [2016] (left) and Montalva et al. [2017] (right) GMPEs. The dot line represents the normal density function of the model and the solid line represents the normal density function of the dataset. Columns correspond to the residual distributions for different oscillator frequencies (PGA, 10Hz, 1.25Hz, 0.75Hz), and rows to the total, within-event and between-event residuals.

The fit of the within-event residuals suggests that both models reasonably describe the variability of path and site effects.

The distribution of the between-event residuals suggests that only the GMPE of *Montalva et al.* [2017] describes the variation of source effects for PGA and the three tested oscillator periods. At periods of 0.8 s and 1.33 s, the between-event residuals of the model of *Abrahamson et al.* [2016] are more scattered than expected from the model.

The between-event residuals distribution does not indicate any magnitude dependency (Figure 4.4). Therefore, these two GMPEs can be used as backbone models for the entire magnitude range from Mw > 4.

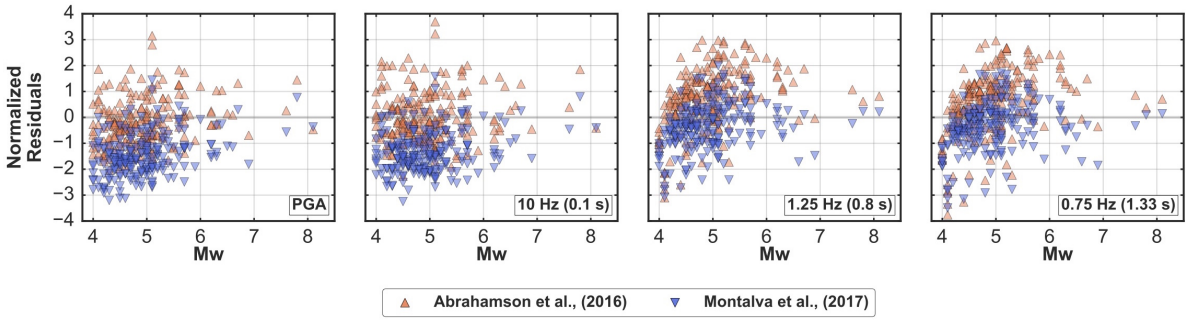

Figure 4.4: Distribution of computed between-event residuals at different frequencies (PGA, 10 Hz, 1.25 Hz, 0.75 Hz) with respect to *Montalva et al.* [2017] (inverted triangles) and *Abrahamson et al.* [2016] (triangles) GMPEs. The between-event residuals do not show any dependency with Mw.

To evaluate the impact of the assumption of a unique value of Vs30 for the whole network, the site terms (δ_{S2S}) have been computed at each station j for oscillator period T as the mean of the n within-event residuals recorded by the station:

$$\delta_{S2S}{}^{j}(T) = \frac{\sum_{i=1}^{n} Z_w{}^{ij}(T)}{n} \tag{4.5}$$

The resulting site terms have been compared with inferred Vs30 values given by Bastías and Montalva [2016]. This comparison shows two interesting results: (1) site amplification at IPOC stations do not depend on the latitude (Figure 4.5 - left), (2) and the correlation between inferred Vs30 and computed site terms is rather poor

(Figure 4.5 - right). This lack of correlation is consistent with several studies [Chiou and Youngs, 2008; Derras et al., 2016], which have shown that GMPEs using inferred Vs30 values are showing large within-event variabilities. These results give further encouragement to promote Vs30 measurements of IPOC accelerometric stations and also indicate that the north-south variations of between-event residuals are not explained by a systematic regional variation of IPOC site conditions.

As a conclusion, the distribution of residuals suggests that the model of Montalva et al. [2017] is the best suited for Northern Chile and that it can therefore be used as a backbone model to study the spatio-temporal variations of ground motions in this area.

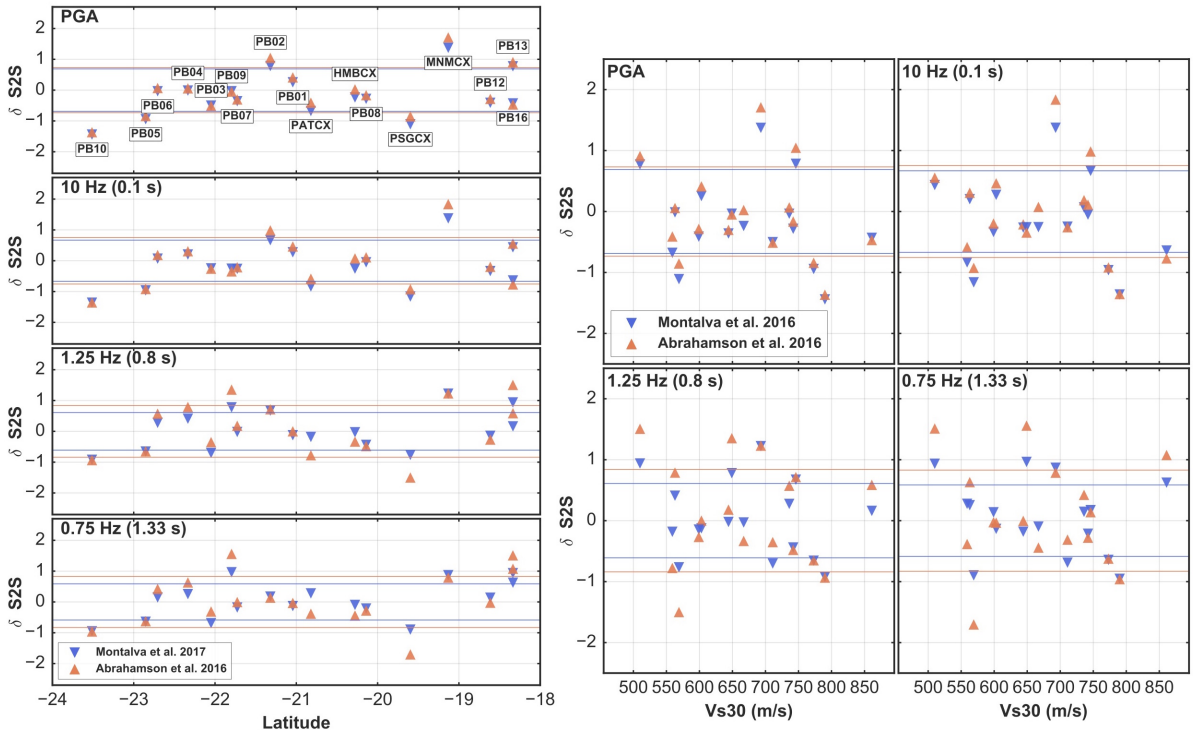

Figure 4.5: *Left* – Stations site terms (δ_{S2S}) at different frequencies according to the of *Montalva et al.* [2017] (inverted triangles) and *Abrahamson et al.* [2016] (triangles) GMPEs with respect to the latitude. *Right* – Stations site terms with respect to the Vs30 obtained by *Bastías and Montalva* [2016]. The horizontal lines represent one standard deviation. No dependency is observed.

4.6 Characterization of the length of energetic phases of ground motion records

Taking into account the large variability in terms of moment magnitudes of the interface earthquakes contained in the catalog, the characterization of the energetic phase of horizontal ground motion on sites with rupture distance of less of 300 km have been done using the “significant duration”. The significant duration is defined as the time length fraction between the 5 and 95% of the cumulative Arias integral [Arias 1970], which represent the length of the records that generate the 90% of the energy of the ground motion records.

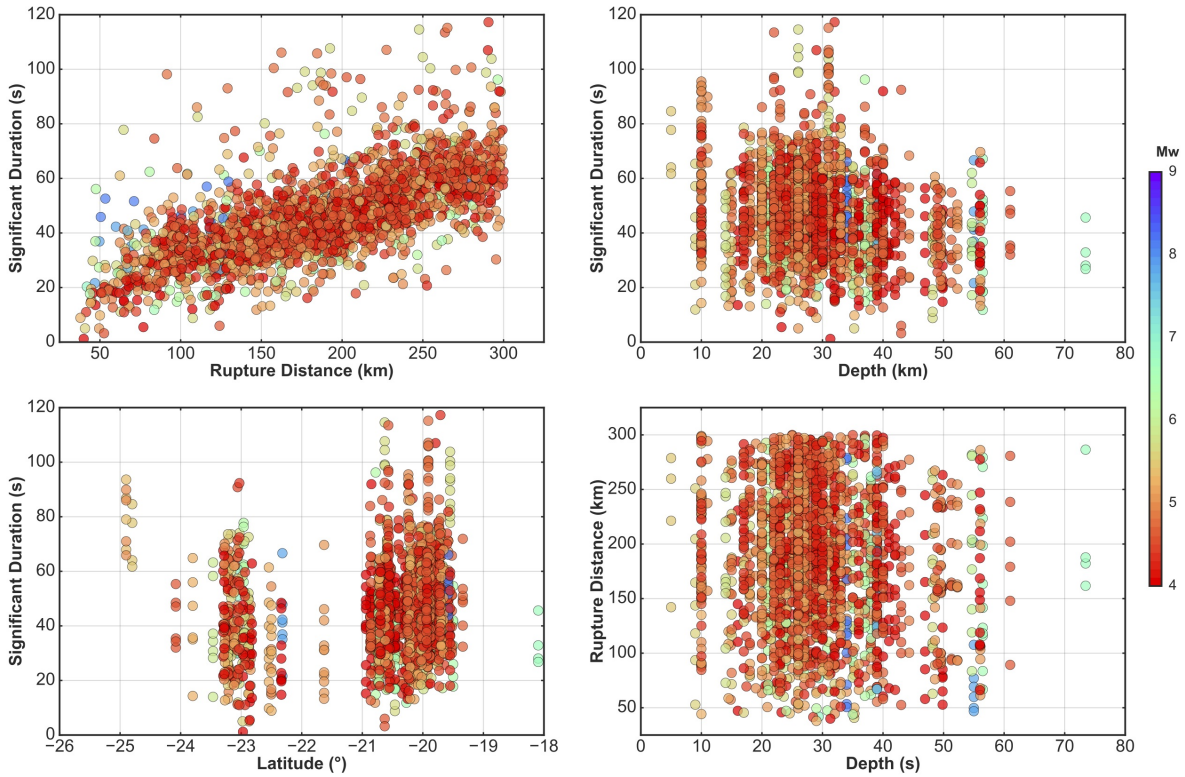

Figure 4.6: Distribution of significant duration of strong ground motion records with respect to the rupture distance (upper-left), epicenter depth (upper-right) and epicenter latitude (bottom-left) color coded by Mw. A strong dependency between significant duration on rupture distance can be observed.

To define the significant duration of the horizontal ground motion records of a given station for a given earthquake, the two horizontal components of the records have been analyzed separately (north-south and east-west components). Thus, the significant duration of the horizontal ground motion record have been defined as the largest significant duration of both component. This has allowed compute at each

station, the significant duration of the horizontal ground motion for each interface earthquake contained in the catalog. In order to analyze bias on frequency contents of offshore and depth earthquakes ground motion records derived from propagation path, correlations between the ground motion significant duration, rupture distance and epicentral depth have been analyzed (Figure 4.6) for each record, and also on the earthquake significant duration average, earthquake rupture distance average and epicentral depth for each earthquake (Figure 4.7).

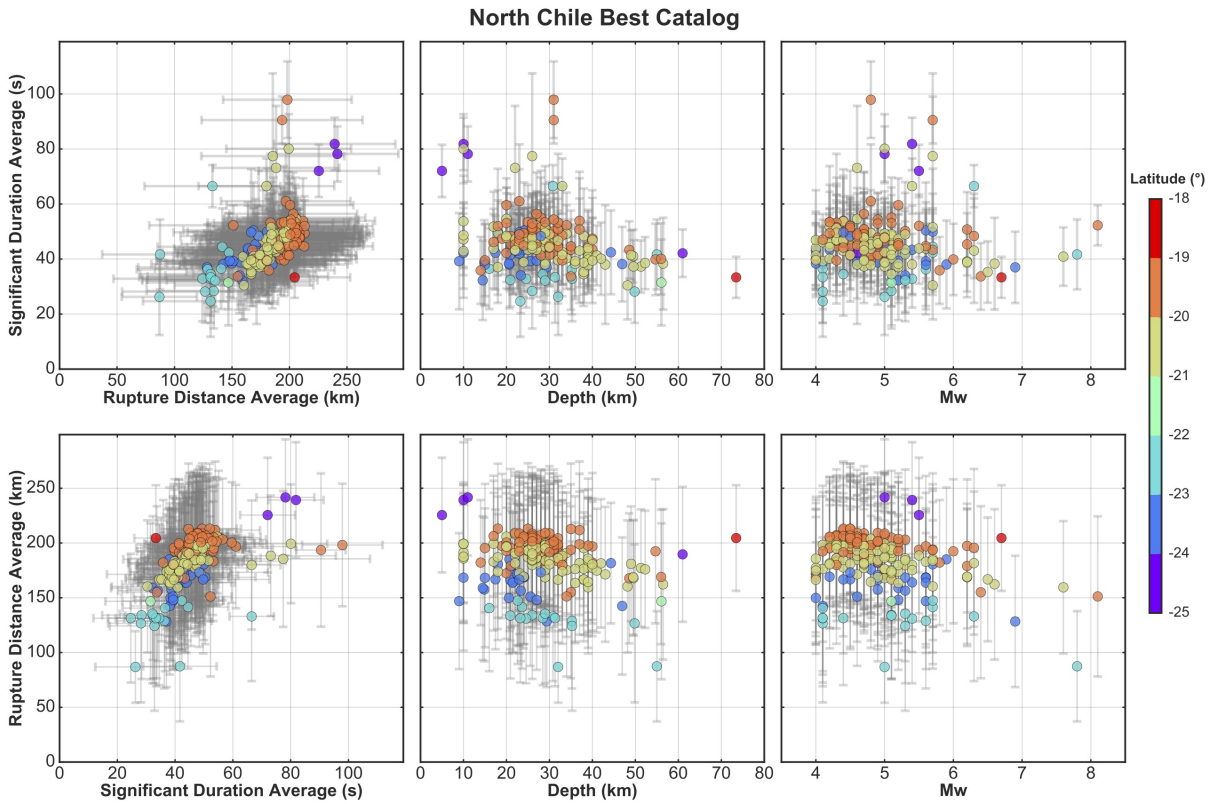

Figure 4.7: *Upper row* – Distribution of the earthquake significant duration average with respect to the earthquake rupture distance average (left), epicenter depth (center) and Mw (right), color coded by epicenter latitude. *Bottom row* – Distribution of the rupture distance average with respect to the significant duration average (left), epicenter depth (center) and Mw (right), color coded by epicenter latitude. Gray error bars represent the standard deviation of rupture distance and significant duration. Only correlation between significant duration average and rupture distance average is observed.

Since no depth dependency is observed on ground motion significant duration, rupture distance and theirs respective averages by earthquake, the bias effects derived from differences of wave propagation paths between offshore and depth earthquakes on the between-event residual can be considered as negligible.

Using the information of significant duration of ground motion records and the rupture distances, the distribution of the total and within-event GMPE residuals of Montalva et al. (2017) model have been checked for PGA and oscillator of fundamental frequencies of 10, 0.1 and 0.75 Hz, as well the distribution of the between-event residuals with respect to the average of the significant durations and rupture distances by earthquakes (Figure 3).

The residuals distribution shows for oscillators of low fundamental frequency (0.1 and 0.75 Hz), that ground motion significant duration and rupture distance do not correlate with the total and within-event residuals, neither between event residuals with their average by earthquakes (Figure 4.8, left side – colors green and yellow respectively). Different is the situation for oscillator of high frequencies (10 Hz) and PGA (Figure 4.8, right side – colors blue and red respectively) where highest total residuals values are related with records of short significant duration. This correlation is more evident in the distribution of the between event residuals with the significant duration average by earthquake, and as expected, is observable also on the distribution of the between-event residuals with respect to rupture distance average, but less clear and more disperse. This suggest that shorter ground motion significant duration are systematically are more rich in high frequency contents than larger ones, but in other hand, the lower level of correlation of the between-event residuals and the rupture distance average, shows that the GMPE model of Montalva et al. [2017] capture well the attenuation and the geometrical spreading of the region and most of the variability of the ground motion significant duration comes from variability of the source rupture.

It result interesting to see that the no clear dependency of within-event residuals is observable with significant duration neither with rupture distance for PGA and all oscillator frequencies (Figure 4.8), this mean that the observations are normally distributed around the predicted acceleration corrected by median of the observations (prediction of the model plus the between-event residual) and they are not spatially dependent. This can be seen also in Figure 4, which show the comparison between the observed ground motion and the ground motion predicted by the GMPE model of Montalva et al. (2017) of four couples of shallow and deep earthquakes for PGA and oscillator of fundamental frequencies of 10, 0.1 and 0.75 Hz.

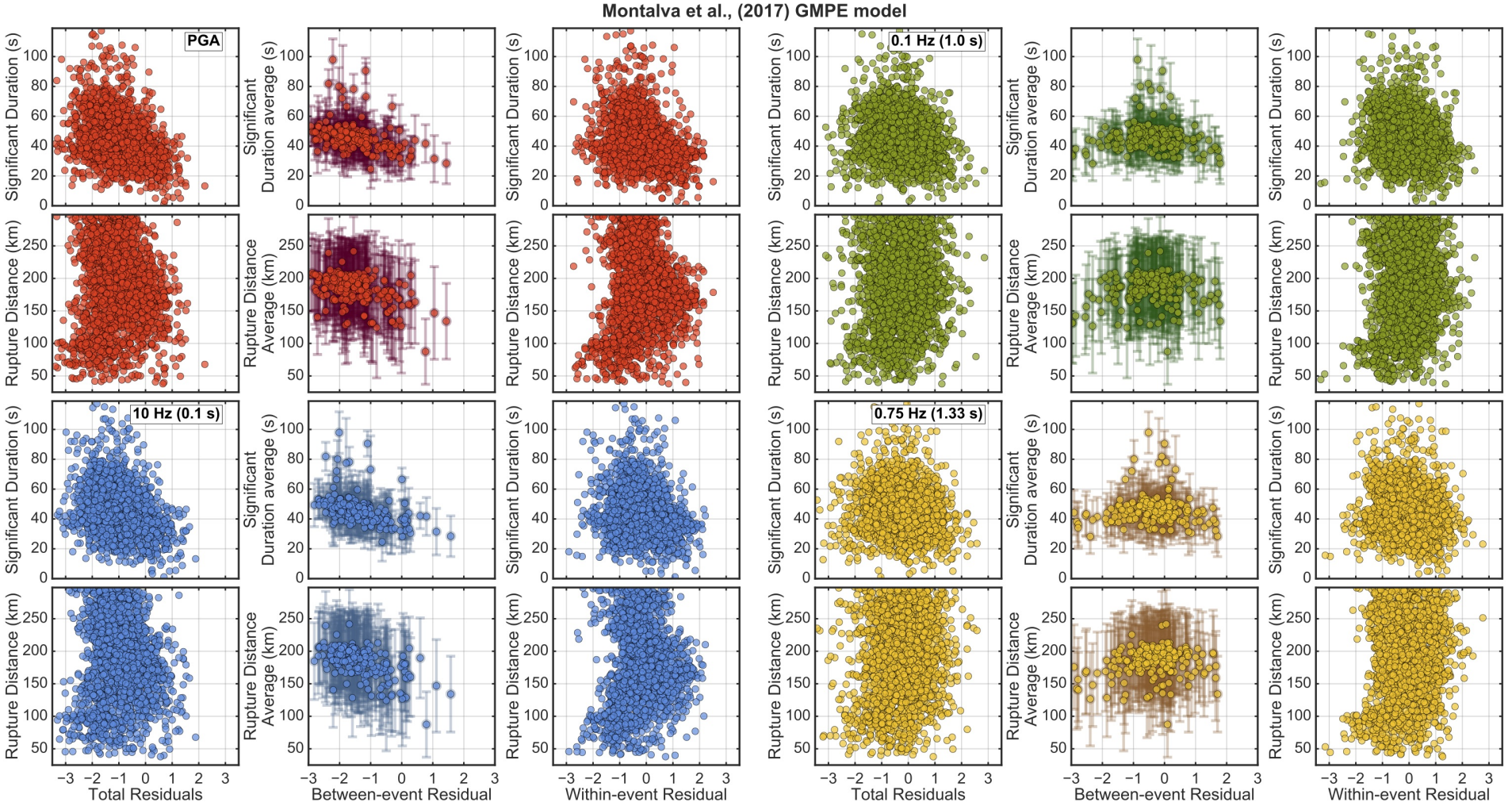

Figure 4.8: Significant duration and rupture distance distribution with respect to total, between-event and within-event residuals of GMPE model of Montalva et al., (2017) for PGA (red) and oscillator of fundamental frequencies of 10 (blue), 0.1 (green) and 0.75 Hz (yellow).

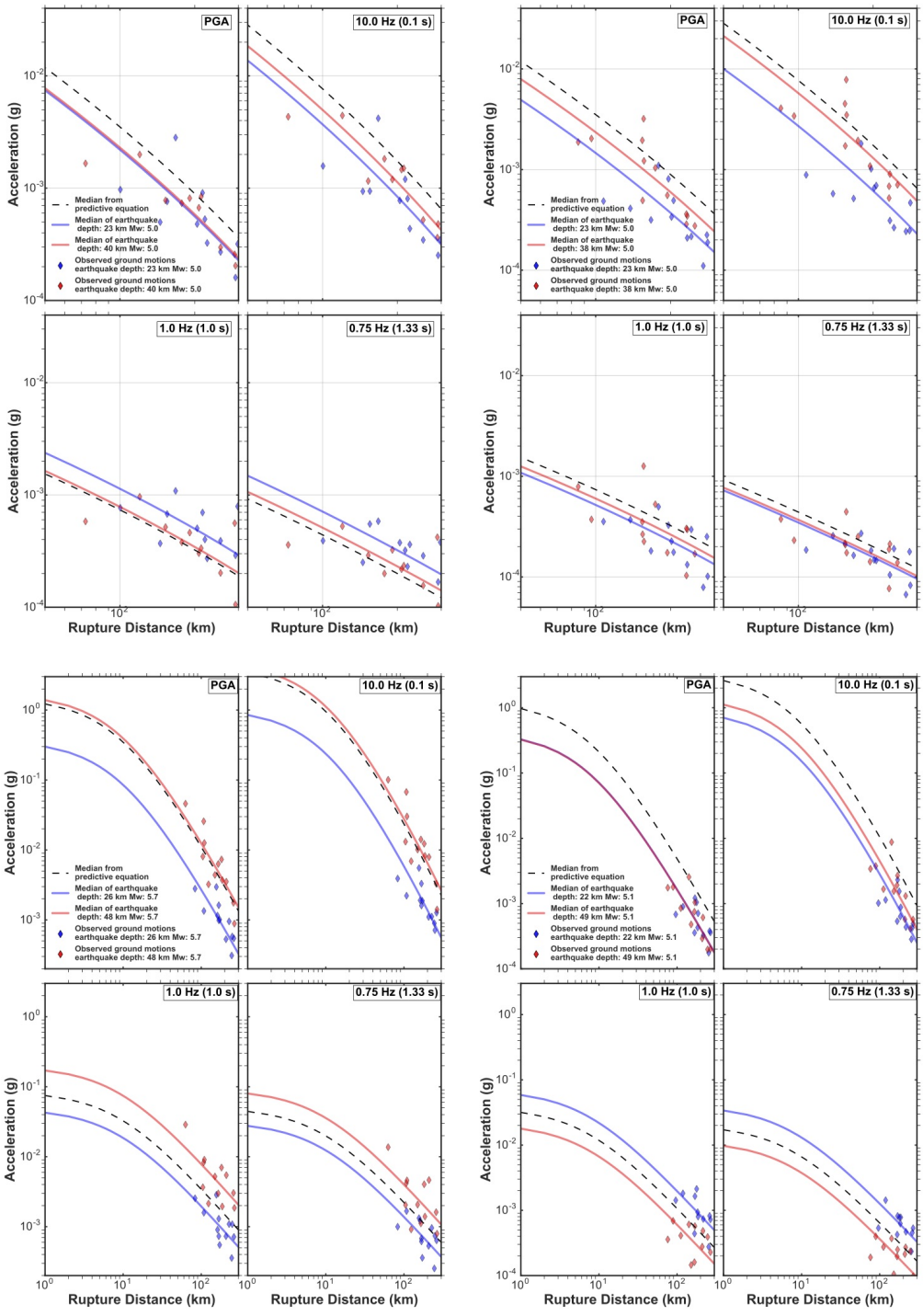

Figure 4.9: Comparison of the observed ground motion acceleration data with the median prediction of the GMPE model of four couples of shallow (blue) and deep (red) earthquakes for PGA and oscillators of fundamental frequencies of 10, 0.1 and 0.75 Hz. The dots (blue and red) show the observed ground motion, the segmented line represent the median prediction of the GMPE model of Montalva et al. (2017), the blue and red lines represents the median of the observations. Note that no spatial dependency affects the observed ground motion.

4.7 Depth and regional dependency of ground-motions

The evolution of the between-event residual with respect to the depth shows a consistent and significant increase with depth of earthquakes radiations at high frequency. This is clearly visible for both regional clusters at low oscillator periods (PGA and 0.1s), while no tendency is observable at medium (0.8s) or high (1.33s) oscillator periods (Figure 4.10). The distribution of between-event residuals along latitude and depth (Figure 4.10 bottom row) shows that for PGA and an oscillator period of 0.1 s, the between-event residuals are clearly differentiated at 40 km depth, where the residual dispersion decreases dramatically and concentrates on higher values. The figure also shows a regional dependency for the medium and high oscillator periods with a lower residual variability and slightly higher residuals values in the northern cluster for earthquakes shallower than 30 km.

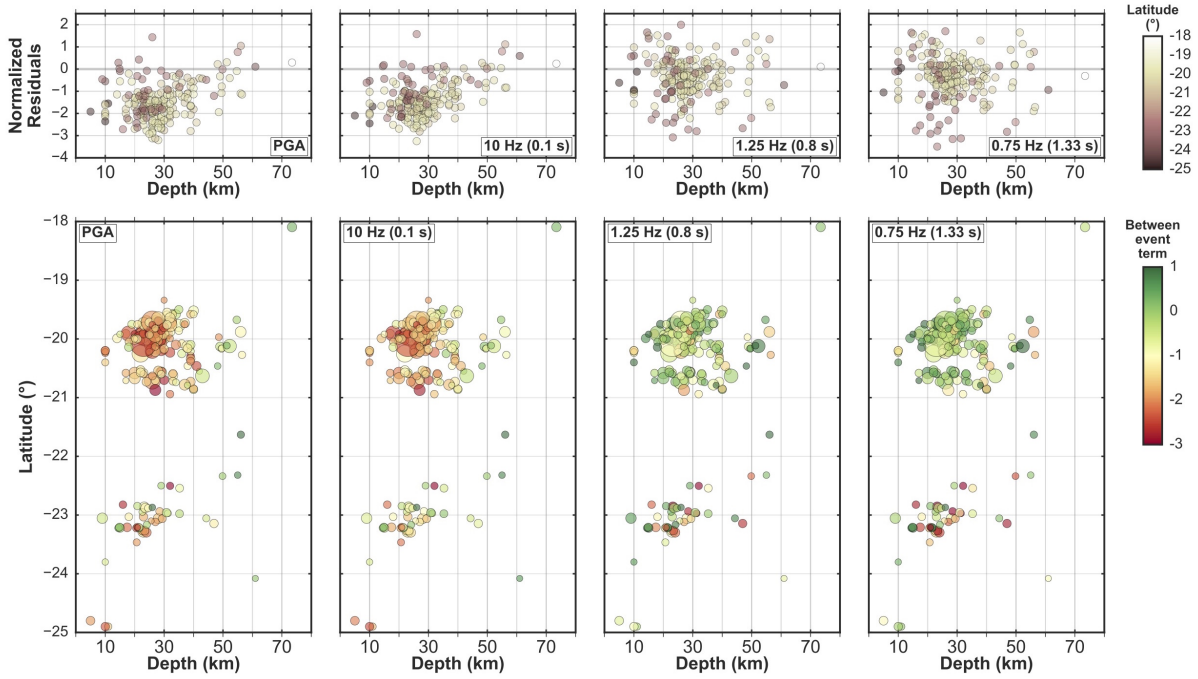

Figure 4.10: Top row – Between-event residuals at different oscillator frequencies (PGA, 10 Hz, 1.25 Hz, 0.75 Hz) with respect to *Montalva et al.* [2017] GMPE as a function of the epicentral depth, the fill show the latitude. An increase of between-event residuals with depth is observable for the PGA and low oscillator periods (0.1 s). Bottom row – Between-event residuals as a function epicenters latitude and depths.

In order to validate the depth dependency of the observed ground motions through between-event residual term distributions, the frequency content of earthquakes have been compared using a Fourier spectral ratio method. This approach has been used recently to compare the frequency content of two subduction earthquakes located at different depths [Lay et al., 2012] Following a similar methodology, we have computed the spectral ratios between pairs of earthquakes, using the horizontal Fourier spectra of the acceleration records of the stations that have recorded both events.

To apply the method, we have used the processed horizontal waveforms to get the Fourier spectra. The Konno and Ohmachi [1998] smoothing function has been applied over each Fourier spectra and for each station record, both horizontal smoothed Fourier Spectra were then averaged to obtain the horizontal Fourier Spectra at each station defined for each frequency f as:

$$F_{hor}(f)=\sqrt{F_{NS}(f)^2+F_{EW}(f)^2} \tag{4.6}$$

where F_{NS} and F_{EW} correspond to the smoothed Fourier Spectra of the North-South and East-West acceleration components respectively, and F_{hor} to the Horizontal Fourier Spectra.

Then, all spectral ratios obtained at each station for a single pair of earthquakes, were averaged with the geometric mean for each frequency, thus, the spectral ratio for each frequency f is defined as:

$$SR_{AB}(f)=\sqrt[n]{\prod_{j=1}^{n}\frac{F_B{}^j(f)}{F_A{}^j(f)}} \tag{4.7}$$

where $F_A{}^j$ and $F_B{}^j$ are the horizontal Fourier Spectra of events A and B, at the station j , and n is the number of stations that have recorded both events.

Pairs of shallow and deep earthquakes with similar magnitudes (ΔMw ≤ 0.1) and relative distance less than 100 km have been selected to compare their frequency contents. The selected pairs of earthquakes consist of one earthquake shallower than 25 km and one earthquake deeper than 40 km. We have limited our analysis to earthquakes for which the theoretical hypocenter is located within a distance of 15 km from the subduction interface, as defined by Tassara and Echaurren [2012]. We found 4 earthquakes pairs that meet these criteria. The spectral ratios were

calculated as the division of the spectra of the deeper event divided by the spectra of the shallower event (Figure 4.11). For all pairs, the spectra amplitude of the deep events is larger than the shallower event for frequencies larger than 1 Hz. This result is in agreement with the depth dependency observed in the GMPEs residuals.

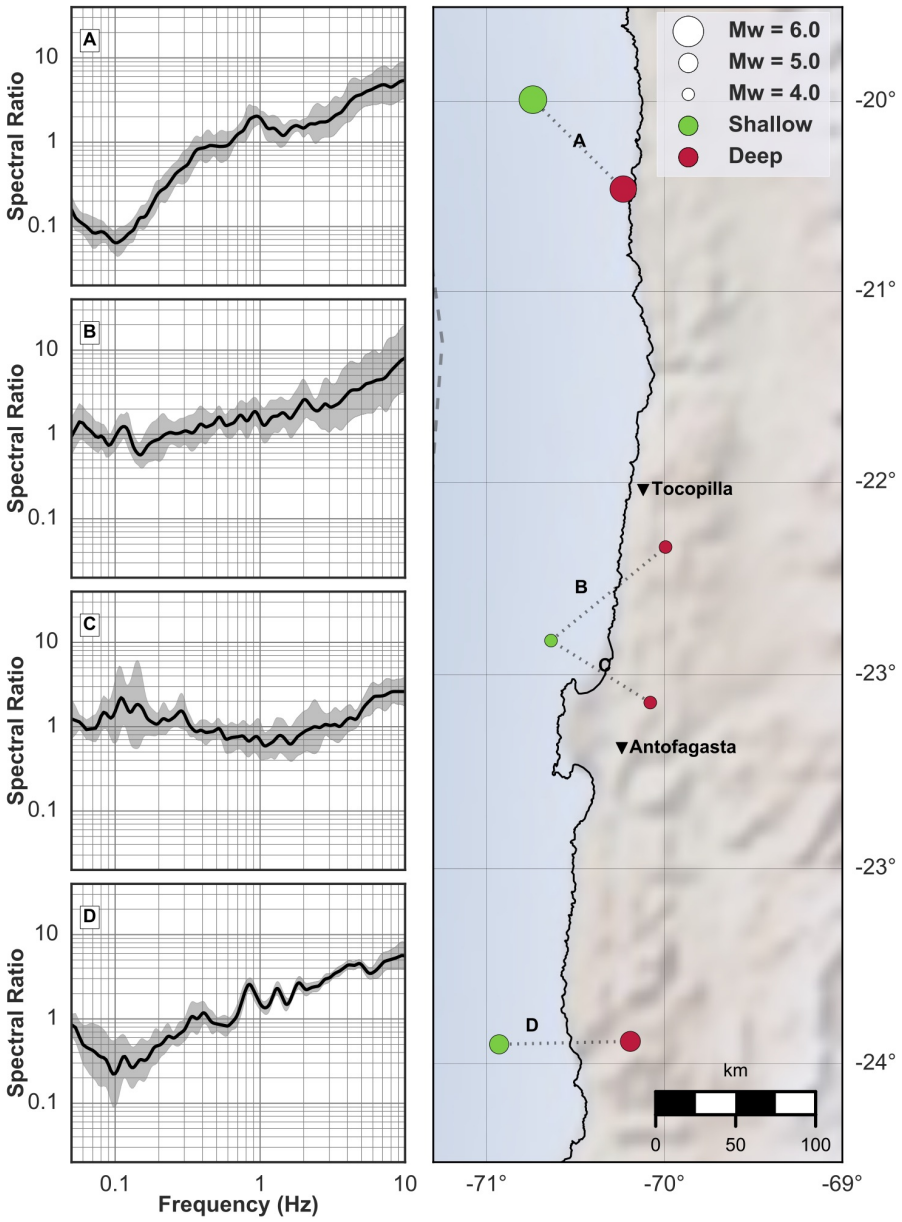

Figure 4.11: *Left* – Spectral ratios computed for pairs of shallow and deep earthquakes. The gray bands show the standard deviation with respect to the geometric mean in the whole frequency band. *Right* – Localization of shallow-deep couples. Deep earthquakes generate higher ground-motions amplitudes at frequencies larger than 1 Hz.

The results of both methods presented here, are consistent with each other and suggest that interface events below 40 km depth release more energy at high frequencies than shallow interface events for the whole region. In addition, shallow seismicity in the northern part of the seismic gap releases more energy at low frequencies than the seismicity in the southern part of the gap.

4.8 Time dependency of ground-motions

To evaluate the time variability of the between-event residuals, we have focused our analysis on the Northern seismicity cluster that is associated with the seismicity of 2014 Mw 8.1 Iquique earthquake [Ruiz et al., 2014; Schurr et al., 2014; Cesca et al., 2016; Kato et al., 2016] . We have grouped the seismicity into three periods of the seismic cycle bracketing the Iquique earthquake [Schurr et al., 2014; Socquet et al., 2017]:

- Interseismic: before August 2013
- Preseismic: August 2013 - March 31st 2014
- Postseismic: after March 31st 2014

Between-event residual terms are compared on Figure 4.12 for the three time period windows at PGA and the three oscillator frequencies selected (10Hz, 1.25Hz and 0.75Hz). For PGA and 10Hz, the between-event residual term decreases from the interseismic to the postseimic period. At frequencies of 1.25 and 0.75Hz, the between-event does not show any important variation from interseismic to preseismic period, and a slight decrease is observed for the postseismic period.

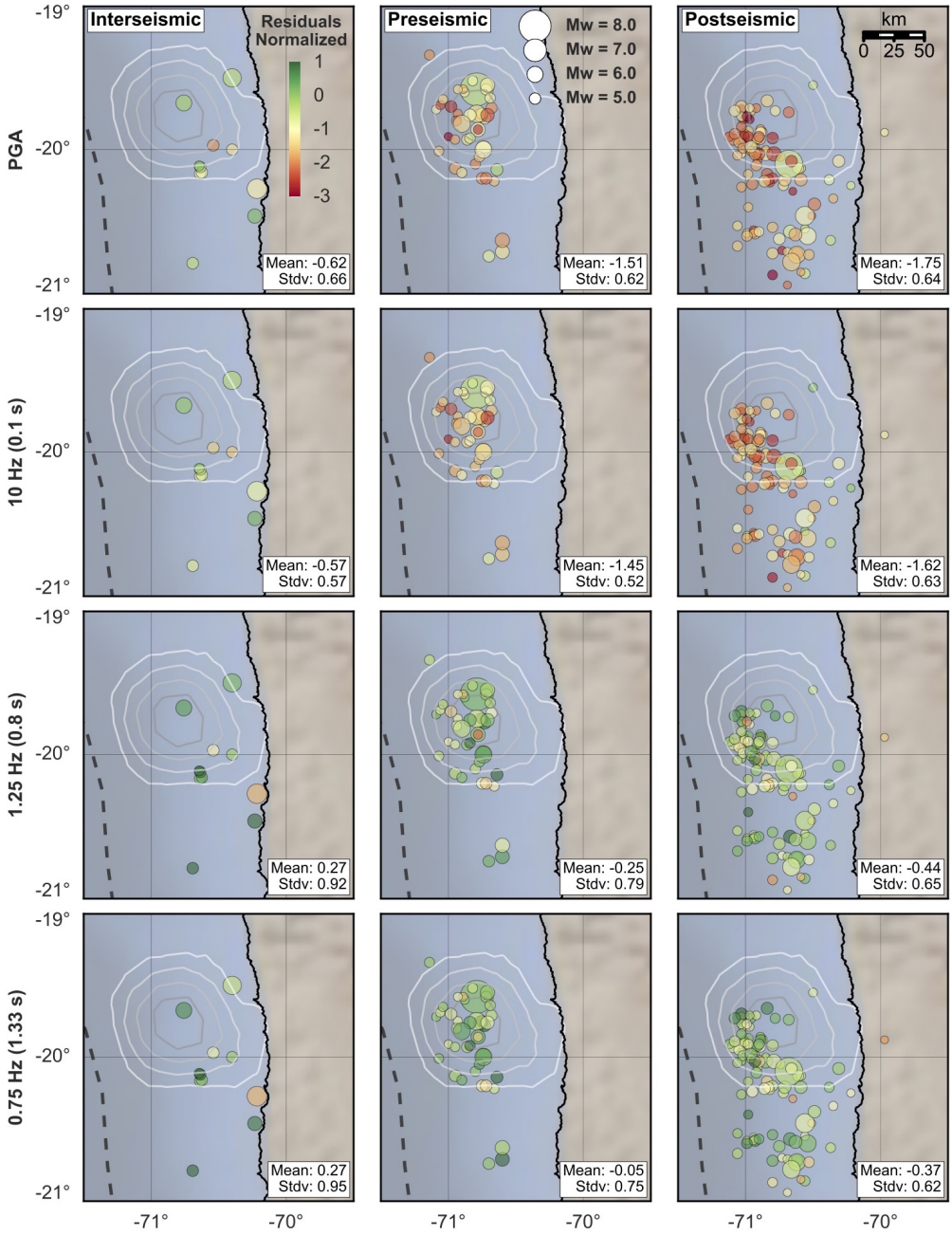

Figure 4.12: Time and space variability of residuals, at different frequencies (PGA, 10 Hz, 1.25 Hz, 0.75 Hz), with respect to *Montalva et al.* [2017] GMPE for earthquakes between -19° and -21°. Columns correspond to a given period of the seismic cycle period (interseismic before August 2013, preseismic between August 2013 and 31st March 2014, post-seismic after 1st of April 2014). The mean and the standard deviation of the between-event residuals showed on each box, are indicate in the right bottom corner. Contours lines correspond to the slip distribution of Mw 8.1 Iquique earthquake (April 1st 2014). PGA and low oscillator period (high frequency, 10Hz) residuals decrease from interseismic to preseismic time-windows.

To complement the analysis of the between-event residual variation, the spectral ratio method was again applied (Equation 4.7). Selected pairs of earthquakes of similar magnitude (ΔMw ≤ 0.1), with differences in depths smaller than 20 km and relative distance smaller than 25 km were selected. 425 pairs of earthquakes meet these criteria. The spectral ratios were computed as the division of the most recent event spectrum by the spectrum of the older one. Then, geometrical means of the spectral ratios are divided into three groups:

- Pairs of earthquakes within the interseismic period
- Pairs of earthquakes belonging to preseismic and interseismic periods
- Pairs of earthquakes belonging to postseismic and interseismic periods

The geometrical means of the spectral ratios over time (Figure 4.13) show that at frequencies lower than 1 Hz, the earthquakes of the interseismic period show lower amplitudes than the earthquakes of the preseismic period. Instead, at frequencies higher than 1 Hz, the earthquakes occurring during the intersesimic period show higher amplitudes than the earthquakes occurring during the preseismic period. A similar pattern is also observable when comparing the earthquakes of the interseismic and postseismic periods, although with a lower intensity. The findings are consistent with the variations observed by the GMPEs residual analysis method (Figure 4.12).

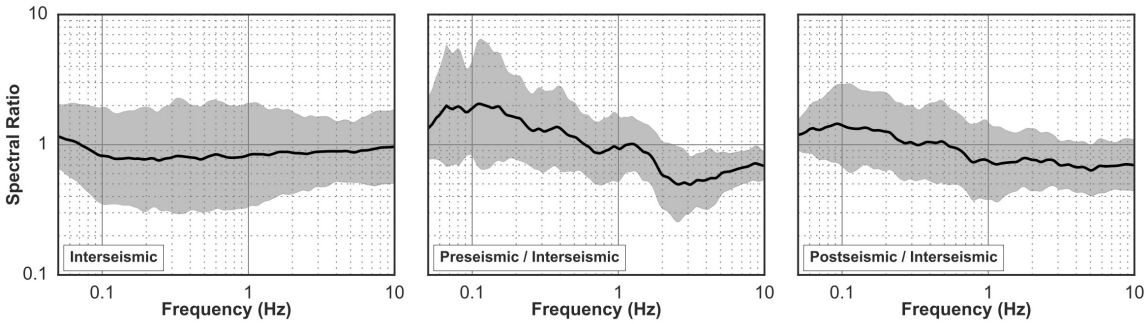

Figure 4.13: Spectral ratios of similar events (ΔMw ≤ 0.1, inter-distance ≤ 25 km) between -19° and -21° of latitude, for the interseismic, preseismic and postseismic periods associated with April 1st, 2014 Iquique earthquake. The gray bands show the standard deviation with respect to the geometric mean in whole frequency band.

4.9 Discussion

The record of the Tocopilla 2007 and Iquique 2014 seismic sequences by the IPOC network provided a unique dataset in terms quality and quantity (more than 1000 records) to (1) test the performance of the most recent subduction GMPEs and to (2) observe the spatiotemporal variations of the ground motions in a region recognized as a mature seismic gap.

The comparison between the GMPE prediction and the observations suggests that the two tested models are able to describe the ground-motion's within-events residuals, which are mainly controlled by site and propagation effects. The main discrepancies between the tested models and the observations are related to the between-event component of the ground-motion variability, which is mainly controlled by source effects.

A possible explanation of this misfit could be due to the limitations of the dataset used to calibrate the ground-motions models. Indeed , the Abrahamson et al. [2016] model is based on a global event catalog with a moment magnitude larger than 6, while the database used in this study includes earthquakes of smaller magnitude ($4 < Mw < 6$).

The Montalva et al. [2017] model has been developed from a seismic catalog with moment magnitudes larger than 5.0 along the entire Chilean trench. This model describes well the ground motion variability of our dataset. The quality of the fit could then be explained by the inclusion of moderate earthquakes ($5 < Mw < 6$) to calibrate the model .

Our data analysis confirms that the energy radiation pattern of interface earthquakes varies with depth, in agreement with the proposal that the subduction interface is segmented down-dip with different frictional properties characterizing each segment [Lay et al., 2012; Lay, 2015]. Such along-dip segmentation is not included so far in the GMPEs models. Indeed, engineering ground-motion models predict ground-motions for large earthquakes, which break the entire seismogenic zone from small to large (60 km) depths. However, due to the nature high frequencies radiation, which is affected by factors such as asperity sizes, source time function, rise time and rupture propagation velocity between others, it results difficult to associate the

variations of the frequency at specific frequency with the heterogeneities size and to do this further investigation are necessaries.

Our findings suggest that below 40 km-depth, a significant change in the signature of the earthquake spectra exists. This change is coincident with the depth of the contact between the continental Moho and the subduction interface in this area [Patzwahl et al., 1999; Béjar-Pizarro et al., 2010]. These two observations are also consistent with the segmentation along depth of the subduction interface and would correspond to the limit between the domains B and C proposed by [Lay et al., 2012].

The Chilean subduction varies from North to South in terms of mechanical behavior and geometry of the interface [Clift and Vannucchi, 2004; Hoffmann-Rothe et al., 2006; Contreras-Reyes et al., 2010]. There is an also influence on the coupling degree that is shown to vary along the trench [Béjar-Pizarro et al., 2010; Métois et al., 2012] and is coherent with the regional segmentation observed for the between event residuals at medium and long oscillator periods for seismicity shallower than 40 km depth (Figure 4.10 bottom row).

Several past crustal earthquakes studies [e.g. Abrahamson et al., 2008] have suggested that aftershocks generate weaker ground motions than the associated mainshock. Our results have shown that the ground motions have started to change several months before the occurrence of 2014 Iquique Earthquake, with a progressive decrease of the released energy at high frequencies. This observation may indicate a change on the subduction interface that may be related to a long-term nucleation process of the megathrust earthquake [Socquet et al., 2017]. The ground motion temporal variation is consistent in time with aseismic slip around the rupture area of the 2014 Iquique earthquake and a slow migration of the foreshock activity [Kato and Nakagawa, 2014; Schurr et al., 2014; Kato et al., 2016; Socquet et al., 2017] similarly to what has been observed before the 2011 Tohoku Oki Mw 9.1 Earthquake [Mavrommatis et al., 2015; Yokota and Koketsu, 2015]. This observation sheds light on the potential processes occurring on the subduction interface through the seismic cycle.

Stress-drop inversions have been used for years by the seismological community to analyze the physics of earthquakes. The stress drop, being proportional to the cube of the corner frequency, it is sensitive to the uncertainty in the corner frequency [e.g. Cotton et al., 2013]. Our study suggests that the analysis of GMPEs between-event residuals could also be used not only for engineering purposes but also to analyze the source characteristics of earthquakes. Indeed, these residuals take into account

both the magnitude effect and the propagation effect (trough the functional form of the GMPE) and it has been shown that response between-event residuals are highly correlated with “classical” Fourier spectrum based stress-drop [e.g. Bindi et al., 2007]. Between-event residuals analysis may therefore constitute a new possibility to compare source-effects of earthquakes with various magnitude and locations.

Finally, the consistency of the results with others studies, opens the possibility to use parameters such as the between-event residuals, stress drop, earthquake spectra and strong motion, as a proxy for the variability of the frictional properties of the subduction interface.

4.10 Conclusion

The testing of GMPEs models is a necessary contribution to seismic hazard assessment in areas that have been recently instrumented. For the specific case of northern Chile, the results presented in this study have shown that the combination of the models of Abrahamson et al. [2016] and Montalva et al. [2017] show different strengths and weaknesses. These two models successfully predict the median values and capture the variability of the ground motions generated by the interface seismicity in different frequency bands, even for a dataset extended out of the validity range of Mw in both models. The results have shown that for a dataset including earthquakes of Mw as low as 4.0, the model of Abrahamson et al. [2016] fits observations better for low oscillator periods (0.8 and 1.33 s), while the model of Montalva et al. [2017] is more suitable for medium and high oscillator periods (PGA and 0.1 s). Considering all frequencies and the magnitude range which is important from a seismic hazard point of view (M>5), the Montalva et al. [2017] model is the best suited for North Chile.

The southern part of the north Chile seismic gap shows weaker ground-motions at low frequencies than the northern part of the gap. This suggests a lateral segmentation of the subduction interface, such along-strike segmentation has also been shown by studies of interseismic coupling [Béjar-Pizarro et al., 2013; Métois et al., 2013; Li et al., 2015] This suggests a potential link between the state of coupling during the interseismic phase, the energy radiation characteristics of interface earthquakes and the friction on the subduction interface that requires further investigations. In addition, using two different methods (GMPEs residuals and the spectral ratios), we showed that the observed ground-motions increase with

hypocentral depth for interface subduction earthquakes. This suggests that the event depth must be considered in the development of future GMPE in order to include in the models interface subduction earthquakes of moderate magnitudes, which are not rupturing the entire seismogenic interface. This could extend the use of the GMPE as backbone ground-motion to study the properties of the subduction interface. Also, this depth dependency confirms previous observations of along-dip segmentation of the subduction megathrust seen in the values of interseismic coupling [Béjar-Pizarro et al., 2010; Lay et al., 2012], and in the geometry since an abrupt change in the subduction angle has been documented in the area [Contreras-Reyes et al., 2012].

Ground-motions have also been shown to vary through time by both methods presented in this work (GMPEs and spectral ratios). The time dependency can be related to the earthquake cycle, and has been observed by studying in great details the seismic events associated with the 2014 Iquique megathrust earthquake. Although one could have expected a significant change in the earthquake frequency content before and after the mainshock, this is not what we observe. Instead, the data shows that the change occurs several months before the mainshock, and is characterized by a progressive decrease of interface earthquake energy release at high frequencies. This change has been shown to concur with an 8-month slow slip event on the subduction interface, and has been interpreted as the long-term nucleation process of 2014 megathrust earthquake [Socquet et al., 2017].

Finally, the dependencies detected on the between-event term, open the possibility to incorporate new factors to improve ground-motion models in the future. An important factor to improve the predictability of the GMPE models is to better take into account depth and regional variations.

4.11 Data and resources

All strong motion data used in this work have been recorded by the CX-network of the Integrated Plate boundary Observatory Chile (http://www.ipoc-network.org). These data are available to registered users at the GEOFON repository (http://geofon.gfz-potsdam.de/waveform/archive/network.php?ncode=CX).

The Harvard CMT and the moment tensor solutions are freely available (http://www.globalcmt.org/CMTsearch.html) as well the GEOFON bulletin information (http://geofon.gfz-potsdam.de/eqinfo/eqinfo.php)

All of the above websites were last accessed on June 2016

Chapter 5: Analysis of Ground motions on the Japanese subduction

5.1 Persistent versus transient segmentation of the Japanese megathrust inferred from Ground Motion Observations

Paper in preparation for Journal of Geophysical Research

Authors: Jesús Piña-Valdés, Anne Socquet, Fabrice Cotton

5.1.1 Abstract

Two GMPE models for subduction zones have been tested using a public ground motion database with records of the KiK-net obtained by automated processing protocols [*Dawood et al.*, 2016]. The database contains records of more than 700 interface earthquakes of the Japan subduction that occurred between 1998 and 2012. The *Zhao et al.* [2006] GMPE has shown to be the best-suited model for the region. It was then used as backbone to analyze the variability of ground motion records. The residuals between observed and predicted ground motions have been used to study the spatial variation of the earthquakes' ground motion frequency content on the Japan megathrust. This analysis revealed a depth dependency of generated ground motions consistent with the down-dip segmentation proposed for subduction interfaces. Likewise, a regional ground motion dependency has been identified, which may be related with lateral variations of the mechanical properties of the subduction interface. This regional ground motion dependency suggests a lateral segmentation of the seismogenic zone of the Japan subduction, consistent with the rupture area of the 2011 Tohoku-Oki earthquake (Mw 9.0), and with geological and geodetic observations made previously in the region.

5.1.2 Introduction

The impact on the frictional sliding behavior of the subduction interface of factors such as temperature, pressure, pore fluids, properties and type of sediments, roughness and fault geometry has been largely discussed [e.g. *Marone and Scholz*, 1988; *Hyndman and Wang*, 1993; *Scholz*, 1998; *Lay and Bilek*, 2007; *Wang and He*, 2008]. Those parameters can vary significantly along and across subduction zones generating lateral and depth variations of the interface frictional properties [*Byrne et al.*, 1988; *Hyndman et al.*, 1997; *Heuret et al.*, 2011]. Indeed, the assent between geological, geodetic and seismological observations suggests that large megathrust ruptures and their associated slip distributions are related with persistent asperities that laterally segment the subduction interface [e.g. *Yamanaka and Kikuchi*, 2004; *Kodaira et al.*, 2006; *Béjar-Pizarro et al.*, 2010; *Loveless and Meade*, 2011; *Moreno et al.*, 2012; *Jara-Munoz et al.*, 2015]. Recently, strong ground motions and teleseismic broadband observations of megathrust ruptures have revealed a depth-frequency dependence of large interface ruptures [*Irikura and Kurahashi*, 2011; *Lay et al.*, 2012], which suggests that the depth segmentation of subduction interface frictional behavior that may impact the earthquake ground motions.

In recent years, the requirement of strong ground motion records of large earthquakes for seismic hazard analysis has promoted the development of ground motion sensors as well as the exponential growth of the networks. This has generated a huge quantity of high-quality strong motion records of low and moderate moment magnitude (Mw) earthquakes. The recent implementation of automated protocols for processing ground accelerations records of Kiban-Kyoshin network (KiK-net) of Japan [*Dawood et al.*, 2016] has allowed access a huge quantity of homogeneously processed ground motions records, offering the opportunity to explore a non exploited database, which can be used to characterize medium and small-scale features of the subduction interface, supplying the lack of information let by other datasets.

The ground motion records are generated by the convolution of the seismic source and the waves propagation, and are affected by magnitude scaling, rupture directivity, geometrical spreading, attenuation, site amplification, topographical effects [e.g. Aki, 1967; Aki, 1993; Boore, 1972; Archuleta and Hartzell, 1981; Sanchez-Sesma, 1987; Bouchon et al., 1996; Somerville, 2003], that render a comparison between events difficult. Modern empirical models of ground motions as the Ground

Motion Prediction Equations (GMPE) predict earthquakes response spectra at a given distance to the source. Those models consider most of the above listed effects [*Edwards and Fäh*, 2014]. Therefore the residuals between the observed ground motions and the predicted ones can help disaggregate the source and site misfits of the models [*Abrahamson and Youngs*, 1992; *Strasser et al.*, 2009; *Al Atik et al.*, 2010]. This allows us to use the GMPE's as backbones to study the variations and uncertainties of ground motions generated by different earthquake sources, which may reflect spatial variations of the frictional properties of the subduction interface.

Japan is located in a complex tectonic context dominated by two subduction zones: the Pacific Plate (PAC) and the Philippine Sea Plate (PHS) that plunge at 80mm/yr and 60mm/yr respectively below mainland Japan [*DeMets et al.*, 1990; *DeMets*, 1992], generating an intense seismic activity and associated seismic hazard (Figure 5.1).

Most of the seismic activity of the region is related to the subduction process and the slip of the subductions interfaces, while only a minor part is related to active volcanoes and magmatic processes. The largest earthquake of the region in the last century was the 2011 Tohoku-Oki Mw 9.0 megathrust earthquake offshore Honshu, while smaller, but still large, earthquakes occurred on the Nankai subduction interface and in the Kuril trench (e.g. 1944 Tonankai Earthquake Mw 8.1, 1946 Nankai Earthquake Mw 8.3, 2003 Tokachi-Oki Earthquake Mw 8.1).

The study of recurrent ruptures of the interface of the PHS along the Nankai Trough allowed to identify segments that are controlled either by persistent features on the subducted plate or by the geometry of the subduction interface, their boundaries having acted as barriers to the propagation of the ruptures for some earthquakes [e.g. *Ando*, 1975; *Cummins et al.*, 2002; *Kodaira et al.*, 2006]. Similarly, geodetic observations and recurrent ruptures of the subduction interface on subduction interface of the PAC, have evidenced persistent asperities along the Japan Trench, the Kuril Trench and also in the bend that connects both trenches (Figure 5.1). The presence of this bend marks a lateral segmentation, with potential implications on the properties that control the seismic coupling of the subduction interface [e.g. *Tanioka et al.*, 1997; *Yagi*, 2004; *Yamanaka and Kikuchi*, 2004; *Hashimoto et al.*, 2009]. The gravity anomalies and the topography of the overriding plate are dominated by persistent asperities controlled by features of the subducted plate [*Song and Simons*, 2003], that exhibits lateral and down-dip variations similar to those observed in the interseismic coupling derived from geodetic observations [*Wells et al.*, 2003; *Loveless and Meade*, 2010].

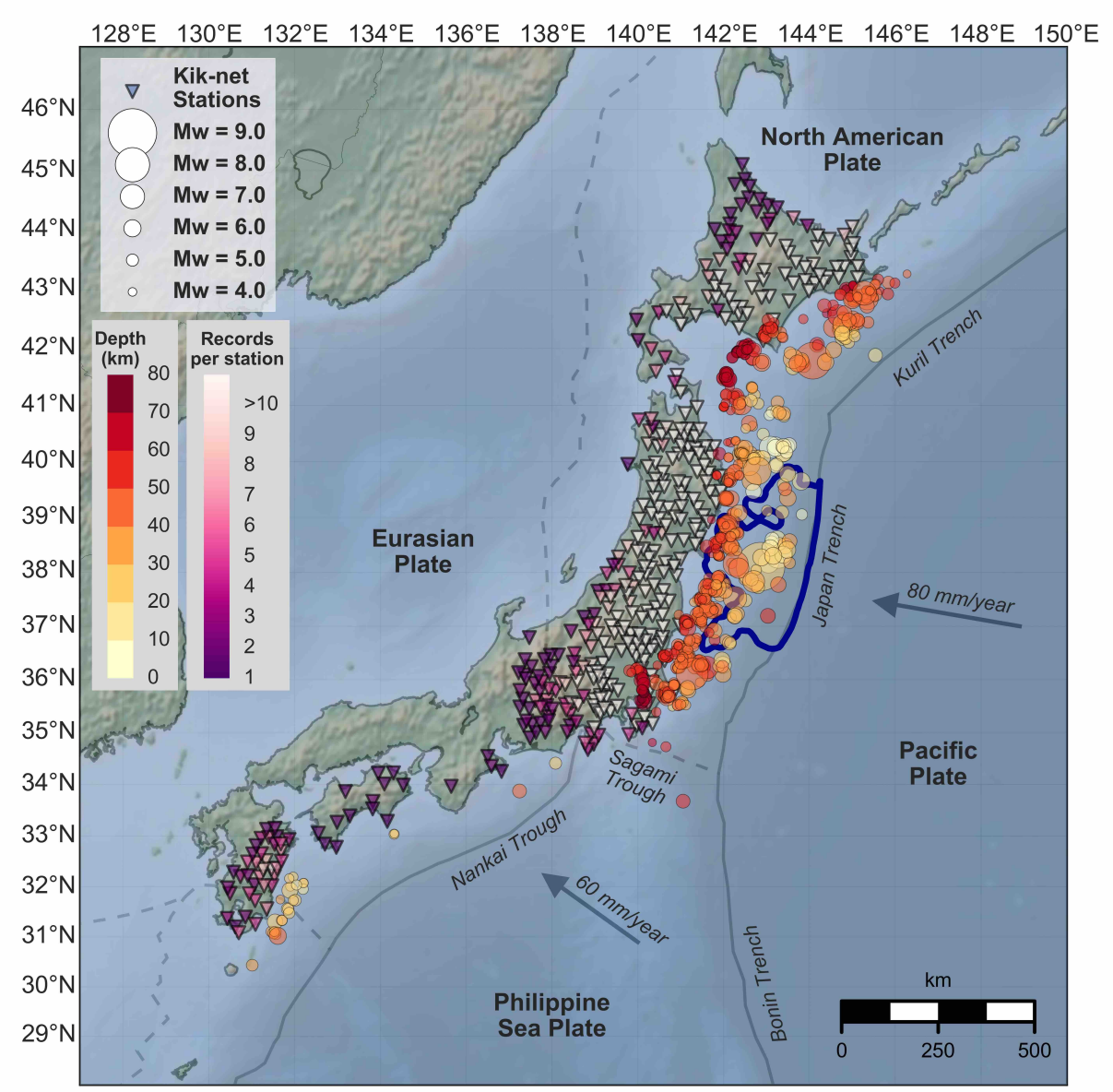

Figure 5.1: Plate boundaries and tectonic plates of Japan [*Bird*, 2003]. The gray lines show the boundaries of the tectonic plates (continuous lines represent the subduction boundaries). The blue contour represents the rupture of 2011 Tohoku-Oki Earthquake Mw 9.0 [*Hooper et al.*, 2013]. The circles show the spatial distribution of the interface seismicity with usable strong motion records contained in the *Dawood et al.* [2016] database. Colors indicate the epicentral depth and the circles size represent the moment magnitude. The inverted triangles show the location of the KiK-net stations that have usable records for subduction interface earthquakes, color-coded by the number of usable records at each station.

The down-dip variability in the slip behavior has also been observed by seismological data along the subduction interfaces in Japan. Deep non-volcanic tremors and associated slow slip events occur offshore Nankai on the PHS subduction interface

between 35 and 45 km depth [*Obara*, 2002]. Those tremors may be related to the geothermal gradient and to the presence of fluids along the subduction interface [*Ito et al.*, 2007]. Further north, offshore Honshu, geodetic observations showed decade-scale transient variations of the slip rate of between 30 and 70 km depth on the PAC subduction interface preceded the rupture of 2011 Tohoku-Oki Earthquake [*Mavrommatis et al.*, 2014; *Yokota and Koketsu*, 2015]. Also seismological studies (ground motions measured by local accelerometric networks, e.g. *Ide et al.* [2011]), and back-projection of the teleseismic waves at different frequencies, [*Kiser and Ishii*, 2012; *Satriano et al.*, 2014], showed that the energy radiated by the Tohoku earthquake varied with depth [*Lay et al.*, 2012].

These different observations suggest that a segmentation of that Japan megathrust exists, both down-dip and along-strike. Some of these segmentation signatures seem to be long-lasting since they correlate with persistent features (e.g. gravity anomalies, topography, offshore basins etc…) [*Song and Simons*, 2003; *Wells et al.*, 2003]. Others are rather characterized by transient behaviors (e.g. transient slip of the deeper part of the seismogenic interface during the decade preceding Tohoku-Oki Earthquake, [*Mavrommatis et al.*, 2014; *Yokota and Koketsu*, 2015], temporal variations of the interseismic coupling [*Loveless and Meade*, 2016]). This suggests that persistent and transient variations of the frictional behavior of the subduction megathrust exist. However, the physical parameters that control the segmentation of the subduction interface, the seismic asperities and the metastable areas, as well their relations with the roughness and the friction, are still not well understood. Assuming that the frequency content of interface earthquakes is representative of the roughness of the subduction interface [*Lay et al.*, 2012], the spatial variation of earthquakes' ground motion frequency content has been used to map the spatial variability of the subduction interface frictional properties, and to compare it with independent observations of long-lasting and transient features along the Japan subduction. Because our data set is dense in this area and because both persistent and transient signals have been described, we will particularly focus on the Pacific Plate subduction offshore Hokkaido and offshore Honshu, including the segment struck by the Mw 9.1 2011 Tohoku-Oki Earthquake.

5.1.3 Interface Ground Motion Database

The KiK-net is a high quality seismological strong motion network with more than 650 stations deployed along Japan. Each station of this network is composed by two ground motion seismographs, one located in a borehole and the second one at the

surface [*Aoi et al.*, 2004; *Fujiwara et al.*, 2004]. Since its installation, this network has generated a huge amount of non-processed (and therefore non-analyzed) seismic ground acceleration records.

The recent implementation of an automated protocol to process ground acceleration records of the KiK-net and the metadata collection from the F-net catalog by *Dawood et al.* [2016] have generated a large database of homogeneously processed records of more than 3.200 earthquakes of Mw ≥ 3.5, classified by type (Intraslab/interface), recorded between January of 1997 and December of 2011. This database contains the response spectra of 873 interface earthquakes distributed along the Japan Trench and the Nankai Trough.

Taking into the account the standard validity range for the rupture distance of the GMPEs only the horizontal surface records with distance to the rupture lower than 300 km contained in the database have been considered. Likewise, to avoid bias in the GMPE residual analysis, the records of earthquakes with less than 4 stations have been removed. Finally, the resulting catalog contains 649 interface earthquakes distributed mainly along the Japan Trench offshore Honshu and Hokkaido (Figure 5.1).

In order to give an appropriate level of consistency to the GMPE residuals analysis and considering the spatial distribution of the interface seismicity as well its data regional-density, the interface seismicity corresponding to the Nankai and to the Izu-Bonin segments was removed from the catalog.

The response spectra contained in our selection of the [*Dawood et al.*, 2016] database have been validated by picking random records and comparing them with manually processed response spectra from KiK-net records. This manual processing was done following the guidelines and recommendations of the COSMOS strong motion record workshop [*Boore and Bommer*, 2005]. The instrument offset was removed from the acceleration time series applying a baseline correction. Then, the signal was tapered and zeros were padded at the beginning and the end of the waveform [*Akkar et al.*, 2014]. Finally, the acceleration response spectrum was calculated with 5% of damping ratio, using the method proposed by *Nigam and Jennings* [1969]. The response spectra obtained by manual processing in the 35 tests performed have not showed significant difference with the response spectra contained in the database.

The resulting strong motion database contains more than 12,000 records with rupture distances between 40 and 300 km (Figure 5.2), which come from 747 Interface

earthquakes of moment magnitude between 3.6 and 9.0. The catalog includes earthquakes that occurred between 2000 and 2011, although almost a third of the earthquakes of the catalog occurred during the year 2011.

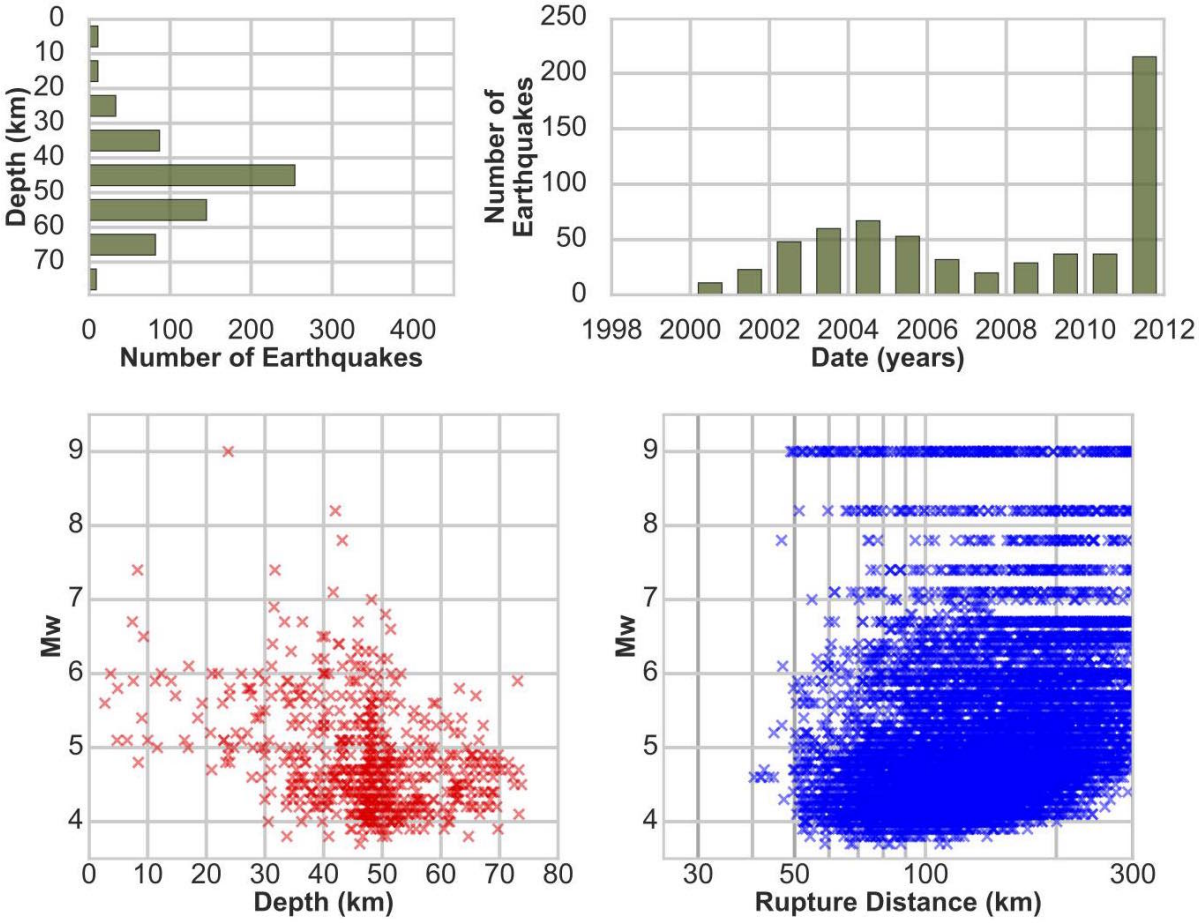

Figure 5.2: *Top* – Depth *(left)* and time *(right)* distribution of the Japan Trench interface seismicity contained in the *Dawood et al.* [2016] database. Most of the seismicity is concentrated between 30 and 60 km depth and no interface seismicity is observed below 80 km depth. The peak of seismicity in the year 2011 is related to the 2011 Tohoku-oki Mw 9.0 earthquake. *Bottom* - Distribution of the magnitude of the Japan Trench interface seismicity contained in the *Dawood et al.* [2016] database as a function of depth *(left)* or distance to the rupture *(right)*. Note that the seismicity of low magnitude (Mw ≤ 5.0) is located between 20 and 80 km depth, with a strong concentration around 50 km depth.

The interface catalog obtained from the strong motion database does not show a homogeneous distribution with depth (Figure 5.2, left). Most of the seismicity is located between 30 and 60 km depth, with a peak of concentration at 50 km depth. Likewise, the earthquakes of Mw < 5.0, are concentrated between 30 and 70 km depth. This low magnitude seismicity bias at shallow depths is likely due to the spatial

disposition of the stations of the KiK-net that are constrained by the geometry of Japan mainland, which is located between 250 to 300 km west of Japan trench. This explains why the completeness magnitude of the catalog decreases near the trench (Figure 5.3). It is therefore difficult to have good strong motions records of low magnitude earthquakes near to the trench.

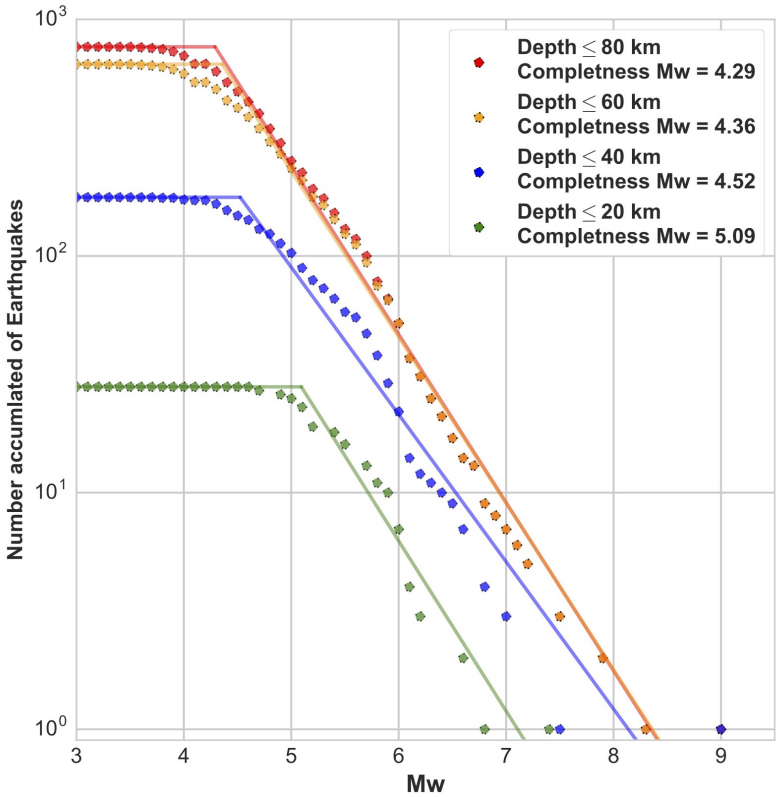

Figure 5.3: Variability of the Gutenberg-Richter law of the interface strong motion seismic catalog as a function of the epicentral depth. Note the inversely proportional relation between the completeness magnitude and the cut-off depth, suggesting the progressive decrease of the KiK-net capability of getting good quality strong motion records for low Mw earthquakes towards the trench

5.1.4 GMPE selection for Japan

To select an adequate GMPE model for the interface seismicity of the Japan subduction, two different models have been tested over the interface ground motion database. The first model considered [*Abrahamson et al.*, 2016] has been developed using a worldwide catalog. It considers non-linear site amplification and differentiates the attenuation of sites located in the forearc from those located back of the volcanic arc. The second selected model [*Zhao et al.*, 2006] has been mainly developed with

records of Japanese earthquakes, and takes the epicentral depth of the earthquakes into account. The ground motions predicted by both of these models have been computed for each record of the database, using the provided metadata on stations positions with respect to the volcanic arc, sites conditions, moment magnitude, epicentral depth, and distance to the rupture.

To evaluate the fit of the models to the ground motion database, the predicted ground motions were compared to the correspondent observed response spectra for Peak ground Acceleration (PGA) and three additional oscillator fundamental-frequencies (10 Hz, 1.0 Hz and 0.66 Hz). The total residuals, which correspond to the difference between the observed and the predicted ground motions normalized by the standard deviation of the model, have been computed. Then, they have been disaggregated into between-event and within-event residuals [*Piña-Valdés et al.*, submitted 2017]. Finally, their dispersion has been compared with the dispersion of both models selected.

The within-event residuals represent the variation of the ground motions generated by a random variability of factors related with the spatial conditions between the site and the source, such as the travel path followed by the waves and site conditions. They are representative of the crustal structure complexity and cannot be captured by simple parameters such as distance to the source, site classification or site shear wave velocity. On the other hand, the between-event residuals represent the variations of ground motions generated by random variability of source parameters not included in the predictive model. They reflect the variation of source factors that cannot be captured by simple source parameters as the magnitude and the epicentral depth, such as the stress drop, the slip distribution, slip velocity or rupture velocity between others [*Strasser et al.*, 2009; *Al Atik et al.*, 2010; *Ktenidou et al.*, 2017].

The total residual distribution shows that the model of *Abrahamson et al.* [2016] describes well the ground motion of the database for oscillators of low frequencies. It also captures well its variability. However it is not the case of high frequencies, for which the standard deviation of the model is exceeded by the variability of the residuals and most of the ground motions are underestimated. The between-event residuals distribution similarly shows a good fit for low frequencies, and a poor fit for high frequencies (Figure 5.4 - left). It is important to note that the records of the ground motion database are away from Mw validity range of the model, that has been calibrated with interface earthquakes of Mw higher than 6 that are the important ones for seismic hazard assessment.

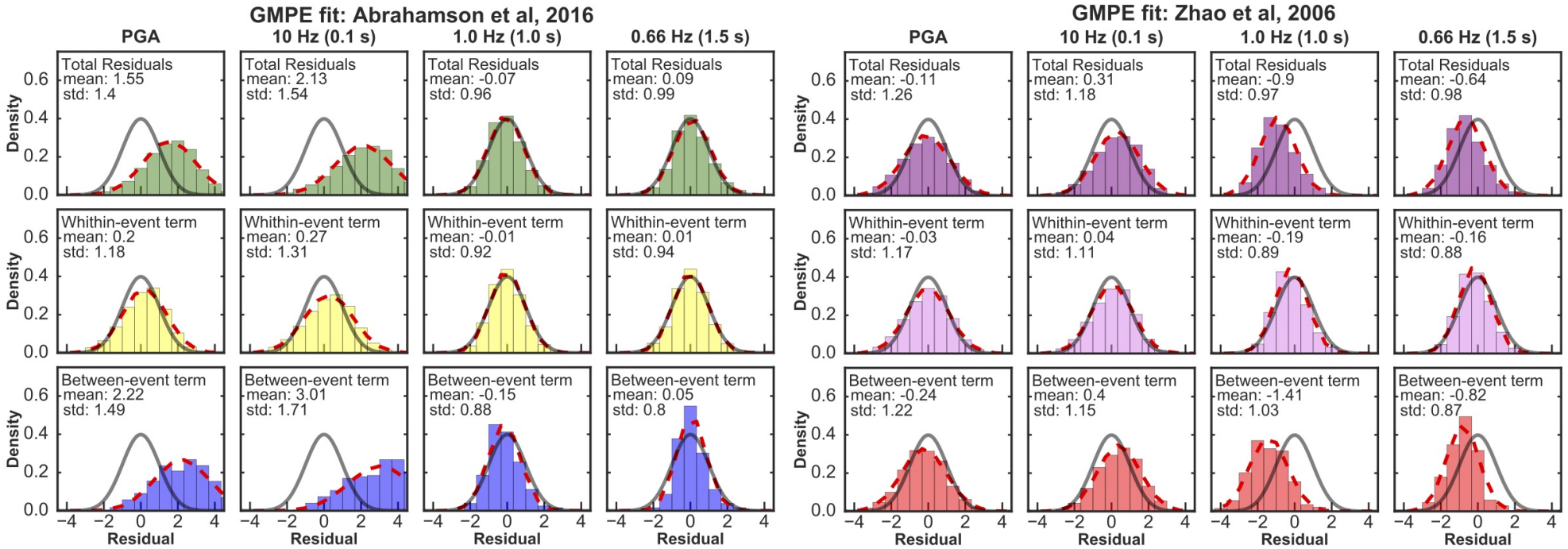

Figure 5.4: Histograms of residuals between Ground motions included in the database and the GMPE models tested (Left : *Abrahamson et al.* [2016] Right : *Zhao et al.* [2006]). The black curve represents the normal density function of the model and the red dashed curve shows the normal density function of the residuals dataset. The columns contain the residual distributions for PGA and oscillator frequencies of 10 Hz, 1 Hz and 0.66 Hz, and the rows contain from top to bottom the total, within-event and between-event residuals.

On the other hand, the total residuals distribution with respect to the *Zhao et al.* [2006] GMPE (Figure 5.4 - right) shows a good fit to the ground motion dataset at high frequencies, its accuracy is decreasing for low frequencies. Its standard deviation suggests that the model captures well the variability of the ground motions for all oscillator frequencies.

For both models, the good fit between the within-event residuals distribution and the model distribution indicates that the models reproduce well the variability associated with the site effects and path attenuations.

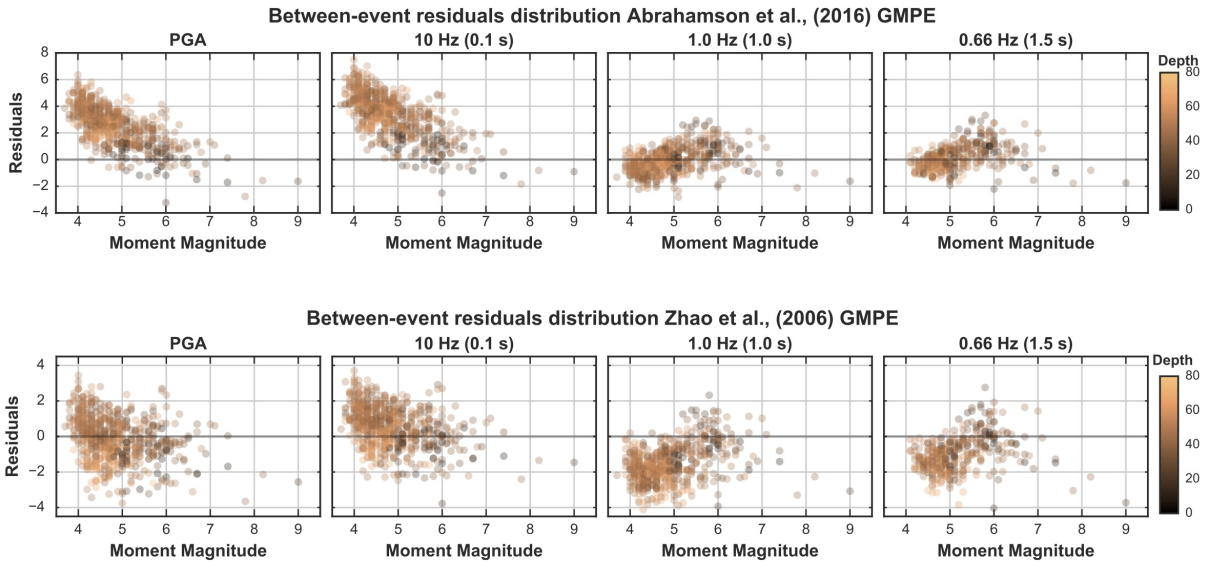

Figure 5.5: Between-event residuals distribution with respect to earthquake moment magnitude for *Abrahamson et al.* [2016] model (Upper row) *Zhao et al.* [2006] model (Bottom row). The colors show the depth of the epicenters.

Since the ground motion database contains an important quantity of earthquakes records largely out of the GMPEs magnitude validity-range, dependencies of between-event residuals on moment magnitude are possible. Indeed, at high oscillator frequencies (PGA and 10 Hz), a strong between-event residuals dependency on magnitude is detected for the *Abrahamson et al.* [2016] model (Figure 5.5), that explain its poor performance for those oscillator frequencies. In the validity range of the model and for moment magnitudes higher than 6.0, the model predicts the ground motions adequately. It is interesting to note that at low oscillator periods, no magnitude dependency is observed. These results suggest that the *Abrahamson et al.* [2016] model is not adequate to describe the ground motion of the

database at high frequencies, but the model seems to capture the source effects that control the ground motion at low frequencies.

The results obtained from the analysis of the between-event residual dependency on magnitude together with the fit of the models show that, from both model tested, only the *Zhao et al.* [2006] model is capable of describing the scaling and variation of ground motions on a large magnitude range (4 - 8). This makes of this model best suited be used as a backbone model to study the ground motion variations of the earthquakes contained in the database.

5.1.5 Regional variations of ground motions and lateral segmentation of the subduction interface

The between-event residuals being computed for each earthquake, their spatial distribution can be analyzed in order to identify regional features. The identification of spatial correlations of between-event residuals of earthquakes that occurred on a large fault may lead the recognition of ground motion dependencies that are currently missing in GMPEs development. Also, such spatial variability may lead in a better description of the variability of fault interface characteristics, such as frictional and roughness properties which may impact the ground motions.

In order to identify possible regional variations of the subduction interface in Japan, the spatial distribution of between-event residuals has been analyzed (Figure 5.6). To evaluate a possible bias coming from stations with particular site conditions, the site term (δ_{S2S}) has been calculated at each station for PGA and the selected oscillator frequencies, as the mean of the within-event residuals recorded by the station [*Ktenidou et al.*, 2017]. The figure confirms that there is no particular regional variations of site amplifications which may bias the regional variation of source-related between-events residuals.

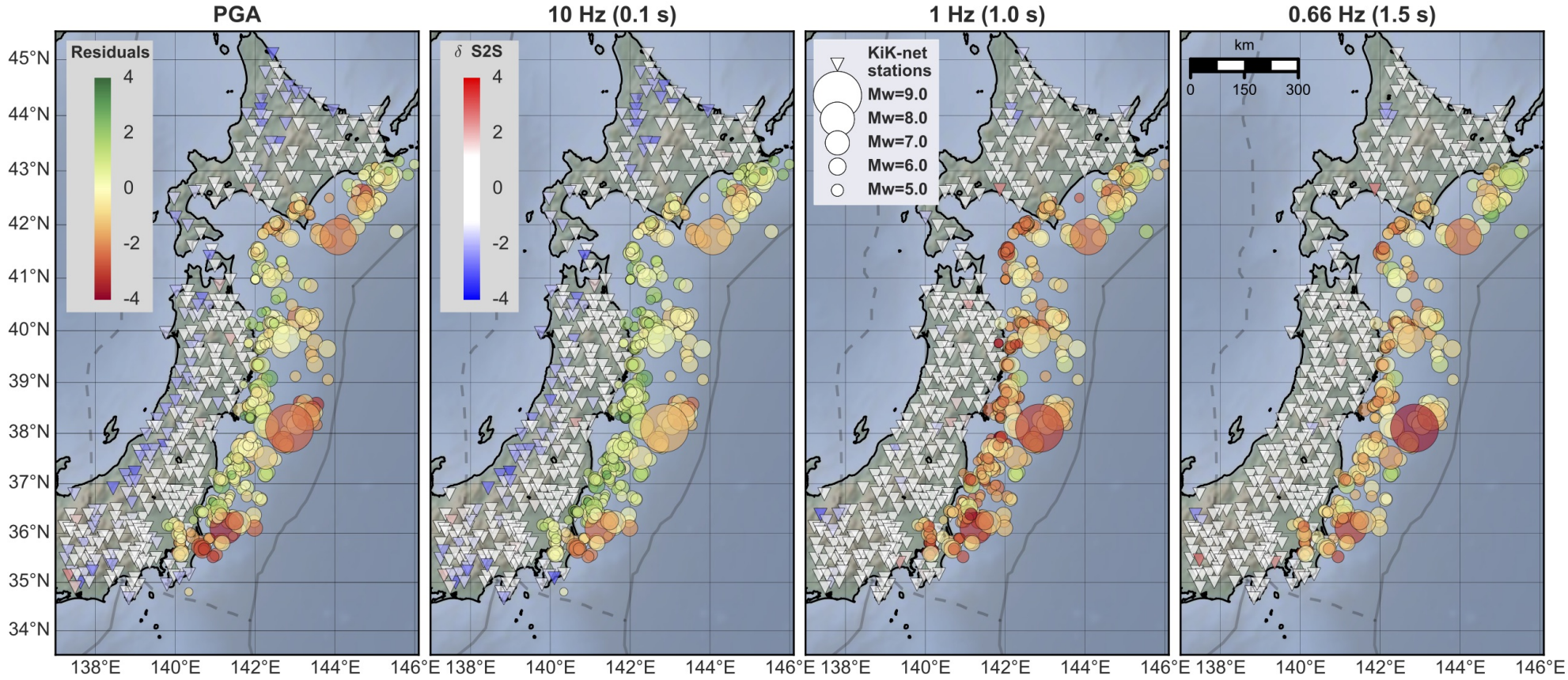

Figure 5.6: Spatial distribution of between-event residuals of *Zhao et al.* [2006] for PGA and oscillator periods of 10, 1 and 0.66 Hz (from left to right). The Circles indicate the location of the interface seismicity, their size depending on the earthquakes magnitudes and their color on the residual value. Inverted triangles represent the stations locations, color-coded as a function of the site term (δ_{S2S}). A dependency with depth is identified on between-event residuals for PGA and 10 Hz (positive values below the coastline and negative values toward the trench). Note that the low values of δ_{S2S} correspond to stations characterized by a low number of records (Figure 5.2) or located far behind of the volcanic arc.

Depth Dependency of the Ground Motions

A first order dependency of the between-event residuals with depth at high frequencies (PGA and 10 Hz) is reflected by the anomalous concentration of positive residuals values below the coastline and their decrease toward the trench (Figure 5.6). Although such depth dependency can be clearly identified by analyzing the spatial distribution of the residuals, a simple plot of the residuals with respect the earthquake depth including all interface earthquakes of the catalogue does not allow to identify any clear depth dependency (Figure 5.7 – bottom row). Moreover, at low oscillator frequencies (1.0 and 0.66 Hz), a slight positive dependency of between-event residuals on depth may be seen, inverse to the one expected and observed at high oscillator frequencies [*Lay et al.*, 2012].

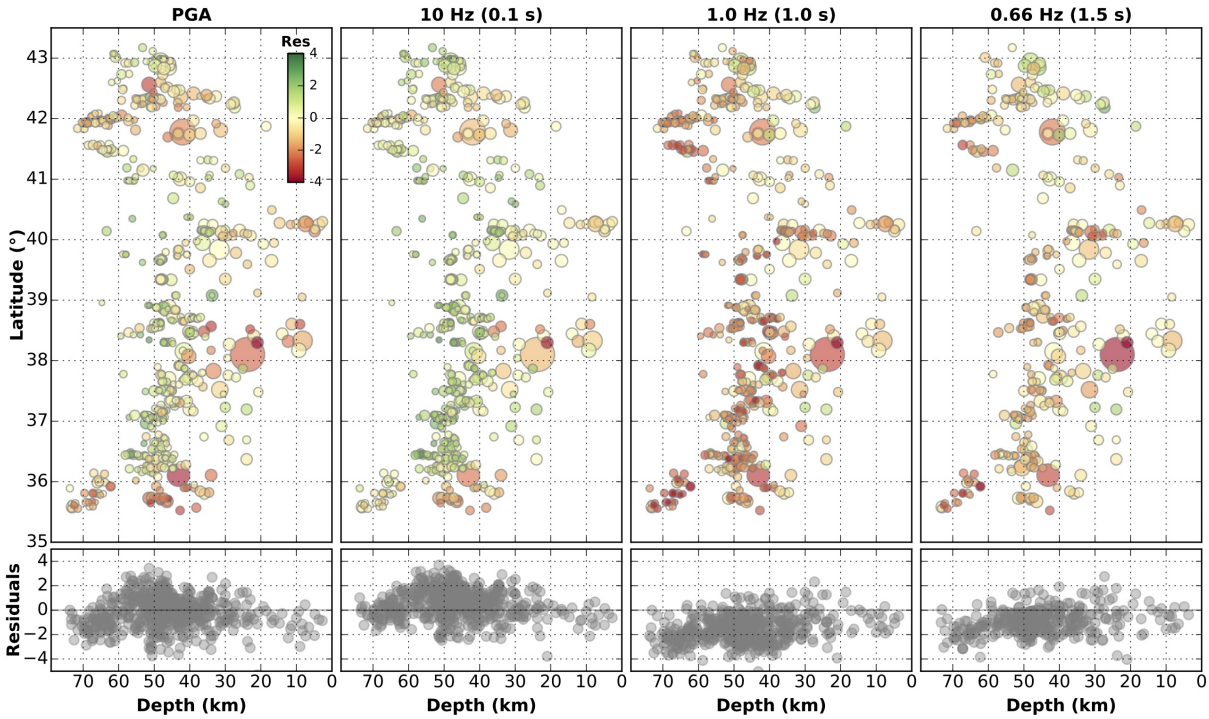

Figure 5.7: *Top* – Between-event residuals of interface seismicity in a latitude - depth plot. The circles size depends on the magnitude, while the colors represent the between-event residuals with respect to *Zhao et al.* [2006] model at different frequencies (PGA, 10 Hz, 1 Hz and 0.66 Hz from left to right). *Bottom* - Between-event residuals as a function of the epicentral depth (All the interface earthquakes included in the database are plot). No depth dependency can be evidenced by examining the complete database in a whole (bottom), while a dependency with depth can be seen segment by segment (top row and Figure 5.6).

The *Zhao et al.* [2006] GMPE model used as a backbone for the computation of the residuals includes a correction for depth in its functional form. Therefore, the fact that no average dependency with depth of between event residuals is seen means that the functional form of the *Zhao et al.* [2006] GMPE model mimics well the overall depth dependency of the interface earthquakes ground motions. It implies that that the deep earthquakes generate larger accelerations than the shallow earthquakes.

A finer spatial analysis reveals a lateral variability in the depth dependency of between-event residuals, and therefore ground motions. The increase of ground shaking with depth at high frequencies can locally vary from the one embedded in the GMPE model of *Zhao et al.* [2006]. Figure 5.7 shows the distribution of the residuals in a latitude-depth diagram, highlighting at least 4 zones along the interface (Figure 7.8), characterized by a different evolution of strong-motions with epicentral depths:

A. The segment north of 42°N, offshore Hokkaido, that only exhibits seismicity between 40 and 60 km depths. There, the between-event residuals computed with respect to [*Zhao et al.*, 2006] model, present an increase with depth at high frequencies (PGA and 10Hz) (Figure 5.7, Figure 5.7 and Figure 5.8)

B. The segment between 41°N and 42°N, that corresponds to a change in the trench orientation, and where seismicity is concentrated between 30 and 75 km depths. No obvious dependency of residuals with depth can be observed.

C. The segment between 36°N and 41°N, which broke during the 2011 Tohoku-Oki Mw 9.0 earthquake, and presents seismicity between 10 and 60 km depths, thus shallower than in other segments of the Japan subduction. These earthquakes present a clear increase with depth of between-event residuals at high frequencies (PGA and 10Hz).

D. The segment south of 36°N offshore Boso, well-known for the occurrence of regular Slow Slip Earthquakes (SSEs) [*Ozawa et al.*, 2007; *Hirose et al.*, 2014; *Ozawa*, 2014; *Reverso et al.*, 2016], concentrates seismicity between 30 and 75 km depths. Like for segment B, despite of the limited number of earthquakes and their large depths, an increase of between-event residuals with depth can be observed.

The distribution of the between-event residuals shows that depth affects the ground-motions on a different manner from one segment to the other. This suggests a persistent non-homogeneous depth dependency of the frequency content of earthquakes that occurred on the Japan subduction interface (Figure 5.8 - Right).

The between-event residual distribution at high oscillator frequencies (PGA and 10 Hz) grouped by segments shows a strongest depth dependency compared to the [*Zhao et al.*, 2006] model on segments A, C and D. In these three segments the impact of depth on the strong-motions is higher than expected by the [*Zhao et al.*, 2006] GMPE model. It is also noticeable that the model overestimates most of the ground motions of the earthquakes of segment D. Finally, only the ground motion generated by the interface seismicity of segment B and their depth dependency seem to be well explained by this model, since the between-event residuals at high frequency oscillators do not show significant correlation with the depth (or even a slight increase with depth).

The between-event residuals distribution suggests that the model overestimates the depth dependency of ground motions at low frequencies for this specific region, predicting higher strong motion for deep earthquakes than for the shallow ones.

Lateral segmentation

The fact that each of these four segments shows its own distribution of between-event residuals with depth supports the idea of a lateral segmentation of the subduction interface. In general, it is possible see that the free air gravity anomalies derived from satellite altimetry [*Sandwell and Smith*, 1997; *Sandwell et al.*, 2013] are spatially correlated with the lateral boundaries of the segments. This is particularly striking in the area affected by the change of direction of the Japan Trench (Figure 5.8 - Left). Additionally, the lateral extension of the highly coupled patches derived from geodesy [*Loveless and Meade*, 2011] shows a first order correlation with the segments boundaries (Figure 5.8- Left).

The segment “A”, located offshore Hokkaido at the northern end of the studied region, is a straight portion of the subduction where the Kuril Trench begins. It does not show interface seismicity below 60 km depth. This segment is characterized by a trench orientation that differs from the main portion of the Japan Trench. This implies that this segment of the subduction is characterized by the oblique convergence of the Pacific Sea Plate with respect to mainland Japan, with a slightly higher velocity than in the main portion of Japan Trench. The deeper part of this segment shows strong positive free air gravity anomalies and a wide negative anomaly towards the trench.

The segment “B” is located at the trench bend that separates two straight segments of different strike. It is affected by the subduction of the Erimo seamount that modifies

locally the geometry of the subduction, impacting the frictional behavior of the subduction interface [*Cadet et al.*, 1987; *Lallemand and Le Pichon*, 1987] and Very Low Frequency earthquakes (VLF) have been observed in the area during the seismic crisis of 2003 Tokachi–Oki Earthquake [*Obara et al.*, 2004; *Asano et al.*, 2008]. On this segment, the interface seismicity can reach 75 km depth (15 km deeper than in adjacent segments). It is dominated by a large negative free air gravity anomaly, extending from the trench until 80km depth, and shows a high geodetic coupling. This zone is characterized by large asperities that have broken in several opportunities in the last century [*Tanioka et al.*, 1997; *Yagi*, 2004; *Yamanaka and Kikuchi*, 2004; *Hashimoto et al.*, 2009].

The segment “C” is defined in the portion of the Japan Trench offshore Honshu that ruptured during the 2011 Tohoku-Oki Mw 9.0 Earthquake [e.g. *Simons et al.*, 2011; *Yomogida et al.*, 2011; *Kato et al.*, 2012; *Hooper et al.*, 2013]. This segment is almost pure thrust and its deeper portion is characterized by a large positive free air gravity anomaly. Before the occurrence of the megathrust, geodetic data have shown that the shallow portion of the interface was locked [*Suwa et al.*, 2006; *Loveless and Meade*, 2011], while the deeper portion of the subduction interface has experimented a very long (~10 years) transient variation of slip rate and interseismic coupling before of the occurrence of 2011 Tohoku-Oki earthquake [*Mavrommatis et al.*, 2014; *Yokota and Koketsu*, 2015; *Loveless and Meade*, 2016]. Interseismic coupling increased in the north deeper portion of the interface, while it decreased (i.e. slow acceleration of slip on the interface) in the central part, below the Tohoku-Oki rupture (Figure 5.8 – Left, blue and purple boundaries respectively). Similarly to segment “A”, this segment does not present interface seismicity below 60 km depth.

Finally, the segment “D”, which is located at the southern limit of the Japan Trench offshore Boso, presents interface seismicity until 75 km depth, like the segment “B”. This area is well known to host regular slow slip events beneath the Boso peninsula with typical recurrence from 6 to 4 years and Mw around 6.5 [*Ozawa et al.*, 2003, 2007]. This segment is characterized by the double subduction of the Philippine Sea Plate, and of the Pacific Sea Plate below mainland Japan making it difficult to separate interface earthquakes from others. This might explain the relative low number of interface earthquakes listed in the database. In this area it could therefore be worth to perform a finer analysis of the database earthquakes in order to perform a more complete classification of interface events, and to identify whether these earthquakes belong to the Pacific plate slab or to the Philippine Sea plate slab.

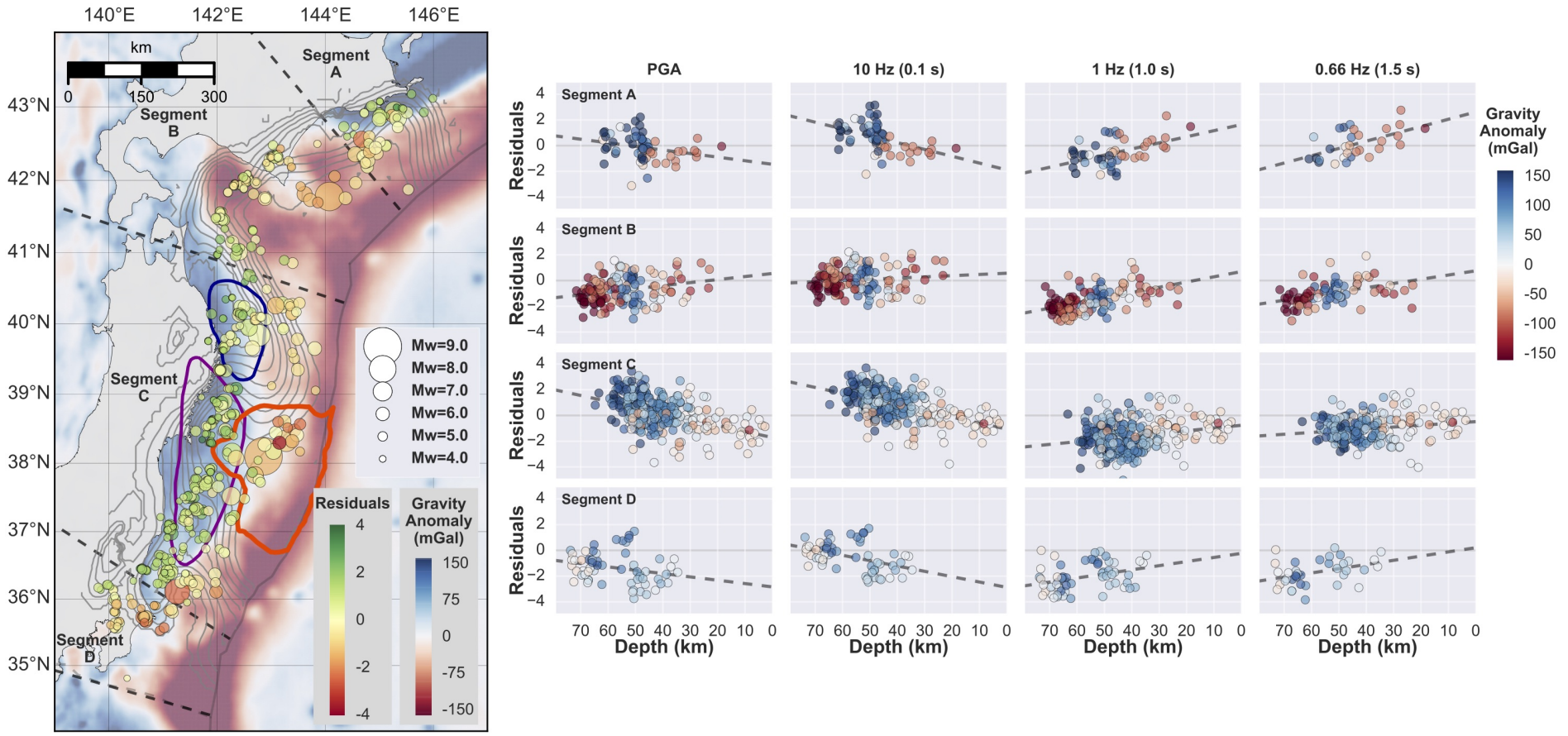

Figure 5.8: L*eft* – Map of free air gravity anomaly derived from satellite altimetry on the Hokkaido and Honshu areas [*Sandwell and Smith*, 1997; *Sandwell et al.*, 2013]. The circles show the location of the interface seismicity, the size represents the moment magnitude and the color represents the between-event residuals with respect to *Zhao et al.* [2006] GMPE model for oscillator frequency of 10 Hz. The gray contours show the geodetic coupling of the subduction interface, contoured for each ΔΦ=0.1 [*Loveless and Meade*, 2011]. The black dashed lines show the boundaries of the lateral segments identified. The purple and blue contours show the areas where transients acceleration and deceleration of slip have been observed on the interface respectively [*Mavrommatis et al.*, 2014]. The red contour shows the 10 m slip boundary of Tohoku-Oki earthquake [*Hooper et al.*, 2013]. *Right* – Distribution of between-event residuals with respect to *Zhao et al.* [2006] GMPE model as a function of the epicentral depth, for PGA and oscillator periods of 10, 1.0 and 0.66 Hz (from left to right) . Segments are sorted from north to south. The colors represent the gravity anomaly at epicenters location.2

5.1.6 Discussion

Validity of the GMPE models tested

The generation of a ground motion database requires the conjugation of two important factors: (1) having a good and well-characterized seismological network able to provide proper records, and (2) having a reliable earthquake catalogue from which the metadata that complement the ground motion records can be extracted. In the case of Japan, the KiK-net provides high quality earthquake acceleration records for one of the most active subduction zone of the world. Its large station density and the high seismicity rate of the region have generated a valuable collection of ground motion records for subduction earthquakes. In addition, the JMA provides a quite complete seismic catalogue of the Japanese subduction zone. In this context, the automated protocol of earthquake accelerations records processing proposed by *Dawood et al.* [2016] has shown to be an efficient tool to generate reliable interface earthquake's ground motion database, which cannot be obtained by manual processing due to large quantity of information contained.

Therefore, to validate the records of the database and their associated metadata, a one-by-one check-up process is not feasible, making a random check process a reasonable option to evaluate the results of the automatic data processing, at least in general terms. In the other hand, evaluating the reliability of the catalogue information is also difficult. Part of the information, such as the earthquake location and depth, could be evaluated analyzing the seismicity spatial distribution and its consistence with the subduction interface geometry. Both solutions are quite limited and only allow having a general idea about where potential error sources could be located, but they do not provide enough information for systematic wrong records removal or their metadata correction. For the database used in this work, the random comparison of records automatically and manually processed did not show significant differences. The spatial distribution of the seismicity only show a few anomalous coordinates for interface earthquakes and their impact on the results should be negligible, which is reflected by the fit to the ground motion database of at least one of the two GMPE models tested.

The global results of the GMPE fit-tests realized have shown that both GMPEs tested can be used to predict the ground motions of interface seismicity of the Japan

subduction, even out of their moment magnitude validity range if precautions are taken. The *Abrahamson et al.* [2016] model has shown to make proper prediction for earthquakes of large magnitude (Mw ≥ 6) at all oscillator frequencies tested (Figure 5.5). For earthquakes of moderate and low magnitude (4.0 ≤ Mw ≤ 6.0) though, it only predicts proper values at low oscillator frequencies. The model of *Zhao et al.* [2006] has shown a good fit at all oscillator frequencies tested for the whole database, although at high magnitudes (M ≥ 7.0) its predictions are less accurate than the model of *Abrahamson et al.* [2016].

Frictional interpretation of the ground motions and link with the interseismic coupling

The good fit of the GMPE model of *Zhao et al.* [2006] to the ground motion database made it possible to use the model as a backbone to evaluate the strong motion records variability in Japan. This has been helpful to identify consistent spatial correlations of the between-event residuals along and across the Japanese subduction interface. Our findings suggest that part of the ground motions dispersion generated by the variations of source parameters do not correspond to random variability, but rather corresponds to a regional dependency of the earthquakes ground motion. Our results show a depth dependency of ground motions generated by interface earthquakes that is consistent with the variation of the energy radiation patterns observed during the 2011 Tohoku-Oki earthquake M 9.0 [*Ide et al.*, 2011; *Irikura and Kurahashi*, 2011; *Kiser and Ishii*, 2012; *Satriano et al.*, 2014], and also in agreement with the down-dip segmentation of the subduction interface [*Lay et al.*, 2012].

The segments “A” and “D” show a significant change at 50km depth in the depth dependency trend for the between-event residual at high oscillator frequencies (PGA and 10 Hz). The segment “C” also shows such a variation of trend, but at 30 km depth (Figure 5.8 - Right). This may be interpreted as the transition between the shallow domain B and the deeper domain C proposed by *Lay et al.* [2012], which are characterized respectively by unstable slip regions hosting large asperities strongly locked during the interseismic period and slipping largely during megathrust events, and the metastable regions dominated by conditionally stable areas with medium-sized to small isolated asperities that radiate a large amount of high frequency energy when they break.

Since the depth variability of the frictional properties of the subduction interface should impact the interseismic coupling, a dependency of the ground motions on the

geodetic interseismic coupling is expected, similar to the one observed on depth. (Figure 5.9) shows that as expected, interface earthquakes generate less high frequency radiations in highly coupled areas, while poorly coupled areas radiate more high frequencies. This variation of the radiated energy at high frequency may be produced by transient stress shadows of dense groups of small asperities of the metastable region, which can generate an average medium geodetic coupling [*Hetland and Simons*, 2010] and are characterized by a rough surface in terms of friction mode, while large persistent asperities would generate smooth ruptures and a nearly full coupling.

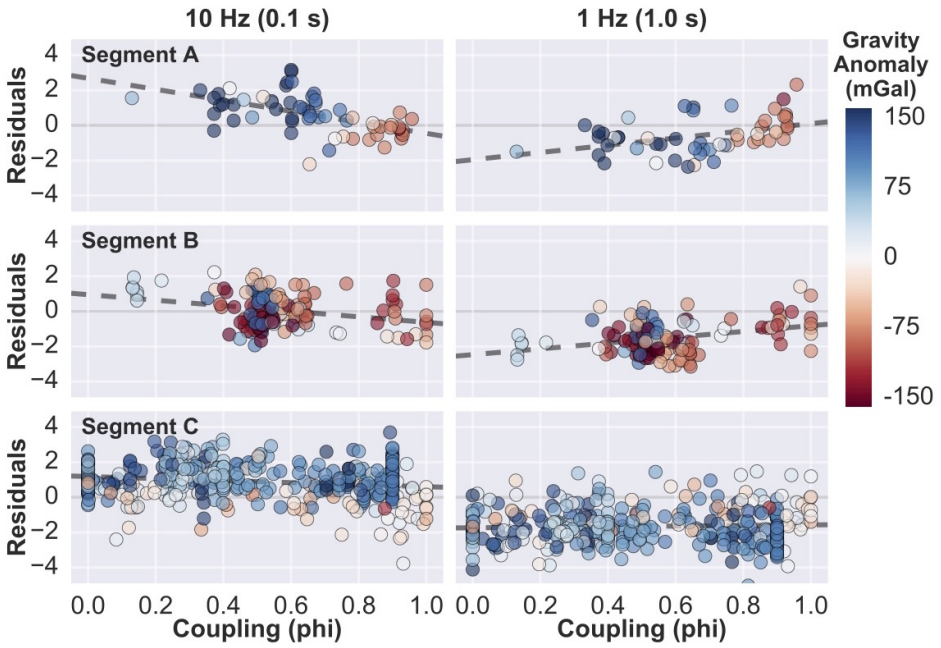

Figure 5.9: Variation of *Zhao et al.* [2006] between-event residuals versus geodetic interseismic coupling [*Loveless and Meade*, 2011], for oscillator frequencies of 10 and 1.0 Hz (left and right respectively). The colors represent the gravity anomaly of epicenters location [*Sandwell and Smith*, 1997; *Sandwell et al.*, 2013]. Segment D has been excluded because the coupling maps are not well constrained offshore Boso. Note that segment C, do not show consistence with the depth dependency observed in Figure 5.8

Persistent versus transient features of the segmentation

The lateral segmentation of the subduction interface correlates with local features of the spatial distribution of the seismicity (eg. the depth range of the seismicity epicenters varies from one identified segment to the other). Additionally, the segments identified and their proposed boundaries are spatially correlated with

geological and geographical markers of the region, as well with the free air gravity anomalies of the region (Figure 5.8 - Left).

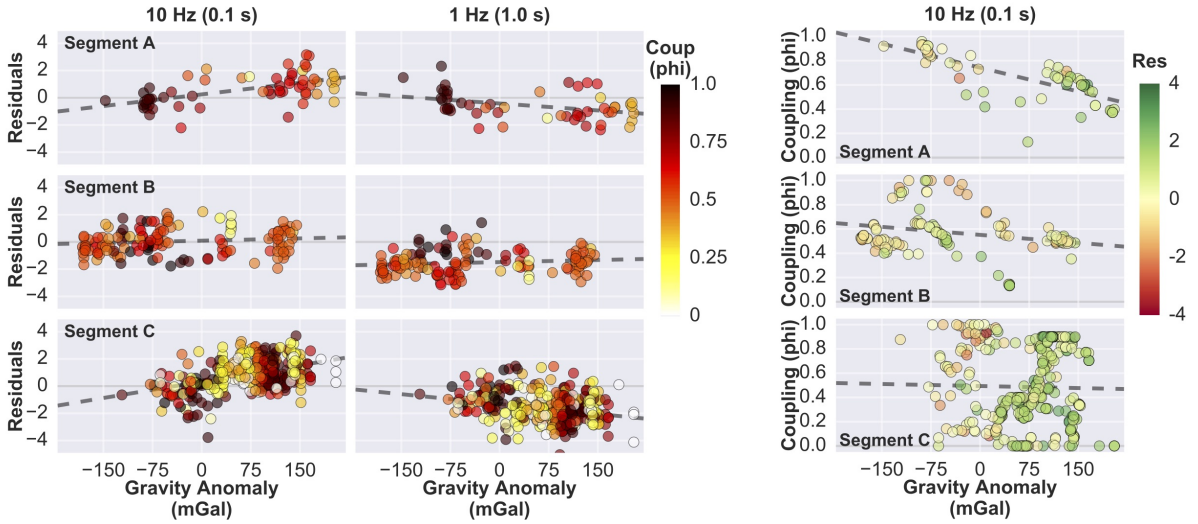

Figure 5.10: Left - Variation of [*Zhao et al.*, 2006] between-event residual with respect to free air gravity anomaly [*Sandwell and Smith*, 1997; *Sandwell et al.*, 2013], for oscillator frequencies of 10 and 1.0 Hz (left and right respectively). The colors represent the geodetic coupling of the epicenters location [*Loveless and Meade*, 2011]. Segment D has been excluded cause the data are not enough to constrain it. Note that segment C, do not show consistence with the depth dependency observed in Figure 5.9

The strongly negative free air gravity anomalies on subduction zones have been related with the increase of shear traction and associated coefficient of friction on the plate interface [*Song and Simons*, 2003]. These high shear tractions and friction coefficients would control the long-term seismic coupling of the subduction interface. The computed between-event residuals show a dependency on free air gravity anomaly consistent with the dependency on depth and on coupling observed before (Figure 5.10 - Left). A similar consistent correlation between geodetic coupling and free air gravity anomaly is observed in segments A and while in the segment C no obvious correlation can be seen. (Figure 5.10 – Right).

Segment C is the segment that has hosted Tohoku earthquake in 2011, and that has undergone a decade on geodetic coupling variation at depth [*Mavrommatis et al.*, 2014; *Yokota and Koketsu*, 2015] The geodetic coupling map plot against the gravity anomaly was derived from a GPS velocity field derived from observations spanning the January 1997 to May 2000 period [*Loveless and Meade*, 2010], hence before the occurrence of the decadal transient slip observed on the interface [*Mavrommatis et al.*, 2014; *Yokota and Koketsu*, 2015]. The location of the deeper coupled patch

region derived from the geodetic coupling is consistent with the location of one of the regions that have shown a transient slip behavior and at the same time, with the location of a strong positive free air gravity anomaly (Figure 5.11 – left). This suggests that this coupled area does not correspond to a long-term persistent asperity. We have therefore performed a detailed analysis of segment C, by separating it into three zones: the area where slip was accelerated before Tohoku (purple contour in Figure 5.8 and Figure 5.11), the area where coupling increased before Tohoku (blue contour in Figure 5.8 and Figure 5.11), and elsewhere (i.e. areas of segment C characterized by a constant coupling through the last decade). The between-event residuals show a dependency on coupling in areas that experienced a steady coupling (Figure 5.11 –top right), while no dependency of the between event residuals is observed for the area that experienced a transient acceleration of slip during the 10 years preceding Tohoku-Oki Earthquake (accelerated area, purple contour). The possible dependency in the decelerated area (blue contour) is not well constrained by the data.

A similar partition can be observed in the distribution of the geodetic coupling with respect to the free air gravity anomaly (Figure 5.11–bottom right). The regions that have experimented transient slip behavior shows inverse correlation than the expected (accelerated slip region) or no correlation (decelerated slip region), while the seismicity that is located outside of these regions shows similar correlation between the geodetic coupling and the free air gravity anomaly than other segments, in agreement with the expected behavior (decrease of the coupling with positive free air gravity anomalies).

These observations suggest that persistent frictional features of the subduction interface seem to be characterized by a positive correlation between the energy of high frequency radiation (i.e. between-event residual at PGA or 10 Hz), free air gravity anomaly and interseismic slip rate on the plate interface (i.e. Vp (1-Φ), where Vp is the rate of plate convergence, and ϕ the interseismic coupling). Instead, areas that do not exhibit such correlations may undergo a transient phenomenon, such as an accelerated aseismic slip, that may change the state of stress in nearby areas, and potentially trigger a seismic rupture. In the areas affected by such transient behavior, the radiation of interface earthquake may be controlled by other mechanisms [*Socquet et al.*, 2017], and its relationship with coupling or aseismic slip rate may differ significantly from the one observed in this study for stable areas.

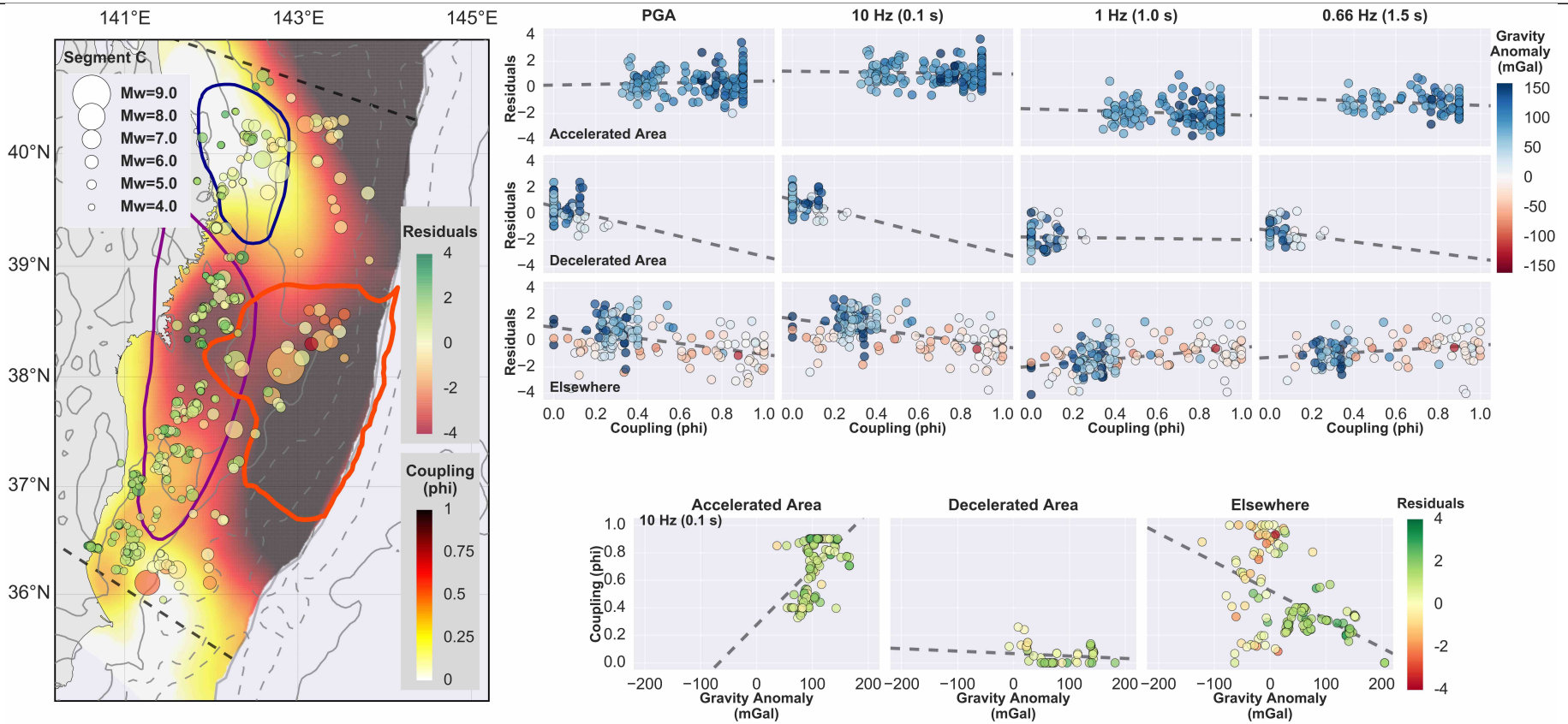

Figure 5.11: *Left* – Map of geodetic coupling of Honshu area [*Loveless and Meade*, 2011], derived from a velocity field spanning January 1997 to May 2000. The circles show the location of the interface seismicity, the size represents the moment magnitude and the color represent the between event residuals of *Zhao et al.* [2006] GMPE for oscillator frequency of 10 Hz. The gray contours show the free air gravity anomaly derived from satellite altimetry [*Sandwell and Smith*, 1997; *Sandwell et al.*, 2013]. The black dashed lines show the lateral boundaries of segment C. The purple and blue contours show the areas where transient acceleration and deceleration slip on the subduction interface derived from GPS time series [*Mavrommatis et al.*, 2014]. The red contour shows the 10 m slip boundary of Tohoku-Oki earthquake [*Hooper et al.*, 2013]. *Right top* – Distribution of between-event residuals with respect to *Zhao et al.* [2006] GMPE model versus the geodetic coupling for PGA and oscillator periods of 10, 1.0 and 0.66 Hz (from left to right), separated by regions showing a different transient coupling in the decade preceding Tohoku earthquake. The colors represent the gravity anomaly of epicenters location. *Right bottom* – Distribution of geodetic coupling at epicenter location with respect to the free air gravity anomaly. The color shows the between-event residual for oscillator periods of 10 Hz.

5.1.7 Conclusion

The GMPE models have been shown to be useful tools not only for seismic hazard analysis purposes. As their functional forms consider the magnitude scaling effect and the propagation effect, they can be used to compare the source-effects of earthquakes. Therefore, the between-event residuals, which have been shown to be correlated with the stress-drops [*Bindi et al.*, 2007; *Bindi et al.*, 2017], can be spatially analyzed in order to identify variations of the frictional properties of large seismogenic faults. The finding presented in this work are in agreement with the down-dip segmentation of the frictional properties on subduction interface [*Lay et al.*, 2012] and with the main features of the frictional segmentation model proposed for Miyagi [*Satriano et al.*, 2014]. This supports the use of the between-event residuals and ground motions generated by earthquakes as a proxy for the variability of the frictional properties of the subduction interface.

The ground motions generated by interface subduction earthquakes are regionally and depth dependent. Since the GMPEs are fundamental tools in the seismic hazard evaluation of regions poorly instrumented or with a limited number historical earthquake records, the implementation of methodologies that allow minimizing the underestimation of the seismic hazard derived from the ground motion regional dependency is imperative. Variations in the earthquake ground motions from one region to another are expected. The calibration of GMPE models with large databases that include records from different regions can lead to a wrong estimation of the effects of parameters that represent the earthquake source. This could even be more important for earthquake records of low and moderate moment magnitude, that do not break the entire seismogenic zone, while for GMPE models that focus on earthquakes of large magnitude, the effects of the regional variability of ground motion should impact less the prediction because these large earthquakes rupture a larger portion of the faults interfaces, therefore smoothing the spatial variability of strong motions.

The regional variability of ground motions, as well the spatial distribution of the interface seismicity and the changes in the geometry of the Japan subduction interface, show an overall good agreement. This information allowed us to define 4 individual segments offshore Hokkaido and Honshu (Figure 5.8 - Left), that show an internally consistent between-event residual distribution. The so-defined segmentation also shows a good agreement with the strong free air gravity

anomalies, which can be interpreted as a proxy for the long-term slip behavior of subduction interface [*Song and Simons*, 2003] and may be related to the lateral variation of parameters that control the frictional behavior of the subduction interface such as temperature gradient, geometry or fault normal stress, which can drive to the variability of the down-dip segmentation boundaries.

The interseismic geodetic coupling maps can be interpreted as the result of an interfingering of seismic asperities and metastable regions, the highly coupled areas being rather constituted by large unstable seismic asperities fully locked between large earthquakes, and the moderately coupled areas being made of small asperities whose stress shadows hinder the slip of surrounding metastable regions (Hetland and Simons, 2009). The inverted correlation between the observed strong radiations of high frequency seismic energy (between event residuals computed at PGA or 10Hz) and the interseismic geodetic coupling corroborates this interpretation. Poorly coupled areas, constituted of an interfingering of small asperities and metastable areas, are characterized by a heterogeneous frictional behavior that likely complicates the seismic rupture and enhance the generation of high frequency radiations. Instead, highly coupled areas are more homogeneous (large unstable seismic asperities) and would generate less high frequency radiations.

It has been shown that strong free air gravity anomalies are related to the long-term features of subduction interface coupling [*Song and Simons*, 2003]. The positive correlations observed between free air gravity anomalies, interseismic coupling and strong motions tend to indicate persistent features. The analysis of between-event residual distribution cross-compared with other geophysical observables could therefore be a helpful method to identify persistent features on the seismogenic subduction interface. Instead, inconsistencies between the strong gravity anomalies, the geodetic coupling and the signature of strong motions seem to occur in regions of the subduction interface affected by a transient behavior. Such inconsistencies, also observed off-shore Chile [*Socquet et al.*, 2017], may therefore be used as a proxy for the identification of such metastable areas affected by a transient slip behavior, and to relate them with a potential enhanced seismic hazard updip.

5.2 Transient signals offshore Honshu : comparison of the temporal evolution of slip on the subduction interface and ground motion

In the decade preceding the 2011 Tohoku-Oki earthquake (Mw 9.0), cGPS time series have shown variations of interseismic velocities in the Honshu region, near the mainshock epicenter [*Mavrommatis et al.*, 2014; *Yokota and Koketsu*, 2015] (Figure 5.12 – Top). The removal of constant interseismic velocity from the time series, have revealed a non-linear displacement after 2002, which indicates an accelerated velocity towards the east in front of the Tohoku rupture area, and a decrease of the eastward velocity in Northern Honshu. These observations suggest the existence of a zone that underwent transient accelerated slip on the deeper portion of the subduction interface at the latitude later ruptured by Tohoku earthquake, while an increase of coupling can be seen in Northern Honshu (Figure 5.12 – bottom left and right).

Similar conclusions have been obtained by analyzing the variation of the background seismicity rate in central Japan [*Marsan et al.*, 2017], using the seismic catalog of the Japanese Meteorological Agency (JMA) between 1990 and 2011. To perform this analysis, the background seismicity of the subduction interface has been obtained removing the aftershock seismic activity by declustering the seismic catalog. Then, a regional nodal analysis using the background seismicity of an area of 50 km around each node was performed. To the cumulative series of background seismicity obtained at each node, a quadratic curve was fitted and the nodes were characterized with the ratio (Φ) of the final and the initial slope of the fitted curve (Figure 5.13). This allowed to differentiate regions where the background seismicity rate increased ($\Phi > 1$) from those where the rate decreased ($\Phi < 1$). The increase of the background seismicity rate may be associated to transient accelerations of the interface slip, since a higher slip velocity may accelerate the load and rupture cycle of the subduction interface seismic asperities. Oppositely, a reduction in the slip velocity may lengthen the load and rupture cycle, which may reduce the background seismicity. The consistency between the seismicity rate variation and the geodetic observations mentioned before supports this interpretation.

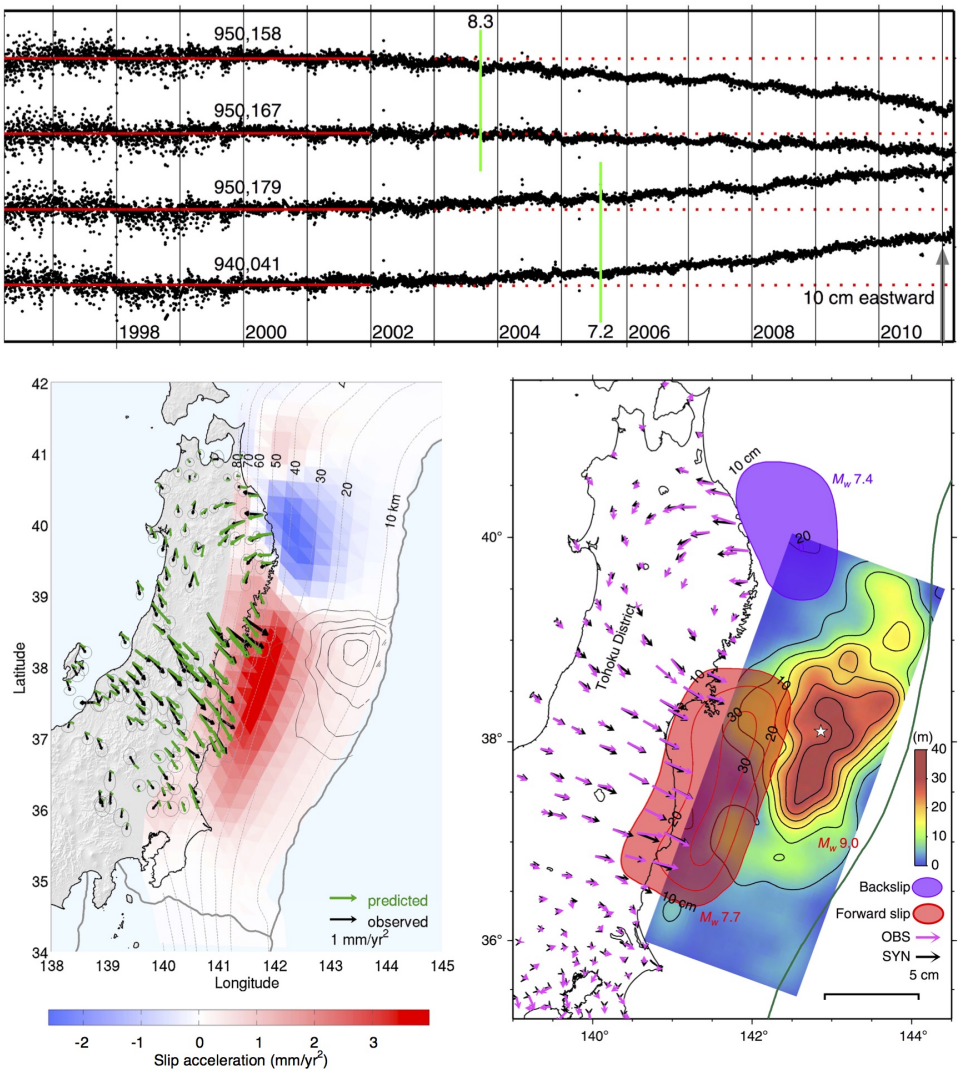

Figure 5.12: *Top:* cGPS time series of 4 coastal stations in central Japan (the two upper curves correspond to stations located at the northern part of Honshu region and the two bottom curves to stations located in the central portion of the 2001 Tohoku earthquake rupture), after removal a constant interseismic velocity from 1996 to 2002, and correction for coseismic offsets and post seismic transients [*Yokota and Koketsu*, 2015]. *Left bottom:* Areas of the subduction interface that have experimented a long term deceleration (blue region) or acceleration (red region) of slip, derived from cGPS time series inversion [*Mavrommatis et al.*, 2014]. *Right bottom:* Slip inversion of detrended cGPS time series: the results suggest that the slip deficit in the decelerated region is equivalent to an earthquake of Mw 7.4, meanwhile in the accelerated area the slip is equivalent to an earthquake of Mw 7.7 [*Yokota and Koketsu*, 2015].

The mechanisms that initiate and arrest the transient slip behavior are still not well understood. They could be related with physical processes that may generate temporal variation of the frictional properties of subduction interface. Since earthquake ground motions are sensitive to the frictional properties of faults, those variations may also impact ground-motions between-event residuals [*Socquet et al.*, 2017]. In order to investigate if transient changes of the frictional properties of the

subduction interface have occurred and are associated with the observed transient slips, the temporal variability of ground-motion between-event residuals have been analyzed for earthquakes in the database that occurred before the 2011 Tohoku-Oki earthquake. For this, we have focused the analysis in the region offshore Honshu, which concentrates most of the seismicity of the used ground motion database [*Dawood et al.*, 2016]. The time series of between-event residuals have been analyzed in the area broken by 2011 Tohoku-Oki earthquake, as well as in the areas that have been shown to present transient features [*Mavrommatis et al.*, 2014; *Marsan et al.*, 2017] (Figure 5.14).

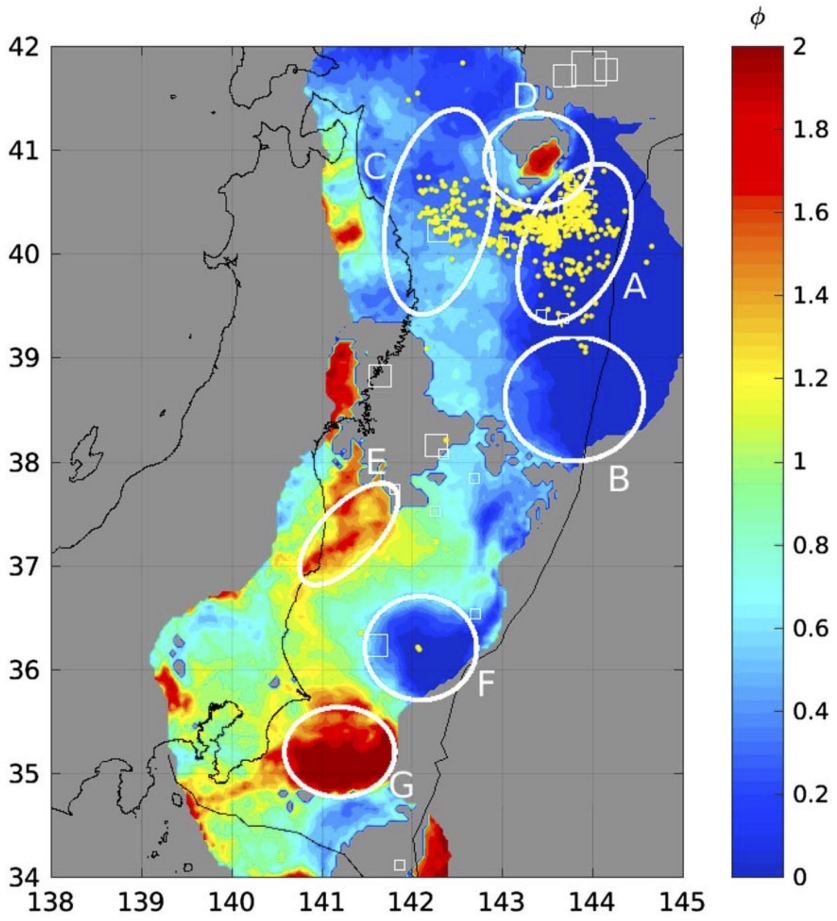

Figure 5.13: Acceleration map of background seismicity rate in Japan, derived from the interface seismicity of magnitude > 3.0 (Φ values higher than 1, indicate acceleration of the seismicity rate and lower than 1 indicate deceleration - after *Marsan et al.* [2017]). The ellipses show the regions which higher variation rates

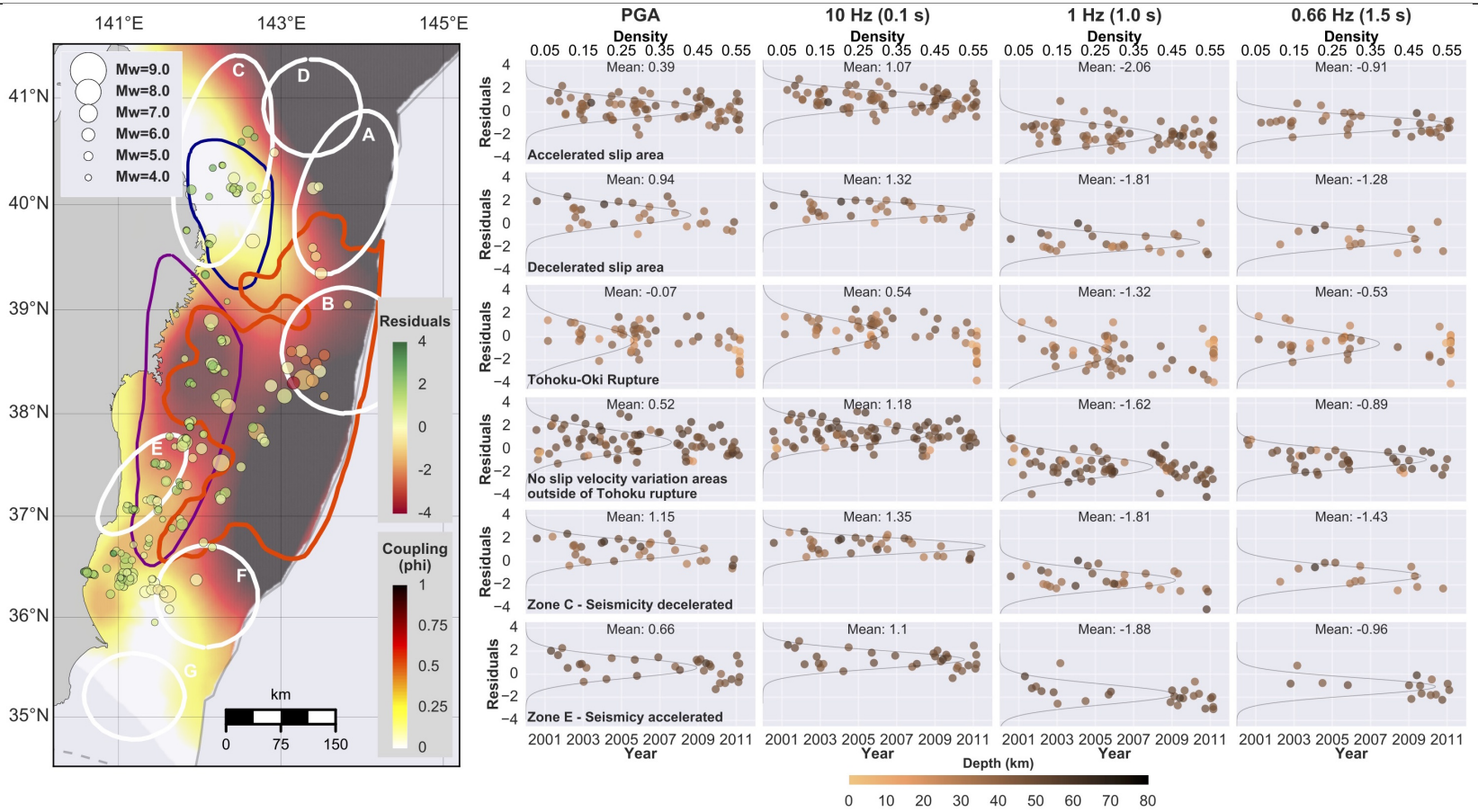

Figure 5.14: *Left* – Geodetic coupling offshore Honshu [*Loveless and Meade*, 2011]. Circles show the interface seismicity, their size represents the Mw and their color the between-event residuals with respect to *Zhao et al.* [2006] GMPE for oscillator frequency of 10 Hz. Purple and blue contours show the areas of transient accelerated and decelerated slip, derived from cGPS time series [*Mavrommatis et al.*, 2014]. Red contour shows the Tohoku-Oki Earthquake rupture [*Hooper et al.*, 2013]. White contours show zones that have experimented transient variations in background seismicity rate [*Marsan et al.*, 2017]: zones A, B, C and F showed deceleration, zones D, E and G showed acceleration. *Right* – Time distribution of between-event residuals with respect to *Zhao et al.* [2006] GMPE model for PGA and oscillator periods of 10, 1.0 and 0.66 Hz. Data are separated by areas showing a different transient slip on the subduction interface in the decade preceding Tohoku earthquake inferred from geodetic and seismological observation [*Mavrommatis et al.*, 2014; *Marsan et al.*, 2017]. The colors represent the epicentral depth. Black curves show the density distribution of the between-event residuals on each area. Only areas with sufficient number of earthquakes during the time span analyzed are shown.

The between-event residuals time series do not show any obvious variation between 2000 and 2011 that would be associated with the 10-year change of slip rate on the subduction interface (Figure 5.15 - Right). Despite of the fact that no obvious change occurs with a dynamics that could directly be related to the change of accelerated / decelerated slip, it is noticeable that the means of the between-event residuals at high oscillator frequencies (PGA and 10 Hz) in the areas that have experimented acceleration of the slip, are slightly higher than the between-event residual means of the areas that have experimented a deceleration. In other words, areas that have increased their interseismic coupling have generated systematically, higher ground motion than those areas where interseismic coupling has decreased, suggesting a slight difference of the frictional properties between both areas. The change in coupling may therefore reflect a return to the equilibrium relation between high frequency radiations and coupling of the interface observed in steady areas of the subduction. Unfortunately, in this segment of the Japanese subduction, the first earthquakes for which ground motion data are available in the database of *Dawood et al.* [2016] occurred in 2000. Therefore we have no good constraints on the state of the ground motions released by interface earthquake before the occurrence of the observed 10-year change of slip rate. A reference is therefore lacking, that would be needed to characterize the between-event residuals at the onset of the process. We are therefore not able to see if a change in the earthquake frequency radiation precedes (and may initiate) the change in slip rate measured by both geodetic data and dynamics of the seismicity.

Even if no temporal trend can be observed in any between-event residual time series, it is interesting to note that, in the area that was later broken during the 2011 Tohoku-Oki earthquake at the end of the time series, a drop in the values of the between-event residuals is detected at high oscillator frequencies (PGA and 10 Hz). This may evidence a diminution of the high frequency energy radiated by the seismic ruptures, which took place two days before to the main rupture of Tohoku-Oki earthquake. Those between-event residuals comes from the records of 10 earthquakes that started with the large interface foreshock of Mw 7.3 on March 9th and finish with the occurrence of the Tohoku-Oki mainshock. They are distributed in a small area nearby the epicenter of Tohoku-Oki earthquake and no large variation in theirs depths is observed. Additionally, the time and space variability of the earthquake is consistent with the second sequence of slow slip that has preceded the 2011 Tohoku-Oki earthquake observed by *Kato et al.* [2012] (Figure 5.15 - Left). Additionally, *Bouchon et al.* [2016] have shown that inslab seismicity of the region, have experimented an increment in the previous month to the occurrence of the Tohoku-Oki earthquake (Figure 5.15 - Right), which is synchronized with the slow slip

interface activity detected by *Kato et al.* [2012]. All this observations, seem to indicate that the region of the subduction interface that host the slow slip occurred previous to the Tohoku-Oki rupture, have experimented a progressive diminution of the friction coefficient before the mainshock. However, the interface seismic activity of the database in the two months previous to the rupture, is very limited (only 11 interface earthquakes between January 1st of 2011 and the mainshock) and by itself does not allow to see an evolution. This lack of interface seismicity can be due to limitations of the automatic classification earthquakes system or to bad quality of the strong ground motion records. Therefore a manual revision of the database may be useful to try to retrieve more information in order to increment the number of interface records in this period.

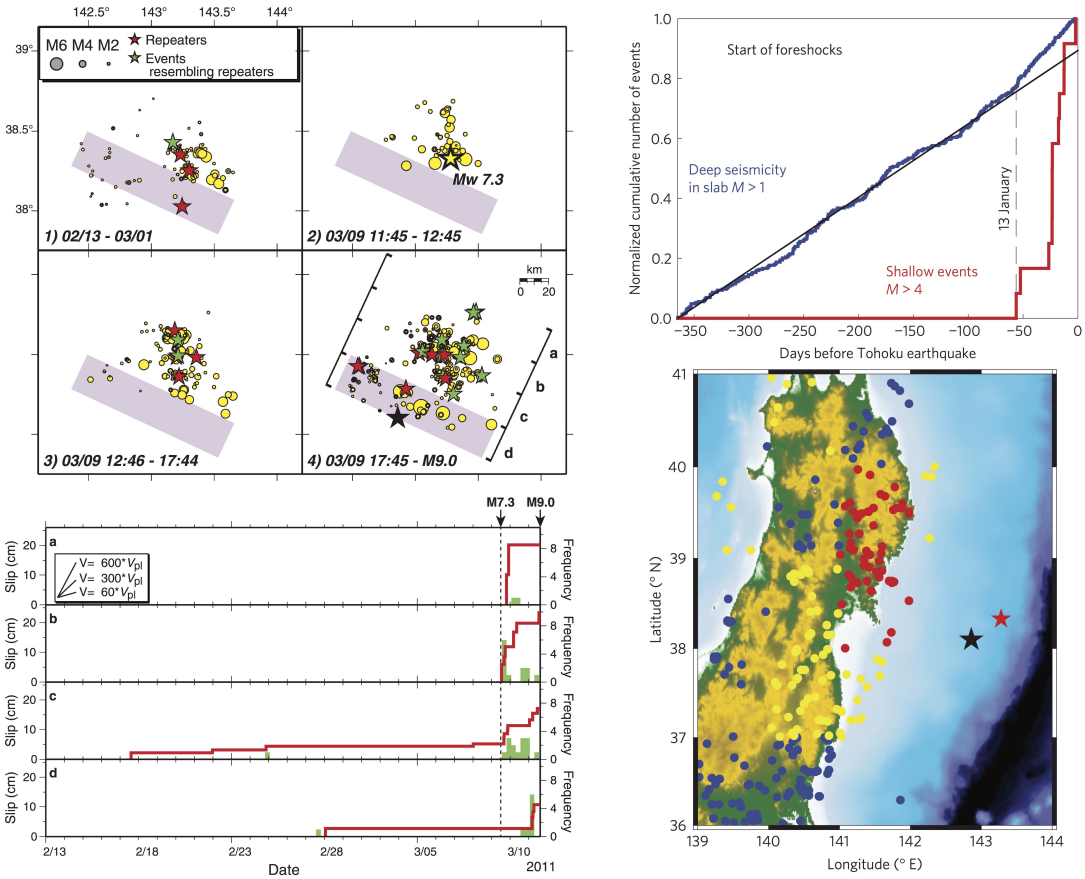

Figure 5.15: *Left* – Space and time distribution of the two sequence of slow slip event that preceded the Tohoku-Oki Earthquake (top) and average cumulative of the quasi-static slip in the areas where the slow slip sequence occurred (Bottom) (after *Kato et al.* [2012]). *Right* – Comparison between the evolution of the depth in-slab seismicity with the evolution of the foreshock of Tohoku-Oki earthquake (Top) and map of the seismic rate variation of deep seismicity (larger than 80 km) between January 2011 and the Tohoku-Oki mainshock (black star), with respect to the seismicity rate observed in the preceding year (bottom), the dot colors represent the variation, blue: decrease, yellow: increase from 0 to 50%, red: increase from 50 to 100%. The red star shows the location of the large foreshock of 9th March Mw 7.3 (after *Bouchon et al.* [2016]).

Chapter 6: Discussion and Perspectives

The present work has raised the challenge of using accelerometric ground motion records of earthquakes of low and moderate moment magnitude to analyze the frictional properties of subduction interfaces. The strong motion records of more than 900 subduction interface earthquakes of Mw ≥ 3.5 have been analyzed in two different subduction zones. We mainly use a method that is based on the analysis of GMPEs residuals and the associated earthquake-to-earthquake comparison of strong ground motion frequency contents.

We have shown that the strong ground motions and their frequency content are depending on the depth of earthquakes, which is in good agreement with the depth dependent subduction fault proposed by *Lay et al.* [2012]. This model has been developed from observations of large megathrust ruptures and our results validate this model with observations of low and moderate Mw earthquakes.

6.1 Methods of earthquake frequency content comparison

Two different methodologies have been explored to compare the strong ground motions frequency contents: the spectral ratio method and the GPMEs residuals analysis method (Chapter 3)

The spectral ratio method has been showed to have a limited applicability due to the effects of magnitude scaling and path attenuations on ground-motions. This methodology has been applied in North Chile and its results have been showed to be consistent with the results obtained by the GPMEs residual method, developed in this study (Chapter 4). Even if this method is applicable to see the differences in the frequency content between shallow and deep seismicity, its application is quite limited for this purpose due to the requirements of proximity and similarity of the

earthquakes to be compared. This left out of the analysis a large volume data. The requirements of proximity also reduce its capability since it makes the method insensitive to the regional variability of earthquakes and ground-motion properties. Despite this limited applicability, different methods based on such spectral ratio technique have given interesting information of source rupture characteristics [e.g. *Ross and Ben-Zion*, 2016; *Yang and Ben-Zion*, 2016].

The GMPEs residual method has showed to be an efficient tool to compare a large number of earthquakes. Since GMPEs residuals are corrected from magnitude scaling and attenuation effects, this method allows to compare the variability of the frequency earthquake contents of large areas. The main limitation of the method comes from the difficulty to have reliable catalogues, metadata and strong motion databases. High quality databases and a large number of data are required to validate a “backbone” GMPE model, reduce the potential biases due to location and depth uncertainties or limit the impact of the error of a given individual data.

This GMPEs residual analysis method has been applied to the study of subduction interfaces. This methodology is however not limited to subduction environments and it can be applied to large strike-slip or normal faults too. This opens a new dimension for this kind of analysis since it may be applied to shallower faults in regions where fault seismic and aseismic behaviors are better constrained. Indeed, some large continental faults are well instrumented and have also generated extended databases of strong ground motions records. These data could also be useful to study the behavior of fault frictional properties during slow slip earthquakes and/or transient slips.

6.2 Depth dependency of the ground motion

The records analysis in North Chile and Japan suggest that at high frequencies, ground motions of interface earthquakes increase with the epicentral depth. These results are consistent with an increment of the roughness of the subduction interface with depth, resulting from the reduction of the asperity size and the surface increase of the areas with conditionally stable behavior in the deeper portion of interface. This model had been proposed by *Lay et al.* [2012]. It is noticeable that this model had been proposed based on observation of megathrust ruptures, but so far, no evidence of the depth-segmentation of the subduction interface have been observed in earthquakes of low and moderate Mw.

The results obtained in Japan also show that the dependency of ground motion on depth is not homogeneous along the subduction trench, which suggest a lateral variability of the frictional properties of the subduction interface. This lateral variability has not been observed in North Chile due to the lack of seismicity between -23° and -21° of latitude, a region where a seismic gap is observed [*Lomnitz*, 2004]. However, differences in the intensities of ground motion have been detected between the ground motion generated at south and north of the gap.

6.3 Lateral segmentation of the subduction interface and regional variability of ground motion

The results obtained in Chile and Japan show a clear regional dependency of the ground motion along the subduction trench. This variability is observed on ground motion intensity. In Japan, regional variations of ground-motions are also associated to different ground motion dependencies on depth. The limited number of earthquakes and the poor seismicity distribution in north Chile do not allow to characterize such regional variations, nevertheless the results obtained in Japan suggest that regional variations occurs abruptly in only few kilometers. Moreover, the correlation of these ground-motions variations with changes of the spatial distribution of the interface seismicity and geometrical variations of the subduction slab, suggest that these variations may be associated to variations of the frictional properties of the subduction interface. These variations may also be correlated with persistent features of the free air gravity anomaly [*Song and Simons*, 2003].

From the point of view of seismic hazard assessment, these results may contribute to the development of GMPEs, which consider regional dependencies of ground motions. Taking into account regional variations this will reduce the uncertainty of the predictions and the standard deviation of the models. Additionally, mixing records of different regions may mask the dependency of the strong motion on parameters such as depth. Such a modeling weakness has been observed in Japan, where the analyzed data do not show a depth dependency larger than the one considered by the GMPE model of *Zhao et al.* [2006] before the regionalization. Therefore regional variations may explain why some GMPEs models do not see depth dependencies of strong ground motions

6.4 Ground motion time variability

A transient variability of ground motions has been detected in Chile before the occurrence of the 2014 Pisagua earthquake Mw 8.1. This transient variability seems to be related with the occurrence of slow slip earthquakes that may have triggered the occurrence of the mainshock [*Socquet et al.*, 2017]. In the case of Japan, where long transient have been detected during the last decade previous to occurrence of the 2011 Tohoku-oki earthquake Mw 9.0 [*Mavrommatis et al.*, 2014; *Yokota and Koketsu*, 2015; *Loveless and Meade*, 2016], the time span of the strong motion database is not long enough large to detect such transients variability. The few records collected two days before the Tohoku earthquake mainshocks show a lower amplitude at high frequency. This observations correspond to a series of earthquakes which occurred near to the mainshock location and which have been identified as part of a sequence of earthquakes occurred during a slow slip earthquake that have preceded the main rupture [*Kato et al.*, 2012]. Surprisingly, the strong ground motion database used is this study does not include interface earthquakes in the few months before to the main rupture. This lack of data limits the characterization of the evolution of strong ground motions in this area. The development of new earthquake classifications procedures [e.g. *Specht et al.*, 2017] may contribute to the identification of additional interface earthquakes and the improvement of our study.

Annex 1: GMPEs Residuals along South America subduction zone

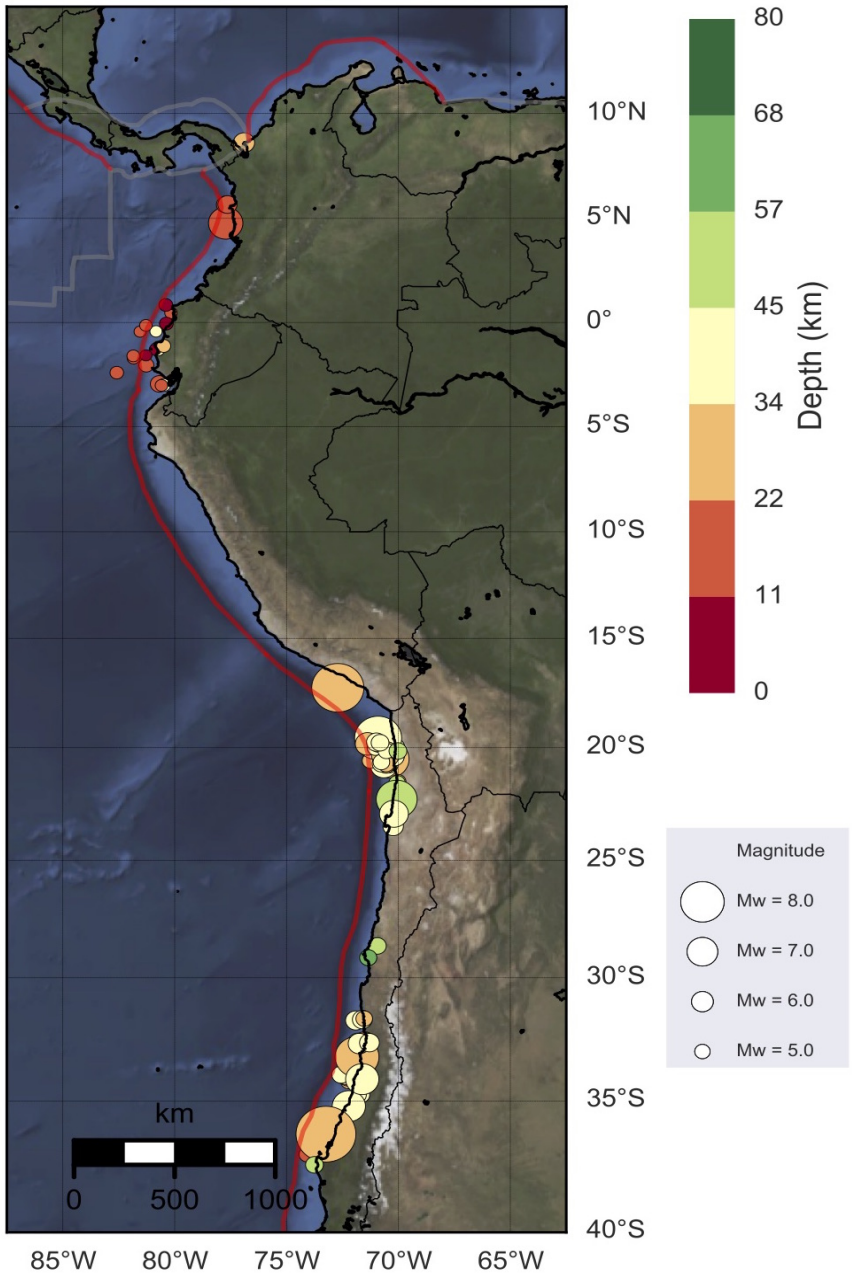

Figure A1.1: Distribution of interface seismicity along South American Subduction zone with Acceleration records for GMPEs Residual analysis (Circles). The size indicates the magnitude and the color indicates the depth

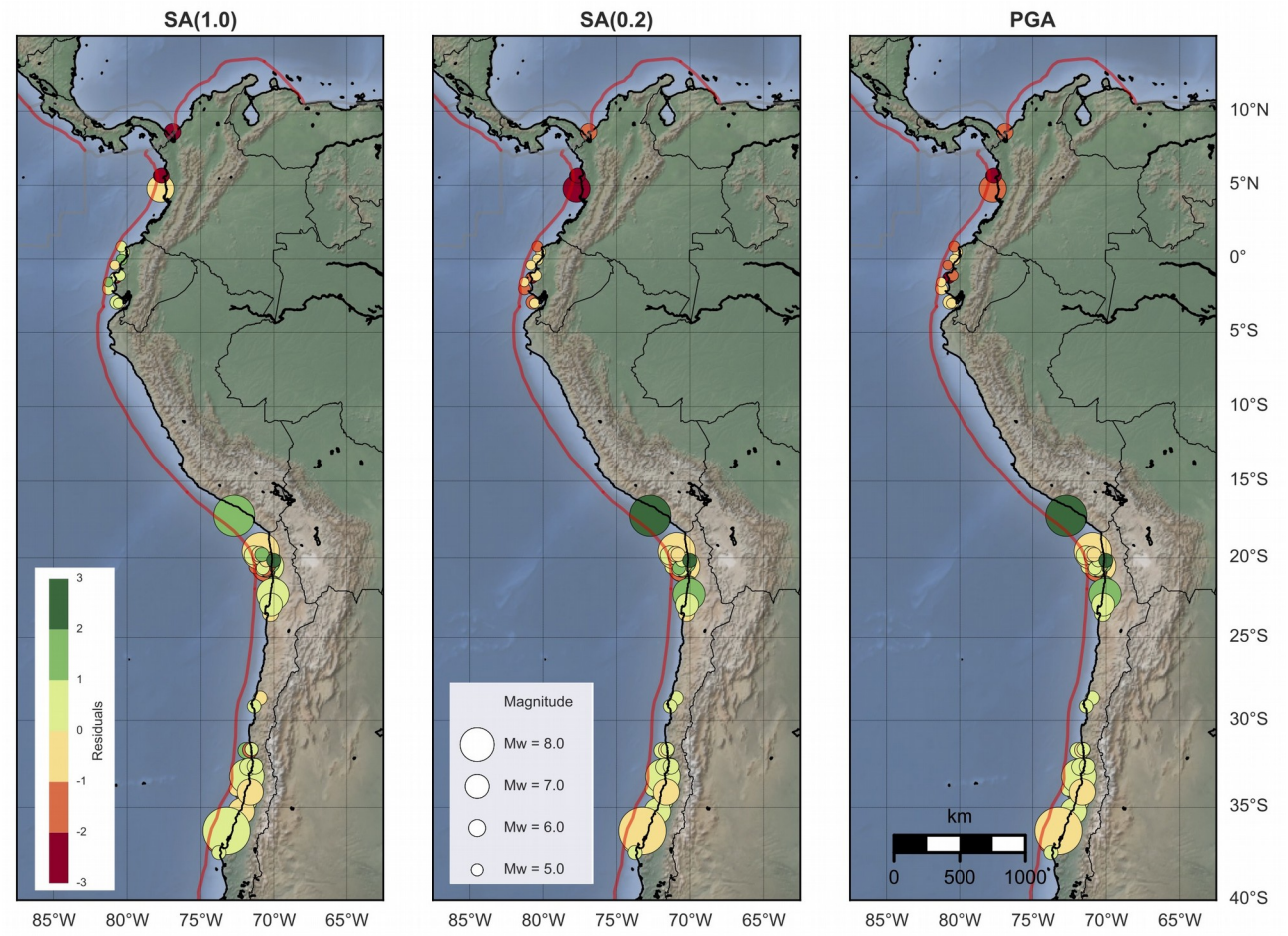

Figure A1.2: Distribution of between-event residuals of *Montalva et al.* [2017] GMPE model, along South American Subduction zone. The circles shows the location of the earthquakes, the size indicates the magnitude and the color indicates the between-event residual value. Seismicity of Ecuador and Colombia generate lower residuals at high frequencies than the seismicity of South Peru and Chile

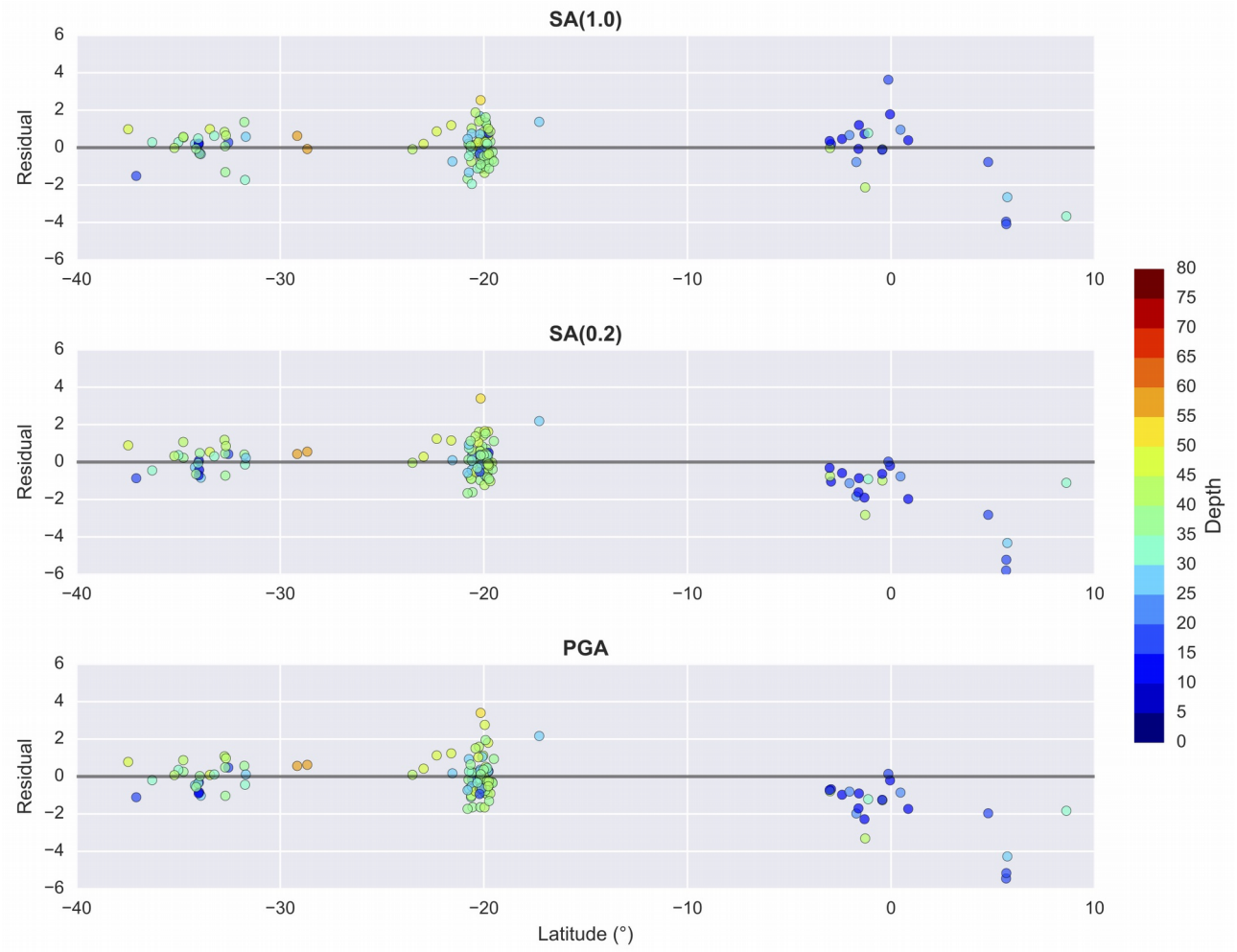

Figure A1.3: Distribution along latitude of between-event residuals of *Montalva et al.* [2017] GMPE model. Colors represent the depth. Earthquakes located at latitudes of Ecuador and Colombia genera the lower residuals at high frequencies than the earthquakes located at south of Peru and Chile. A first order of depth dependency can be appreciated.

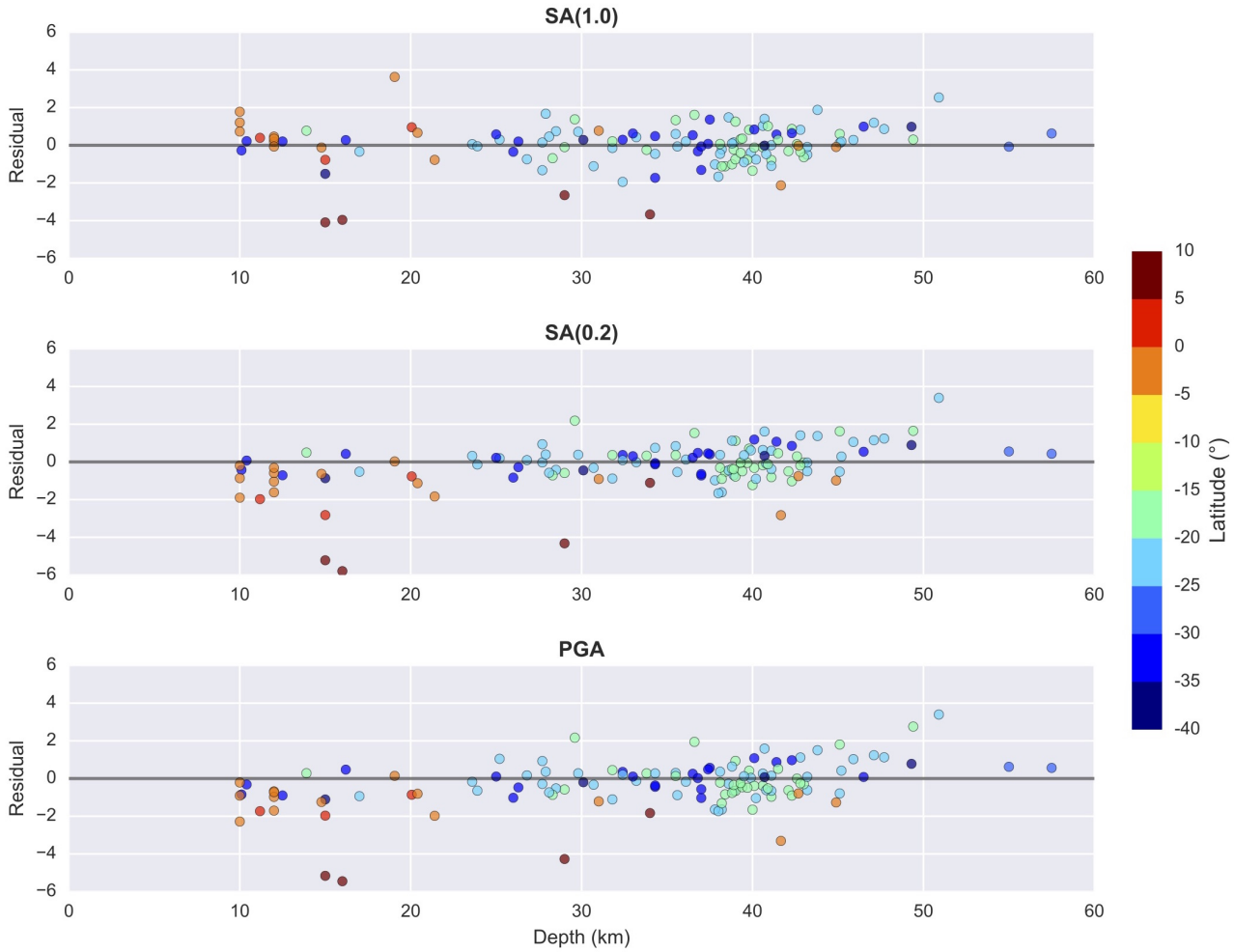

Figure A1.4: Depth distribution of between-event residuals of *Montalva et al.* [2017] GMPE model. Colors represent the Latitude. A depth dependency can be appreciated at high frequencies deeper than 30 km.

Annex 2: GMPEs Residuals along the Japanese subduction zone

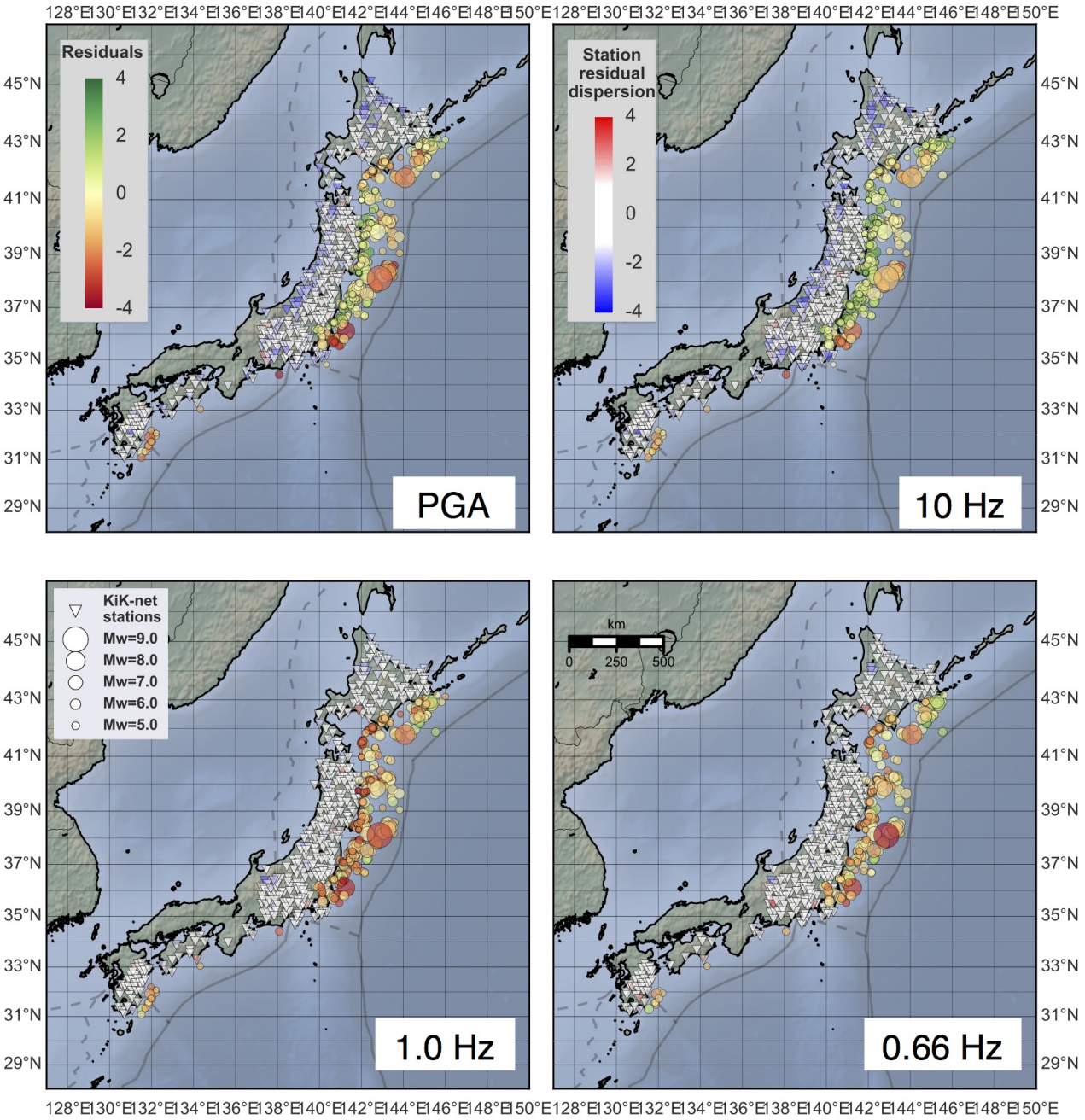

Figure A2.1: Between-event residual distribution of *Zhao et al.* [2006] GMPE model for whole interface catalog contained in the database of *Dawood et al.* [2016], for PGA and Oscillator frequencies of 10, 1.0 and 0.66 Hz. Circles shows the location of the interface seismicity, its size represent the magnitude and colors show the residual value. Inverted triangles show the location of the stations of KiK-net with records and the colors shows the site term (δ_{S2S}).

Annex 3: An 8 month slow slip event triggers progressive nucleation of the 2014 Chile megathrust

Publication in Geophysical Research Letters with participation as coauthor

AGU PUBLICATIONS

Geophysical Research Letters

RESEARCH LETTER
10.1002/2017GL073023

Key Points:
- Westward acceleration of coastal GPS stations 8 months before the main shock reveals a M_w6.5 aseismic slow slip event on fault interface
- Interface foreshocks underwent a diminution of their radiation at high frequency, suggesting a modification in source parameters
- Slow sliding of subduction interface and gradual enlarging of seismic ruptures are the precursory mechanisms leading to the main shock

Supporting Information:
- Supporting Information S1

Correspondence to:
A. Socquet,
anne.socquet@univ-grenoble-alpes.fr

Citation:
Socquet, A., J. P. Valdes, J. Jara, F. Cotton, A. Walpersdorf, N. Cotte, S. Specht, F. Ortega-Culaciati, D. Carrizo, and E. Norabuena (2017), An 8 month slow slip event triggers progressive nucleation of the 2014 Chile megathrust, *Geophys. Res. Lett.*, *44*, 4046–4053, doi:10.1002/2017GL073023.

Received 31 OCT 2016
Accepted 28 MAR 2017
Accepted article online 29 MAR 2017
Published online 8 MAY 2017

An 8 month slow slip event triggers progressive nucleation of the 2014 Chile megathrust

Anne Socquet[1], Jesus Piña Valdes[1], Jorge Jara[1], Fabrice Cotton[2,3], Andrea Walpersdorf[1], Nathalie Cotte[1], Sebastian Specht[2,3], Francisco Ortega-Culaciati[4,5], Daniel Carrizo[5], and Edmundo Norabuena[6]

[1]Université Grenoble Alpes, Université Savoie Mont Blanc, CNRS, IRD, IFSTTAR, ISTerre, Grenoble, France, [2]German Research Centre for Geosciences, GFZ Helmholtz Centre Potsdam, Potsdam, Germany, [3]Institute of Earth and Environmental Science, Potsdam University, Potsdam, Germany, [4]Department of Geophysics, Faculty of Physical and Mathematical Sciences, University of Chile, Santiago, Chile, [5]Advanced Mining Technology Center, Faculty of Physical and Mathematical Sciences, Universidad de Chile, Santiago, Chile, [6]Instituto Geofisico del Peru, Lima, Peru

Abstract The mechanisms leading to large earthquakes are poorly understood and documented. Here we characterize the long-term precursory phase of the 1 April 2014 M_w8.1 North Chile megathrust. We show that a group of coastal GPS stations accelerated westward 8 months before the main shock, corresponding to a M_w6.5 slow slip event on the subduction interface, 80% of which was aseismic. Concurrent interface foreshocks underwent a diminution of their radiation at high frequency, as shown by the temporal evolution of Fourier spectra and residuals with respect to ground motions predicted by recent subduction models. Such ground motions change suggests that in response to the slow sliding of the subduction interface, seismic ruptures are progressively becoming smoother and/or slower. The gradual propagation of seismic ruptures beyond seismic asperities into surrounding metastable areas could explain these observations and might be the precursory mechanism eventually leading to the main shock.

1. Introduction

Some earthquakes have been preceded by an intense foreshock activity [*Bouchon et al.*, 2013; *Schurr et al.*, 2014; *Ruiz et al.*, 2014; *Lay et al.*, 2014; *Bedford et al.*, 2015; *Cesca et al.*, 2016; *Kato et al.*, 2016; *Meng et al.*, 2015; *Hasegawa and Yoshida*, 2015; *Kato et al.*, 2012; *Ozawa et al.*, 2012, *Sato et al.*, 2013; *Bouchon et al.*, 2011] raising the possibility that earthquake forecasting may be achieved through a better understanding of precursory mechanisms. Two concurrent models have been proposed to explain the initiation of seismic rupture [*Dodge et al.*, 1996]. A first model assumes that the accelerated moment release observed before large earthquakes [*Bowman and King*, 2001] is triggered by a slow slip event on the fault interface [*Bouchon et al.*, 2013; *Ruiz et al.*, 2014; *Dodge et al.*, 1996]. Alternatively a slow cascade of failures eventually may trigger the main shock [*Dodge et al.*, 1996].

The precursory phase of earthquakes is most usually studied using seismological data, which is readily available in some regions. Because of limited in situ monitoring combined with lower detection thresholds, geodetic data are less commonly used to study earthquake precursors. Therefore, the link between foreshock activity and associated deformation transients has never been directly established for periods exceeding a few weeks, although it has been observed and suggested [*Obara and Kato*, 2016, and references therein].

The M_w8.1 2014 Iquique earthquake occurred within the North Chile seismic gap, which had not experienced a megathrust rupture since 1877 [*Bejar Pizarro et al.*, 2013; *Metois et al.*, 2016]. The earthquake ruptured an ~ 150 km long portion of the subduction zone [*Schurr et al.*, 2014; *Ruiz et al.*, 2014], in an area that was partially locked before the earthquake [*Bejar Pizarro et al.*, 2013; *Metois et al.*, 2016]. The earthquake was preceded by a series of earthquake swarms beginning in July 2013 [*Schurr et al.*, 2014; *Ruiz et al.*, 2014].

Given the presence of detailed seismic and geodetic monitoring of the Chilean subduction zone, this earthquake is an excellent case to monitor the precursory seismic activity and associated deformation. Previous studies focused mostly on the 20 days immediately preceding the earthquake when a strong transient signal occurred [*Schurr et al.*, 2014; *Ruiz et al.*, 2014; *Lay et al.*, 2014; *Bedford et al.*, 2015; *Cesca et al.*, 2016]. Nevertheless, a debate remains on the mechanisms leading to this foreshock activity, notably on the existence or not of aseismic slip preceding the earthquake. Apart from the study of the foreshock

AGU Geophysical Research Letters 10.1002/2017GL073023

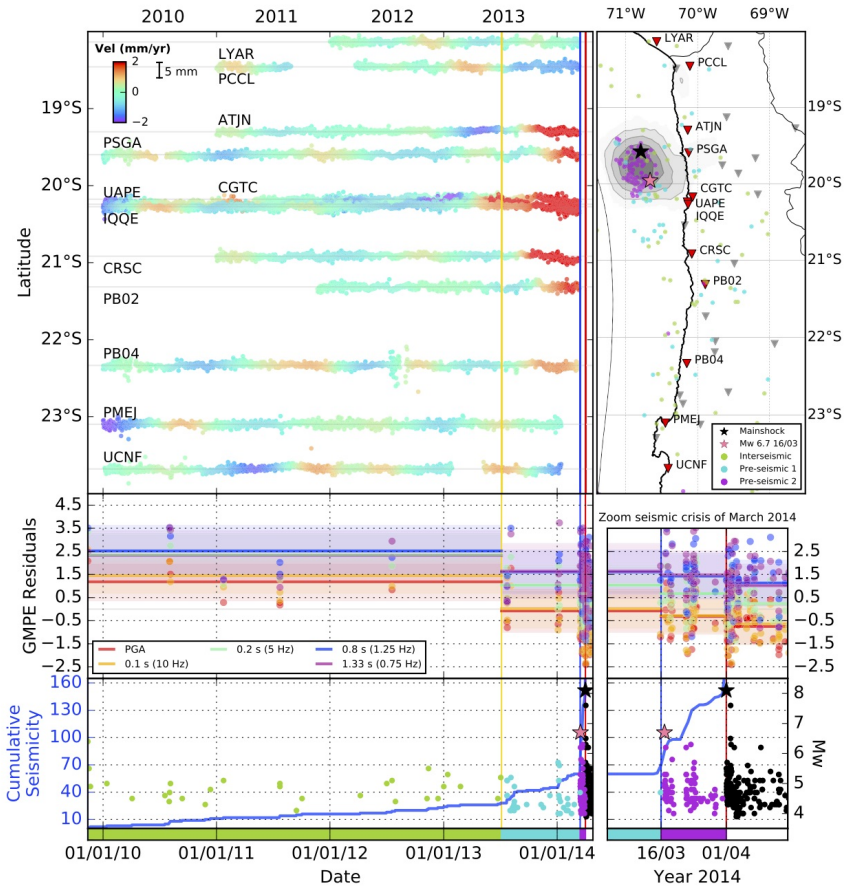

Figure 1. Preseismic ground deformation and foreshock frequency content over a 4 year period, before the 1 April 2014 megathrust in North Chile. (top right) Map of seismicity: foreshock activity color coded by periods, epicenters of M_w8.1 main shock and M_w6.7 foreshock are indicated by black and pink stars, M_w8.1 slip distribution with 1 m contours. Triangles indicate the location of GPS stations, the red ones being stations whose time series are shown to the left. (top left) Trench perpendicular, detrended time series of coastal cGPS, sorted by latitude. Colors show the variation of average GPS velocities computed in 6 month sliding windows. (middle left) Frequency content evolution of interface foreshocks. Lines show average values of normalized residuals with respect to GMPE model [*Abrahamson et al.*, 2015] at high (reddish) and low (bluish) frequencies computed for each time period. Standard deviation of the model is shown by shaded colors, while dots show single earthquakes residuals. (bottom left) Foreshock activity over time (dots). Blue curve shows the cumulative number of earthquakes. Red, blue, and yellow vertical lines separate the three preseismic periods and depict respectively the M_w8.1 main shock on 1 April 2014, the M_w6.7 foreshock of 16 March 2014 that is followed by an increase of seismicity rate 2 weeks before the main shock, and the July 2013 swarm.

sequence [*Schurr et al.*, 2014; *Ruiz et al.*, 2014; *Lay et al.*, 2014; *Bedford et al.*, 2015; *Cesca et al.*, 2016; *Kato et al.*, 2016; *Meng et al.*, 2015], very little is known about any potential long-term precursors, in particular in terms of deformation.

Here we use geodetic and seismological observations to document the precursory deformation and foreshock frequency content for the 2 years preceding the Iquique earthquake.

2. Data and Methods

GPS data from several networks monitoring the North Chile subduction (IPOC, LIA Montessus de Ballore, ISTerre, Caltech Andean Observatory, IGS) have been processed in double differences, including

AGU Geophysical Research Letters 10.1002/2017GL073023

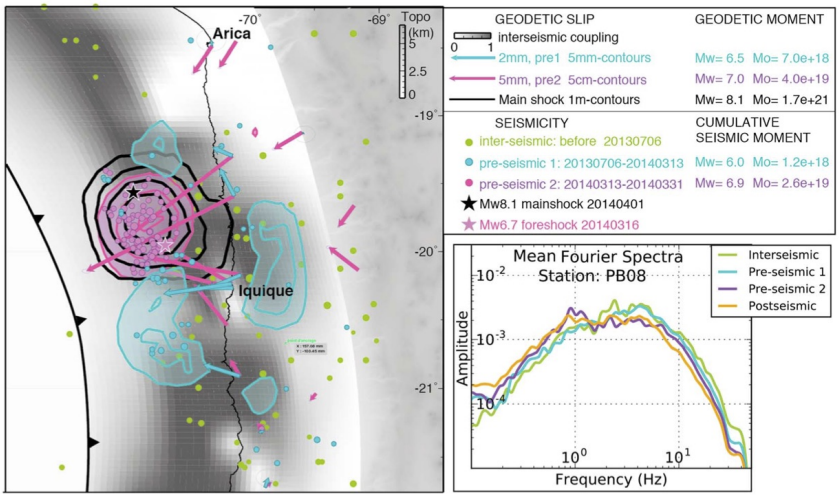

Figure 2. (left) Long- and short-term slip events (in blue and purple, respectively), preceding the M_w8.1 main shock, superimposed on the interseismic coupling distribution [*Metois et al.*, 2016] in gray, and the coseismic slip 1 m contours in black. Foreshock seismic activity for the same periods is also shown (in blue, purple, and green, $M_w > 4$). Epicenters of the main shock and the M_w6.7 foreshock are shown as black and pink stars. (right inset) Mean Fourier spectra computed for interface earthquakes ($5.1 < M_w < 5.2$) grouped into four different time periods: interseismic in green, preseismic 1 in cyan, preseismic 2 in purple, and postseismic in orange. Station PB08 being located at an even distance of the earthquakes studied, the computed variations in Fourier spectra shapes should be unaffected by variations in attenuation but, instead, characterize earthquake's source.

tropospheric delays and gradients [*Boehm et al.*, 2006], and mapped into the ITRF 2008 [*Altamimi et al.*, 2011] (see supporting information for further details). The trend, as well as seasonal signals and common modes were removed from the time series. In order to study the long-term transient in our time series, we excluded data after 15 March 2014 (when a strong preseismic signal occurred) and then computed the average velocity variations, by fitting a linear regression in a 6 month sliding window of the detrended and denoised time series (Figure 1). In a second step, we compute the displacement during two preseismic periods (preseismic 1: July 2013 to 13 March 2014 and preseismic 2: 14 March 2014 to 31 March 2014), by taking as a reference the mean interseismic loading trend before July 2013 (Figures S2 and S3).

The surface deformation fields were then inverted to retrieve the distribution of slip on the subduction interface (Figure 2), by discretizing it as a series of dislocations buried in a layered elastic half space [*Wang et al.*, 2003]. A Laplacian smoothing has been applied; the best compromise between model roughness and data-model misfit has been chosen [*Jonsson et al.*, 2002]. The power of our data to constrain the slip on the interface [*Loveless and Meade*, 2011] is high from 15 km depth to more than 70 km depth in general (Figures S4–S6). Although the details of slip distributions can vary from one inversion to the other, the estimated geodetic moment of preseismic slow slip events vary within less than 10% (Figure S7).

To complement the geodetic analysis, we analyzed the frequency content of interface seismicity. The interface seismicity catalog (Figure S9) was compiled using the GEOFON moment tensor catalog and the Global CMT catalog. We use a data driven algorithm to automatically determine focal mechanism clusters with similar style of faulting (strike, rake, and dip, Figure S10).

The horizontal response and Fourier spectra of interface earthquakes were computed from the acceleration records of stations belonging to the IPOC network (Figure S9). The raw acceleration records were demeaned and tapered, and a zero pad has been applied at the beginning and the end before being

AGU Geophysical Research Letters 10.1002/2017GL073023

used to compute the spectra [*Boore et al.*, 2012; *Chiou et al.*, 2008]. The response spectra were also computed for each horizontal component of the records following the *Nigam and Jennings* [1969] method with a damping of 5%. Finally, both Fourier and response horizontal spectra were computed as the geometrical mean of the two horizontal response spectra at each station. Fourier source spectra depend on source, propagations, and site effects. Also, there is then a need to deconvolve the records from propagation and site properties to analyze earthquake source properties. In order to compare the shape of Fourier spectra during the different time span studied, we selected three IPOC stations located at equal distance from the earthquakes swarm to get rid of the attenuation effects and performed our analysis on earthquakes within a 0.1 magnitude range (Figures S11 and 2 (right inset)).

Second, we compared the measured ground accelerations, at different frequencies, with the response spectra predicted by the recent Ground Motion Prediction Equation (GMPE) developed for subduction interface earthquakes by *Abrahamson et al.* [2015]. *Abrahamson et al.*'s [2015] model is recognized as one of the leading models to predict ground motions in subduction areas and has been recently selected for the Global Earthquake Model [*Stewart et al.*, 2015]. The analysis of the obtained residuals confirmed that this model is well suited for our data set (see supporting information for details). Between-event residuals were computed, for each frequency (0.75 Hz, 1 Hz, 1.25 Hz, 5 Hz, 10 Hz, and PGA) and each earthquake, as the difference between the median of the observations of the given earthquake and the median of the model [*Abrahamson and Youngs*, 1992]. The Ground Motion Prediction Equations is acting here as a backbone model which takes into account first-order magnitude and propagation effects. The analysis of relative time and spatial variations of between-event residuals allow us to compare the source effects of earthquakes with various magnitude and locations [*Strasser et al.*, 2010, *Atik et al.*, 2010; *Youngs et al.*, 1995]. It has been shown that response between-event residuals are fully correlated with "classical" Fourier stress drops [*Bindi et al.*, 2007], so there is no information lost using response spectra and GMPEs compared to a more classical stress drop analysis. The between-event residuals were then organized as a function of time, space, and magnitude, in order to represent their variations and temporal evolution during the different periods before or after the main shock (Figures 3 and S15).

3. Results

3.1. Precursory Slow Slip and Associated Seismicity

We detected a westward acceleration of some permanent GPS stations with respect to the average interseismic velocity (Figure 1). This acceleration begins ~8 months before the main shock and affects mostly coastal stations located within an area 100 km south of the M_w8.1 source, which was also affected by foreshock seismicity during the same period (Figure 1, blue dots). For comparison, during the preceding interseismic period, the seismicity is evenly distributed within the deeper part of the seismogenic zone (green dots in Figures 1 and 2). Inversion of these 8 month preseismic displacements (from July 2013 to mid-March 2014) suggests that a slow slip event occurred on the subduction interface (Figure 2, blue contours), surrounding the main shock slip patch. South of the main shock, the slow slip occurs in a zone of low coupling during the interseismic period [*Metois et al.*, 2016], while it rather affects areas characterized by intermediate locking downdip and north of the main shock. The geodetic precursor is collocated with long-term foreshock activity (Figure 2, blue dots). The comparison between geodesy and seismology shows that this long-term preseismic signal is at least 80% aseismic in nature; the cumulative seismic moment release (1.2×10^{18} N m) representing 17 to 19% of the slip derived from GPS observations (6.4 to 7.0×10^{18} N m).

On 16 March 2014, a M_w6.7 intraplate earthquake [*Cesca et al.*, 2016] occurred 2 weeks before the main shock, north of the creeping area (pink star, Figure 2). This foreshock is the largest of the whole sequence. It is followed by an abrupt increase of the seismicity rate and associated *b* value [*Schurr et al.*, 2014], some of them in the upper plate, and most of them on the subduction interface [*Cesca et al.*, 2016], affecting the area that later ruptured during the M_w8.1 megathrust. During this 15 day preseismic period, GPS stations were affected by a large deformation transient [*Ruiz et al.*, 2014] (Figure 2). This preseismic slip measured by geodesy resembles the one released seismically: the location and shape of geodetic slip mimics the spatial distribution of epicenters (Figure 2, purple contours and dots) [*Schurr et al.*, 2014], while the seismic moment is 65–67% of the geodetic moment (the remaining 33–35% is aseismic).

AGU Geophysical Research Letters 10.1002/2017GL073023

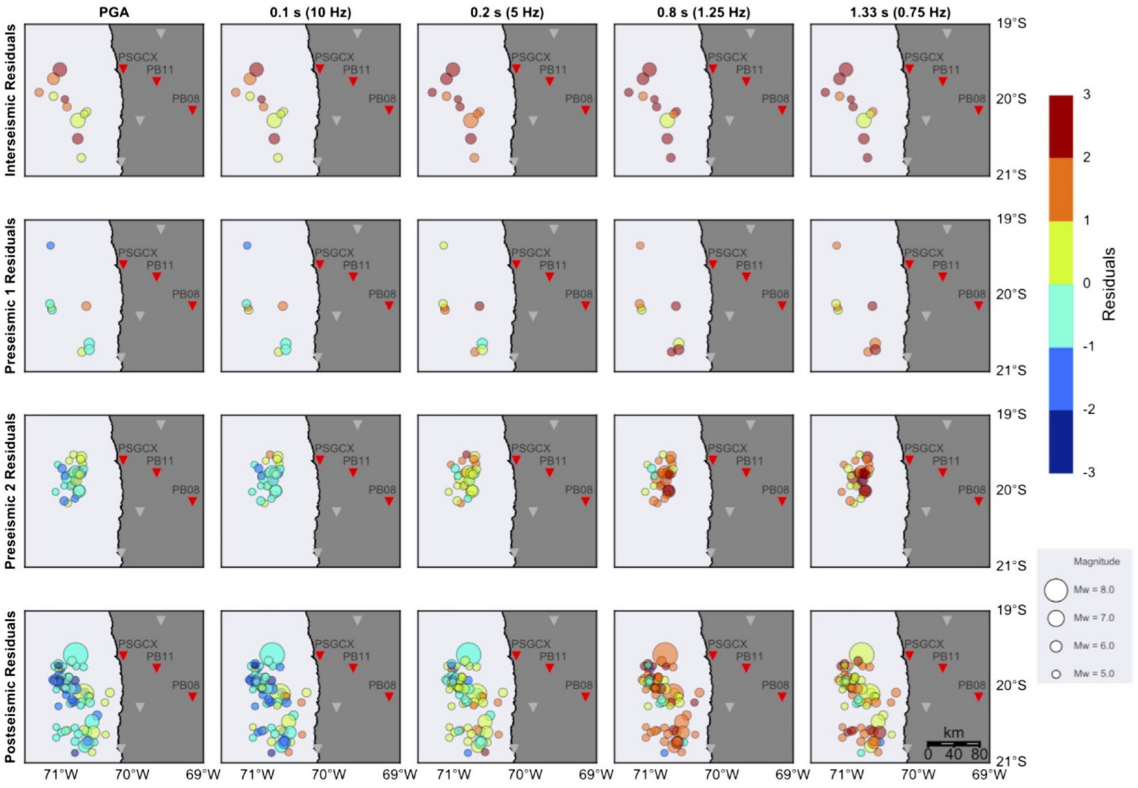

Figure 3. Time-space evolution of between-event residuals at the different frequency values shown in Figure 1 (middle row). Residuals are normalized by the standard deviation of the GMPE model. Therefore, average temporal changes can be considered significant from one standard deviation.

3.2. Evolution of Interface Earthquakes Ground Motions

To complement these findings, we analyzed the frequency content of interface seismicity [*Specht et al.*, 2017; *Strasser et al.*, 2009]. Mean Fourier spectra at stations equidistant to the seismic crisis events show a consistent temporal decrease in high frequencies from interseismic to preseismic and, eventually, postseismic periods (Figures 2 and S11).

The comparison of the measured accelerations for interface earthquakes with respect to the ground motion model [*Abrahamson et al.*, 2015] provides an independent assessment of ground motion temporal variations [*Händel et al.*, 2014]. The time, space, and magnitude dependencies of between-event residuals have been analyzed in order to search for a potential evolution of the source characteristic (Figures 3 and S15). Measured residuals do not depend on earthquakes magnitude (as expected given the fact that the ground motion predictive equation acts as a backbone model correcting for magnitude and propagation effects). However, at frequencies of 5 Hz and above, a clear clustering of between-event residuals as a function of their time of occurrence is observed (Figure S15), indicating a diminution of high-frequency energy release from interseismic period to preseismic period and later. Also, the temporal evolution of residuals differs from one frequency band to the other: at frequencies below 1.25 Hz residuals remain more or less constant with time, while at higher frequencies (5 Hz and above) residuals decrease between interseismic period to preseismic and postseismic periods (Figures 1–3). During the second preseismic period (i.e., during the 15 days between the largest foreshock and the main shock) and the postseismic period, interface earthquakes show no significant change of their energy radiation.

AGU Geophysical Research Letters 10.1002/2017GL073023

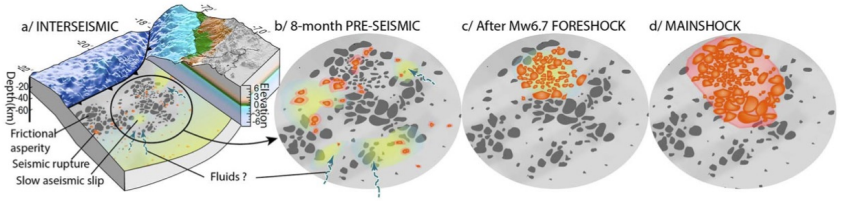

Figure 4. Schematic interpretation of the precursory phase of M_w8.1 earthquake. (a) During the interseismic phase, the subduction interface slowly creeps (yellow) at depth and in low coupling areas, where frictional asperities are sparse. The rupture of small frictional asperities resisting this slow slip generates the background seismicity (red). (b) Eight months before the main shock, slow slip accelerates in the seismogenic zone (maybe facilitated by fluids migration), around the area ruptured by the main shock. Seismic ruptures start to propagate into the conditionally stable area surrounding the frictional asperities (light red). (c) After the largest foreshock on 16 March (M_w6.7), slow slip goes on but is superimposed onto a rough seismic signal generated by the postseismic cascade. (d) On 1 April 2014, M_w8.1 earthquake ruptures a large portion of the subduction interface, breaking both frictional asperities (red) and surrounding conditionally stable areas (light red).

These two independent assessments of interface earthquake ground motions indicate a reduction of the high-frequency radiation, which is coincident with the preseismic acceleration in GPS velocities 8 months before the main shock.

4. Discussion

Our results indicate that a geodetic precursor occurred simultaneously with an identified increase in the seismicity rate (Figure 1, bottom row), and a decrease in the *b* value [*Schurr et al.*, 2014]. Such observations can be modeled as an aseismic slow slip on the subduction interface collocated with long-term foreshock activity (Figure 2, blue dots). This is consistent with the slow sliding of conditionally stable area on the subduction interface, spread out by sparse, small seismic asperities [*Hetland and Simons*, 2010], the seismic activity arising from the response of seismic asperities to the aseismic forcing.

Seismic radiation spectra of interface events have been proposed, on average, to be representative of the different frictional regimes of a subduction interface [*Scholz*, 1998; *Lay et al.*, 2012]; regions of unstable sliding can have large slip but generate modest amounts of short-period radiation upon failure, while smaller patchy regions of unstable sliding produce coherent short-period radiation when loaded to failure by creep of conditionally stable surrounding regions [*Lay et al.*, 2012; *Meng et al.*, 2015].

The reduction in high-frequency radiated energy often indicates a reduction in earthquake stress drop (i.e., a decrease of corner frequency). This phenomenon might be explained either by (a) smoother ruptures [*Radiguet et al.*, 2009], (b) lower rupture velocities, or (c) increasing high-frequency attenuation. Given the foreshocks sequence does not migrate through time, a change in attenuation characteristics over such a short period of time seems unlikely. Rapid fluid migration within the fault zone may change the attenuation locally, within the few hundred meters of the damaged fault zone (high pore fluid pressures are accompanied by very low Qs/Qp ratios—0.1 to 0.4 for saturated basalt that are primarily due to increased shear attenuation [*Tompkins and Christensen*, 2001]). However, once integrated over the whole path followed by seismic waves through continental crust (a few hundred meters with increased attenuation versus tens of kilometers with no change), this local change in attenuation accounts for a minor part of the overall attenuation and only at large frequencies (higher than 15–20 Hz). It will be considered as part of the source, distance independent, high-frequency (kappa) attenuation. Therefore, the observed change of frequency content at 5–10 Hz rather seems related to a modification of the earthquake source parameters, such as a wider rupture area or slower rupture velocity. This is also compatible with the observed reduction in *b* value during the precursory time period, implying an increasing proportion of large to small earthquakes. Such a decrease in *b* value has been proposed as a precursor to major macrofailure [*Smith*, 1981]. Our observations suggest that a slow aseismic forcing that started 8 months before the main shock triggerred an increased number of seismic events together with a modification of the earthquake frequency content, interpreted as a widening of rupture surfaces [*Lay et al.*, 2012]. This suggests a progressive expansion of failures into the conditionally stable areas surrounding small seismic asperities, in a mechanism that will eventually lead to the main rupture nucleation (Figure 4b).

AGU Geophysical Research Letters 10.1002/2017GL073023

Two weeks before the main shock, the largest foreshock of the sequence triggered an increased deformation, seismicity, and *b* value. This seismicity, which is much more focused both spatially and temporally, might have been triggered by the M_w6.7 foreshock that induced a significant increase of the Coulomb stress in the area. The seismicity and associated slow slip observed within the 15 days before the main shock may therefore result from a regular aftershock sequence and associated afterslip following the M_w6.7 event, overprinting the preexisting slow aseismic slip (Figure 4c).

On 1 April 2014, the M_w8.1 megathrust nucleates immediately north of the seismicity surge, in an area of increased stress resulting from adjacent preseismic slip. The maximum slip (Figure 2, black contours) occurs close to the area that started to slip before the main shock (pink), slightly downdip associated foreshock activity (pink dots), including repeating earthquakes [*Meng et al*., 2015]. However, the rupture extends deeper to areas that were fully locked during the interseismic period [*Metois et al*., 2016]. To the south, the rupture stops abruptly when it reaches the metastable areas affected by the long-term aseismic precursor (blue).

5. Conclusions

These observations confirm that a long-term aseismic slip of the subduction interface led to the nucleation of the M_w8.1 Iquique megathrust earthquake. During the interseismic period, the seismicity was evenly distributed within the deeper part of the seismogenic zone (green dots on Figures 1 and 2) and ruptured small frictional asperities in response to deep interplate aseismic sliding (Figure 4). Eight months before the main shock, this slow sliding of plate interface started to accelerate within the seismogenic zone. South of the main shock this precursory creep occurs in an area characterized by little interseismic coupling, while downdip and north of the main shock, the slow slip affects more coupled areas (Figure 2) [*Metois et al* .,2016] and may be seen as the slow rupture of locked patches surrounding the main shock. Small seismic asperities scattered in this area ruptured repeatedly [*Meng et al*., 2015; *Lay et al*., 2012]. The change in the earthquake frequency content during the foreshock sequence (a reduction of the stress drop) suggests that seismic failures widen progressively, decelerate, and start to extend into the slowly sliding, conditionally stable areas surrounding frictional asperities. This process can be seen as the start of the precursory phase that will eventually lead to the megathrust rupture.

The simultaneous occurrence of slip acceleration, increased seismic activity, and the slow decrease of the high-frequency radiations of foreshocks may provide a way to detect the preparation of great earthquakes. Identifying aseismic slip combined with changes in associated earthquake spectra may therefore significantly help to mitigate seismic hazard at plate boundaries.

Acknowledgments
We are very grateful to Departamento de Geofísica de la Universidad de Chile (DGF) (http://www.dgf.uchile.cl/), Centro Sismológico Nacional de Chile (CSN) (www.sismologia.cl), International Plate Boundary Observatory Chile (IPOC) (http://geofon.gfz-potsdam.de/waveform/), LIA "Montessus de Ballore" International Laboratory (www.lia-mb.net), Central Andean Tectonic Observatory Geodetic Array (CAnTO) (http://www.tectonics.caltech.edu/resources/continuous_gps.html), and Instituto Geofisico del Peru for making raw GPS and strong motion data available. This work has been supported by PNTS-2014-08, LabeX OSUG@2020, SMINGUE, IRD AO-Sud, and INSU-Aléas grants. J.P.V. and J.J. acknowledge support provided by CONICYT through "Becas Chile" PhD fellowships. F.O. acknowledges support from Proyecto Fondecyt 11140904 (CONICYT). The authors warmly thank J.M. Nocquet for making PYACS software available. Thank you to J. Hollingsworth for editing the English writing. This work benefited from fruitful discussion with PY. Bard, C. Beauval, D. Bindi, M. Bouchon, R. Bürgmann, M. Métois, G. Montalva, D. Marsan, and J. Ruiz among others.

References

Abrahamson, N., N. Gregor, and K. Addo (2015), BC Hydro ground motion prediction equations for subduction earthquakes, *Earthquake Spectra*, doi:10.1193/051712EQS188MR.

Abrahamson, N. A., and R. R. Youngs (1992), A stable algorithm for regression analyses using the random effects model, *Bull. Seismol. Soc. Am.*, *82*, 505–510.

Altamimi, Z., X. Collilieux, and L. Métivier (2011), ITRF2008: An improved solution of the international terrestrial reference frame, *J. Geod. 85*, 457–473, doi:10.1007/s00190-011-0444-4.

Atik, L. A., N. Abrahamson, J. J. Bommer, F. Scherbaum, F. Cotton, and N. Kuehn (2010), The variability of ground-motion prediction models and its components, *Seismol. Res. Lett.*, *81*(5), 794–801, doi:10.1785/gssrl.81.5.794

Bedford, J., M. Moreno, B. Schurr, M. Bartsch, and O. Oncken (2015), Investigating the final seismic swarm before the Iquique-Pisagua 2014 M_w8.1 by comparison of continuous GPS and seismic foreshock data, *Geophys. Res. Lett.*, *42*, 3820–3828, doi:10.1002/2015GL063953.

Bejar Pizarro, M., A. Socquet, R. Armijo, D. Carrizo, J. Genrich, and M. Simons (2013), Andean structural control on interseismic coupling in the North Chile subduction zone, *Nat. Geosci.*, doi:10.1038/NGEO1802.

Bindi, D., S. Parolai, E. Görgün, H. Grosser, C. Milkereit, M. Bohnhoff, and E. Durukal (2007), ML scale in northwestern Turkey from 1999 Izmit aftershocks: Updates, *Bull. Seismol. Soc. Am.*, *97*(1B), 331–338, doi:10.1785/0120060071.

Boehm, J., B. Werl, and H. Schuh (2006), Troposphere mapping functions for GPS and very long baseline interferometry from European Centre for Medium-Range Weather Forecasts operational analysis data, *J. Geophys. Res. 111*, B02406, doi:10.1029/2005JB003629.

Boore, D. M., A. A. Sisi, and S. Akkar (2012), Using pad stripped acausally filtered strong motion data, *Bull. Seismol. Soc. Am.*, *102*(2), 751–760.

Bouchon, M., H. Karabulut, M. Aktar, S. Özalaybey, J. Schmittbuhl, and M. P. Bouin (2011), Extended nucleation of the 1999 M_w 7.6 Izmit earthquake, *Science*, *331*(6019), 877–880, doi:10.1126/science.1197341.

Bouchon, M., V. Durand, D. Marsan, H. Karabulut, and J. Schmittbuhl (2013), The long precursory phase of most large interplate earthquakes, *Nat. Geosci.*, *6*(4), 299–302, doi:10.1038/NGEO1770.

Bowman, D. D., and G. C. P. King (2001), Accelerating seismicity and stress accumulation before large earthquakes, *Geophys. Res. Lett.*, *28*, 4039–4042, doi:10.1029/2001GL013022.

Cesca, S., F. Grigoli, S. Heimann, T. Dahm, M. Kriegerowski, M. Sobiesiak, C. Tassara, and M. Olcay (2016), The M_w 8.1 2014 Iquique, Chile, seismic sequence: A tale of foreshocks and aftershocks, *Geophys. J. Int.*, *204*(3), 1766–1780.

Chiou, B., R. Darragh, N. Gregor, and W. Silva (2008), NGA project strong-motion database, *Earthquake Spectra*, *24*(1), 23–44.
Dodge, D. A., G. C. Beroza, and W. L. Ellsworth (1996), Detailed observations of California foreshock sequences: Implications for the earthquake initiation process, *J. Geophys. Res.*, *101*, 22,371–22,392, doi:10.1029/96JB02269.
Händel, A., S. Specht, N. M. Kühn, and F. Scherbaum (2014), Mixtures of ground-motion prediction equations as backbone models for a logic tree: An application to the subduction zone in Northern Chile, *Bull. Earthq. Eng.*, *13*(2), 483–501, doi:10.1007/s10518-014-9636-7.
Hasegawa, A., and K. Yoshida(2015), Preceding seismic activity and slow slip events in the source area of the 2011 M_w 9.0 Tohoku-Oki earthquake: A review, *Geosci. Lett.*, *2*(1), 6, doi:10.1186/s40562-015-0025-0.
Hetland, E. A., and M. Simons (2010), Post-seismic and interseismic fault creep: II. Transient creep and interseismic stress shadows on megathrusts, *Geophys. J. Int.*, *181*, 99–112, doi:10.1111/j.1365-246X.2009.04482.x.
Jonsson, S., H. Zebker, P. Segall, and F. Amelung (2002), Fault slip distribution of the 1999 M_w 7.1 hector mine, California, earthquake, estimated from satellite radar and GPS measurements, *Bull. Seismol. Soc. Am.*, *92*(4), 1377–1389, doi:10.1785/0120000922.
Kato, A., K. Obara, T. Igarashi, H. Tsuruoka, S. Nakagawa, and N. Hirata (2012), Propagation of slow slip leading up to the 2011 M_w 9.0 Tohoku-Oki earthquake, *Science*, *335*(2), 705–708, doi:10.1126/science.1215141.
Kato A. et al. (2016), Accelerated nucleation of the 2014 Iquique, Chile M_w 8.2 earthquake, *Nat. Sci. Rep.*, *6*, 24792, doi:10.1038/srep24792.
Lay, T., H. Kanamori, C. J. Ammon, K. D. Koper, A. R. Hutko, L. Ye, H. Yue, and T. M. Rushing (2012), Depth-varying rupture properties of subduction zone megathrust faults, *J. Geophys. Res.*, *117*, B04311, doi:10.1029/2011JB009133.
Lay, T., H. Yue, E. E. Brodsky, and C. An (2014), The 1 April 2014 Iquique, Chile, M_w 8.1 earthquake rupture sequence, *Geophys. Res. Lett.*, *41*, 3818–3825, doi:10.1002/2014GL060238.
Loveless, J. P., and B. J. Meade (2011), Spatial correlation of interseismic coupling and coseismic rupture extent of the 2011 M_W = .0 Tohoku Oki earthquake, *Geophys. Res. Lett.*, *38*, L17306, doi:10.1029/2011GL048561.
Meng, L., H. Huang, R. Bürgmann, J. P. Ampuero, and A. Strader (2015), Dual megathrust slip behaviors of the 2014 Iquique earthquake sequence, *Earth Planet. Sci. Lett.*, *411*, 177–187, doi:10.1016/j.epsl.2014.11.041
Metois, M., C. Vigny, and A. Socquet (2016), Interseismic coupling, megathrust earthquakes and seismic swarms along the Chilean subduction zone (38°–18°S), *Pure Appl. Geophys.*, *194*(3), 1283–1294, doi:10.1007/s00024-016-1280-5.
Nigam, N. C., and P. C. Jennings (1969), Calculation of response spectra from strong-motion earthquake records, *Bull. Seismol. Soc. Am.*, *59*(2), 909–922.
Obara, K., and A. Kato (2016), Connecting slow earthquakes to huge earthquakes, *Science*, *353*(6296), 253–257, doi:10.1126/science.aaf1512.
Ozawa, S., T. Nishimura, H. Munekane, H. Suito, T. Kobayashi, M. Tobita, and T. Imakiire (2012), Preceding, coseismic, and postseismic slips of the 2011 Tohoku earthquake Japan, *J. Geophys. Res.*, *117*, B07404, doi:10.1029/2011JB009120.
Radiguet, M., F. Cotton, I. Manighetti, M. Campillo, and J. Douglas (2009), Dependency of near-field ground motions on the structural maturity of the ruptured faults, *Bull. Seismol. Soc. Am.*, *99*(4), 2572–2581.
Ruiz, S., M. Metois, A. Fuenzalida, J. Ruiz, F. Leyton, R. Grandin, C. Vigny, R. Madariaga, and J. Campos (2014), Intense foreshocks and a slow slip event preceded the 2014 Iquique M_w 8.1 earthquake, *Science*, doi:10.1126/science.1256074.
Sato, T., S. Hiratsuka, and J. Mori (2013), Precursory seismic activity surrounding the high-slip patches of the 2011 M_w 9.0 Tohoku-Oki earthquake, *Bull. Seismol. Soc. Am.*, *106*(6), 3104–3114, doi:10.1785/0120130042.
Scholz, C. H., Earthquakes and friction laws, *Nature*, *391*, 37–42 (1998) doi:10.1038/34097.
Schurr, B., et al. (2014), Gradual unlocking of plate boundary controlled initiation of the 2014 Iquique earthquake, *Nature*, doi:10.1038/nature13681.
Smith, W. D., The *b*-value as an earthquake precursor, *Nature, 289*, 136–139 (1981) doi:10.1038/289136a0.
Specht, S., O. Heidbach, F. Cotton, and A. Zang (2017), Data-driven earthquake focal mechanism cluster analysis, *Sci. Tech. Rep. STR; 17/01*, Potsdam : GFZ German Res. Cent. for Geosci., doi:10.2312/GFZ.b103-17012.
Stewart, J. P., J. Douglas, M. Javanbarg, Y. Bozorgnia, N. A. Abrahamson, D. M. Boore, K. W. Campbell, E. Delavaud, M. Erdik, and P. J. Stafford (2015), Selection of ground motion prediction equations for the global earthquake model, *Earthquake Spectra*, *31*, 1, 19–45, doi:10.1193/013013EQS017M.
Strasser, F. O., N. A. Abrahamson, and J. J. Bommer (2009), Sigma: Issues, insights, and challenges, *Seismol. Res. Lett.*, *80*(1), 40–56. doi:10.1785/gssrl.80.1.40
Strasser, F. O., M. C. Arango, and J. J. Bommer (2010), Scaling of the source dimensions of interface and intraslab subduction-zone earthquakes with moment magnitude, *Seismol. Res. Lett.*, *81*, 941–950.
Tompkins, M. J., and N. I. Christensen (2001), Ultrasonic *P*- and *S*-wave attenuation in oceanic basalt, *Geophys. J. Int.*, *145*(1), 172–186, doi:10.1046/j.0956-540x.2001.01354.x.
Wang, R., F. Lorenzo-Martín, and F. Roth (2003), Computation of deformation induced by earthquakes in a multi-layered elastic crust—FORTRAN programs EDGRN/EDCMP, *Comput. Geosci.*, *29*(2), 195–207.
Youngs, R. R., N. Abrahamson, F. I. Makdisi, and K. Sadigh (1995), Magnitude-dependent variance of peak ground acceleration, *Bull. Seismol. Soc. Am.*, *85*(4), 1161–1176.

AGU PUBLICATIONS

Geophysical Research letters

Supporting Information for

An 8-month slow slip event triggers progressive nucleation of the 2014 Chile megathrust

Anne Socquet[1], Jesus Piña Valdes[1], Jorge Jara[1], Fabrice Cotton[2,3], Andrea Walpersdorf[1], Nathalie Cotte[1], Sebastian Specht[2,3], Francisco Ortega-Culaciati[4,5], Daniel Carrizo[5], Edmundo Norabuena[6]

[1] Univ. Grenoble Alpes, Univ. Savoie Mont Blanc, CNRS, IRD, IFSTTAR, ISTerre, F-38000 Grenoble

[2] GFZ Helmholtz Centre Potsdam, German Research Centre for Geosciences, Telegrafenberg, 14473 Potsdam, Germany.

[3] Potsdam University, Potsdam, Germany

[4] Department of Geophysics, Faculty of Physical and Mathematical Sciences, University of Chile, Santiago, Chile.

[5] Advanced Mining Technology Center, Faculty of Physical and Mathematical Sciences, Universidad de Chile, Santiago, Chile.

[6] Instituto Geofisico del Peru, Lima, Peru

Contents of this file

Introduction

This supporting information provides a general description of the methods and processing steps used and supplementary figures that support our findings.

Text S1: Methods

cGPS data analysis

Daily cGPS processing

We used data from several cGPS networks spanning the whole central Andes subduction (IPOC, LIA Montessus de Ballore, ISTerre, and Caltech Andean Observatory), together with IGS stations. These cGPS data were analyzed in double differences, in two distinct regional subnetworks, plus a global network **(Figure S1)**. The fifty stations available during the period 2000–2014 were used to design the first regional subnetwork. The second regional subnetwork includes 50 stations running from 2007 to 2014, 33 stations overlapping with the first subnetwork in order to ensure consistency between the subnetworks. The global network includes 99 IGS sites worldwide, 22 of them in South America, with 49 stations overlapping with the two regional subnetworks. 24-hour sessions were reduced to daily estimates of station positions using the GAMIT 10.5 software, choosing the ionosphere-free combination, and fixing the ambiguities to integer values. We use precise orbits from the International GNSS Service for Geodynamics, precise EOPs from the IERS bulletin B, IGS tables to describe the phase centers of the antennas, FES2004 ocean-tidal loading corrections, as well as atmospheric loading corrections (tidal and non-tidal). We estimated one tropospheric zenith delay parameter every two hours and one couple of horizontal tropospheric gradients per 24h session, using the Vienna Mapping Function (VMF1) [Boehm et al., 2006], to map the tropospheric delay in zenithal direction, with a priori ZHD evaluated from pressure and temperature values from the VMF1 grids. Daily solutions are combined using the GLOBK software in a "regional stabilization" approach, and mapped it into the ITRF2008 reference frame [Altamimi et al., 2011] by adjusting selected stations coordinates to those defined in the ITRF in a least square iterative process.

Time series analysis and identification of transient movements

Annual and semi-annual signals were removed from the obtained daily time series, as well as the long-term constant deformation associated with interseismic loading, by fitting a linear regression together with a pair of sinusoids terms. The remaining noise has been reduced by removing the common-mode, obtained by selecting stations located within a distance range of 50-500km from the source region (SJUA, ATIC, CHRA, PTCL, LYAR, UTAR, PCCL, PB02, PB04, MLCA, PB05, PMEJ, JRGN, UCNF, NZCA, AREQ, TORA, TQPL, DANC, TRTA, PALC, PTRE, MNMI, COLC, CHMZ, PB11, PCHA, PB08, PB01, PB07, PB03, CDLC, RADO, PB06, CBAA, VLZL, CJNT) and by averaging their detrended signals. Then, in order to mitigate the residual loading signal present in our signal, we removed from each time series the mean annual residual seasonal movement computed between 2010 and 2013. This procedure reduced significantly the scatter in our time series. In order to study the long term transient in our time series, we excluded data after March 15th, 2014 (when a strong preseismic signal occurred), and then computed the average velocity variations, by fitting a linear regression in a six-month sliding window of the obtained detrended and de-noised time-series. The results indicate a velocity change in July 2013 (appr. eight months before the mainshock) at coastal stations located at 20.3°S close to the city of Iquique. This velocity change propagated bilaterally and reached stations located within a distance of appr. 100km parallel to the strike of the subduction (parallel to the coastline). In a second step, we compute the average velocities by fitting a linear regression to the detrended cGPS

time series on three different time periods before July 2013 (interseismic), July 2013- 13th March 2014 (preseismic 1), 14th March 2014-March 31st 2014 (preseismic 2) **(Figures S2 and S3)**. Uncertainties on linear regressions correspond to standard deviation of one for each linear regression. Displacements for both pre-seismic periods have been obtained by multiplying each station velocity by the time span. For the preseismic period 1, we selected only stations showing a continuous time series since 2012, to avoid artifacts associated with jumps or data holes in the time series. For both preseismic periods, we discarded noisy time series generating the largest uncertainties in the displacement computation.

Slip distribution inversion and resolution

The surface deformation fields associated with the coseismic and preseismic phases were modeled using a dislocation buried in a layered elastic half space [Wang et al., 2003], taking crust1.0 as a velocity model. The fault geometry was constrained by the trace of the trench at the surface. We assumed a uniform dip of 15° and a variable rake, so that the slip direction is parallel to the plate convergence (76°), and is taken constant at all patches.

The fault was discretized into an array of 24 × 11 elements, measuring approximately 15x15km, although their size varies locally since the fault follows the trench geometry **(Figures S4, S5 & S6)**. To solve for the slip distribution along the 264 fault patches, we used a least squares minimization with a non-negativity constraint on the slip. Slip was forced to zero at the edges of the fault. To limit oscillations of the solution, we applied smoothing by minimizing the second-order derivative of the fault slip. We determined the optimal solution roughness [Jonsson et al., 2002] that was used in our final models searching for a compromise between the roughness and misfit of the solution. We estimate the sensitivity of our data set to unit displacements on each node of the grid by summing the horizontal deformation on the whole network after Loveless et al. [2011]. The power of our data to constrain the coupling on the interface is high from 15 km depth to more than 70 km depth in general.

The coseismic offsets extracted from cGPS time series were used to invert for the coseismic slip **(Figure S4)**. The roughness of the preferred co-seismic distribution is 0.04 cm/km for a RMS (L2-norm misfit) of 1.20 cm. The seismic moment is 1.7 10^{21}N.m, and corresponds to a Magnitude 8.1. The inverted slip distribution for pre-seismic period 2 **(Figure S5)** corresponds to a moment Mo=3.9 10^{19}N.m (Mw=7.0) and a fit to the data with RMS= 1.3mm. The inverted slip distribution for pre-seismic period 1 **(Figure S6)** corresponds to a moment Mo=7 10^{18}N.m (Mw=6.5) and a fit to the data with RMS= 0.5mm **(Figure S7)**. Because we were able to estimate accurately the long term transient displacement on a subset of stations only, mostly located along the coast, the slip distribution for pre-seismic period 1 less well constrained than the co-seismic and pre-seismic period 2. However, the patches that are found to be slipping by our inversions are located in zones that are well constrained by our data **(Figure S6)**. Depending on the smoothing applied to the model, the estimate of the geodetic moment of pre-seismic slow slip events (for periods 1 and 2) vary within less than 10% **(Figure S7)**, and the main features of the slip distribution are quite stable whatever the smoothing applied **(Figure S8)**.

Interface Seismic Catalog

The interface seismicity catalog **(Figure S9)** was compiled from the GEOFON moment tensor catalog (http://geofon.gfz-potsdam.de/eqinfo/list.php?mode=mt) and the Global CMT catalog (http://www.globalcmt.org/CMTsearch.html). We use ACE, a data driven algorithm to automatically determine focal mechanism clusters with similar Style-of-Faulting (strike, rake, and dip). The algorithm is also capable to identify the nodal planes as rupture and auxiliary planes, therefore allowing the computation of the rupture plane distance. Since the rupture plane size is unknown, we used a rupture plane scaling relation [Strasser et al., 2009]. Hypocenters are not directly required to classify the data and therefore, classification errors are reduced, compared to classical deterministic classification scheme. We checked that this data-driven procedure was giving results consistent with a more classical classification and that the locations of the earthquakes identified as interface earthquakes were consistent with the known subduction fault plane geometry. This procedure allowed us to build a catalogue containing 125 interface earthquakes in North Chile between January 2008 and June 2014, from 19°S to 21°S and 72°W to 67°W, shallower than 80 km, with Mw equal or higher than 4.5 **(Figures S9 and S10)**. Location and depth of earthquakes can be poorly constrained in the area (see the dispersion in the seismicity and the discrepancy with the trace of the slab in **Figure S10**), demonstrating that the strategy of using the focal mechanisms to identify interface events is better adapted than a strategy based on earthquakes depth or location.

Validation of the Ground Motion Prediction Equations (GMPEs) for the studied seismic crisis

The prediction of ground motion was done using the Abrahamson et al. [2015] Prediction Model. GMPEs predict the Acceleration Response spectra, which correspond to the maximum acceleration experimented by an oscillator of a given mass with one degree of freedom (at different fundamental periods) for different input parameters (e.g. distance to the source, site conditions, magnitude). Abrahamson et al. [2015] model is recognized as one of the leading models to predict ground-motions in subduction areas and has been recently selected for the Global Earthquake Model [Stewart et al., 2015]. To apply this model, Vs30 = 850 m/s was assumed for all stations of the network based on the information that the stations are located on bedrock. The distance between each site and the rupture plane has been estimated directly from the hypocentral distances [Händel et al., 2014].

The fit of the model was tested for oscillators frequencies of 0.75 Hz, 1 Hz, 1.25 Hz, 5 Hz, 10 Hz and for PGA. Residuals have been computed and normalized by the standard deviation of the GMPE model. Therefore a residual value of one means that the observation is offset from the mean predicted value by one model standard deviation. The distribution of absolute residuals allows to evaluate how good is the predictive model in terms of consistency (i.e. do the residuals follow a similar probabilistic distribution than the random error of the model with respect to dataset used to calibrate the model?), precession and accuracy (i.e. are the observed normalized residuals centered on zero?). The obtained absolute residual distribution shows both a good residual distribution and a reasonable fit of the model, with a somewhat lower accuracy between 0.75 Hz and 5 Hz (**Figure S12**).

GMPEs residuals can be separated in two residuals terms: between-event and within-event residuals [Abrahamson and Youngs 1992]. The within-event residuals correspond to the difference between each observation and the median of the observations. Its distribution provides an estimation of the variability of record specific factor as site amplification (i.e. variability in site conditions effects) [Strasser et al. 2010, Al Atik et al, 2010]. The within-event residual distribution shows also a good fit, indicating that site effects variability is well estimated by the model (**Figure S13**).
The between-event residuals represent the difference between the median of the observations of a given event, with respect to the median of the model [Abrahamson and Youngs, 1992]. The between-event residual distribution (**Figure S14**) can be interpreted as the variability of wave radiation due to source parameters (e.g. stress-drop) that are not included in the prediction model [Atik et al., 2010; Youngs et al., 1995]. Tests performed with other recent subductions GMPE's did not show a better global agreement and therefore the Abrahamson et al. [2015] model was chosen as the backbone model to predict ground-motions for the North Chile subduction area.

References:

Abrahamson N., Gregor N., K. Addo, BC Hydro Ground Motion Prediction Equations For Subduction Earthquakes. Earthquake Spectra, (2015) doi: http://dx.doi.org/10.1193/051712EQS188MR.

Abrahamson, N. A., and R. R. Youngs (1992). A stable algorithm for regression analyses using the random effects model, Bulletin of the Seismological Society of America **82** 505-510.

Z. Altamimi, X. Collilieux, L. Métivier, ITRF2008: An improved solution of the international terrestrial reference frame. J. Geod. 85, 457–473 (2011). doi:10.1007/s00190-011-0444-4

Atik L. A., Abrahamson N., Bommer J. J., Scherbaum F., Cotton F., Kuehn N. (2010). The Variability of Ground-Motion Prediction Models and Its Components. Seismological Research Letters, 81(5), 794-801. doi:10.1785/gssrl.81.5.794

Bindi, D., S. Parolai, E. Görgün, H. Grosser, C. Milkereit, M. Bohnhoff, E. Durukal (2007). ML scale in Northwestern Turkey from 1999 Izmit aftershocks: updates., Bull. Seism. Soc. of Am., Vol. 97, No. 1B, pp. 331–338, doi: 10.1785/0120060071

Boehm J, Werl B, Schuh H, Troposphere mapping functions for GPS and very long baseline interferometry from European Centre for Medium-Range Weather Forecasts operational analysis data, J Geophys Res 111:B02406. doi:10.1029/2005JB003629, (2006).

Boore D. M., Sisi A. A., Akkar S., Using Pad Stripped Acausally Filtered Strong Motion Data. Bulletin of the Seismological Society of America, 102(2), 751-760 (2012).

Chiou B., Darragh R., Gregor, N., Silva W., NGA project strong-motion database. Earthquake Spectra, 24(1), 23-44 (2008).

208 Händel A., Specht S., Kühn N. M., Scherbaum, F. (2014). Mixtures of ground-motion
209 prediction equations as backbone models for a logic tree: an application to the
210 subduction zone in Northern Chile. Bulletin of Earthquake Engineering, 13(2),
211 483-501. doi:10.1007/s10518-014-9636-7.

212 Jonsson, S., H. Zebker, P. Segall, and F. Amelung, Fault Slip Distribution of the 1999
213 Mw 7.1 Hector Mine, California, Earthquake, Estimated from Satellite Radar and
214 GPS Measurements, Bull. Seismol. Soc. Am., 92(4), 1377–1389, (2002). doi:
215 10.1785/0120000922.

216 Loveless, J. P., and B. J. Meade (2011), Spatial correlation of interseismic coupling and
217 coseismic rupture extent of the 2011 MW = 9.0 Tohoku Oki earthquake,
218 Geophys. Res. Lett., 38, L17306, doi:10.1029/2011GL048561.

219 Nigam N. C., Jennings P. C. (1969). Calculation of response spectra from strong-motion
220 earthquake records. Bulletin of the Seismological Society of America, 59(2), 909-
221 922.

222 Stewart J. P., Douglas J., Javanbarg M., Bozorgnia Y., Abrahamson N. A., Boore D. M.,
223 Campbell K. W., Delavaud E., Erdik M., Stafford P. J. (2015) Selection of
224 Ground Motion Prediction Equations for the Global Earthquake Model.
225 Earthquake Spectra, 31, 1, 19-45, doi:
226 http://dx.doi.org/10.1193/013013EQS017M.

227 Strasser F. O., Abrahamson N. A., Bommer J. J., Sigma: Issues, Insights, and Challenges.
228 Seismological Research Letters, 80(1), (2009) 40-56. doi:10.1785/gssrl.80.1.40

229 Strasser, F. O., M. C. Arango, and J. J. Bommer (2010). Scaling of the Source
230 Dimensions of Interface and Intraslab Subduction-zone Earthquakes with Moment
231 Magnitude, Seismological Research Letters 81 941-950.

232 Wang R., F. Lorenzo-Martín, F. Roth, Computation of deformation induced by
233 earthquakes in a multi-layered elastic crust - FORTRAN programs
234 EDGRN/EDCMP, Computer and Geosciences, 29(2), 195-207 (2003).

235 Youngs R. R., Abrahamson N., Makdisi F. I., Sadigh K. (1995). Magnitude-dependent
236 variance of peak ground acceleration. Bulletin of the Seismological Society of
237 America, 85(4), 1161-1176.
238

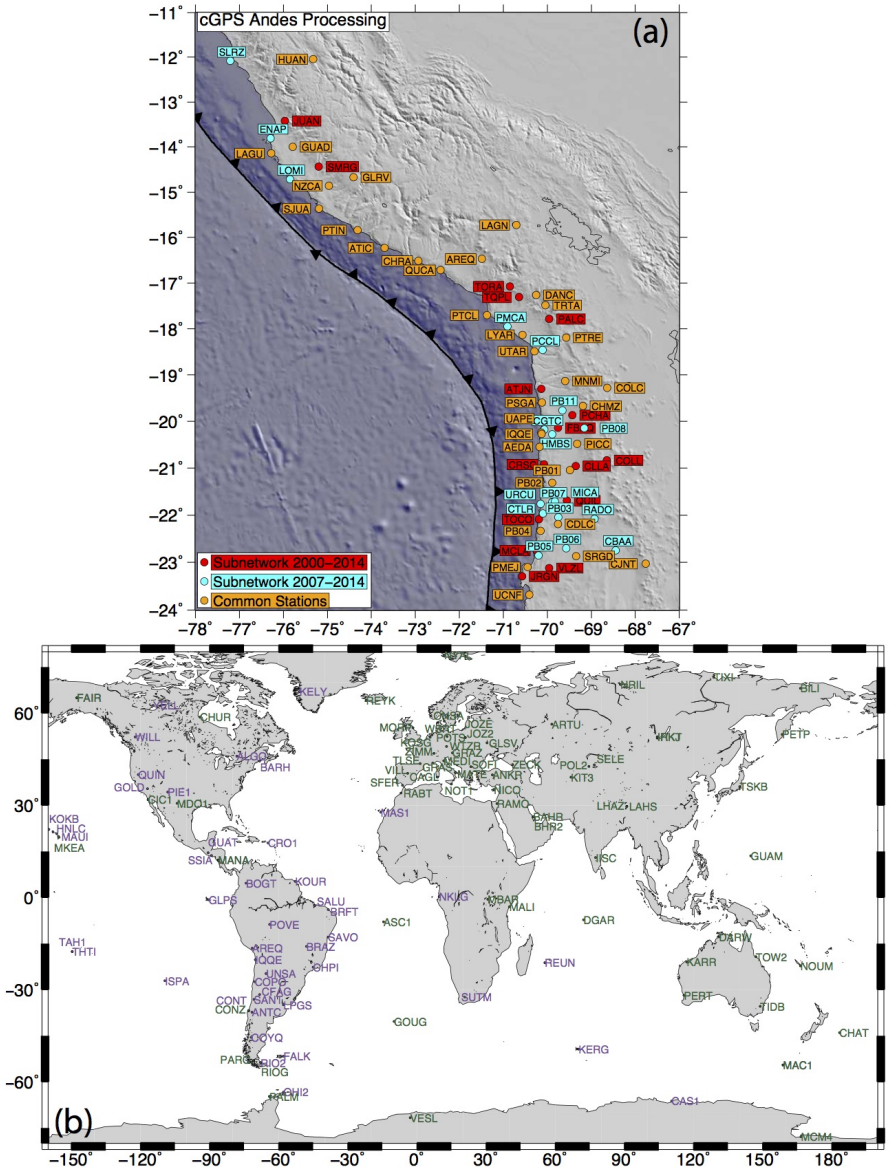

Figure S1 : Map of the network used in this study, showing the three subnetworks (Andes 2000 – 2014, Andes 2007 – 2014 (a) , and the Global Network (b)), as well as the stations used for the reference frame computation. Green color in (b) indicates IGS stations included for global processing, while purple indicates IGS stations overlapping with the Andes subtnetworks.

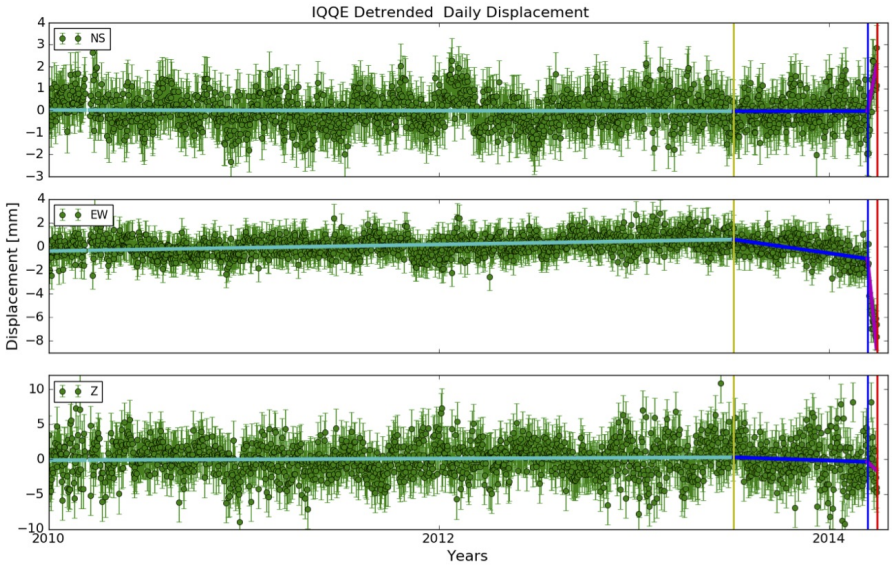

Figure S2 : N, E, U detrended daily displacements for IQQE station since 2010. Vertical lines indicate the dates of the swarm of July 2013 (yellow), the Mw6.7 foreshock on March 16th 2014 (blue) and the Mw 8.1 main shock on April 1st 2014 (red). Linear regressions for the three preseismic periods are shown.

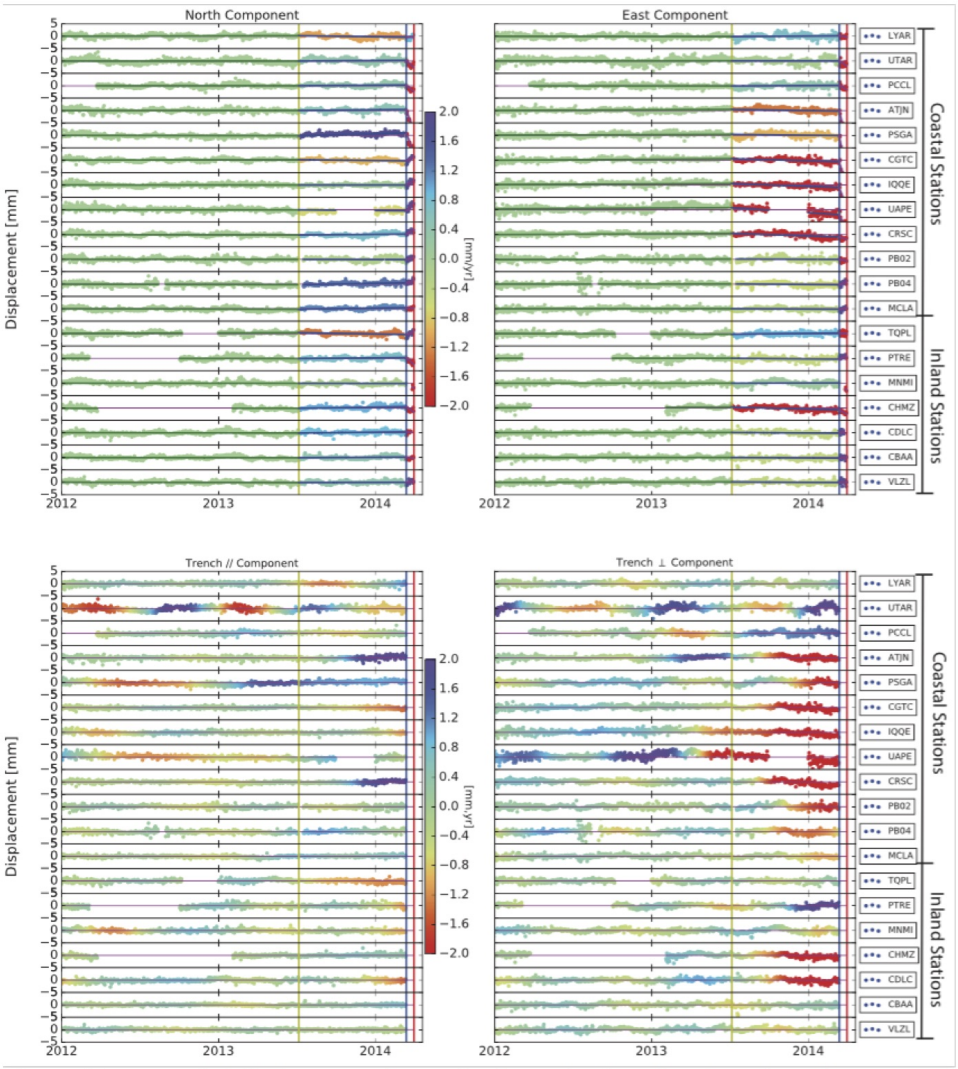

Figure S3 : Detrended displacement time series for a selection of stations along the coast and inland. Bottom 2 panels: Colors, indicate the trench parallel (left panels) and trench perpendicular (right panels) velocities obtained by computing the average velocity over a six-month sliding window. Top 2 panels: Colors, indicate the N-S (left panels) and E-W (right panels) velocities obtained by fitting a linear regression on the displacement time series for the three preseismic periods.

261

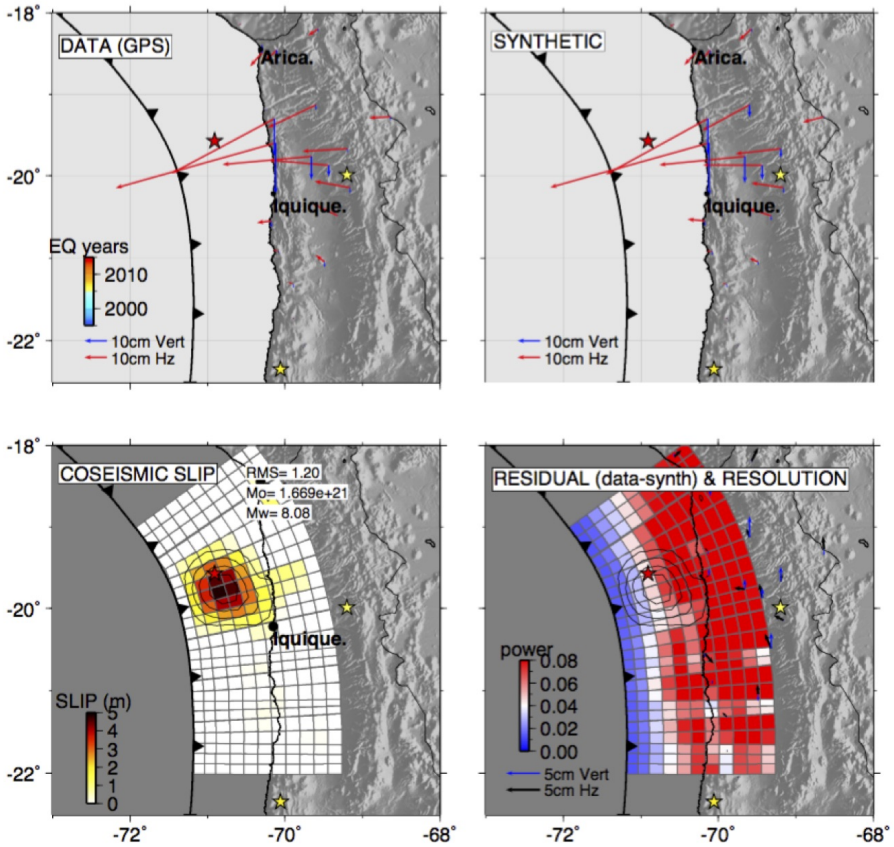

262
263 **Figure S4** : Co-seismic displacements (observed : top left, and modeled: top right), co-
264 seismic slip distribution inverted from surface displacements (bottom left), residuals and
265 power of GPS stations to constrain plate interface behavior (i.e., sum of the partial
266 derivatives relating GPS displacement to unit slip [Loveless & Meade, 2011]) (bottom
267 right). One-meter contours are drawn.
268
269

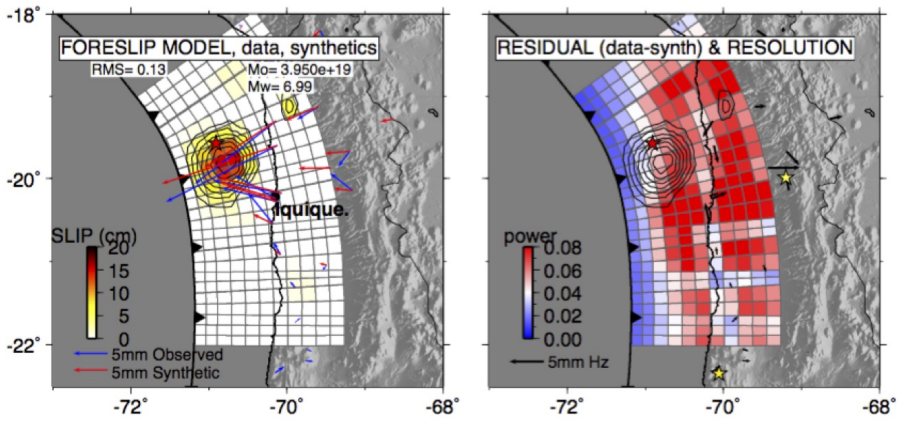

Figure S5 : Left: Displacements (observed: blue, modeled: red) during preseismic period 2 (March 14th 2014 to March 31st 2014) and preseismic slip distribution for the two weeks preceding the main shock inverted from surface displacements, Right: residuals and resolution. Two-cm contours are drawn.

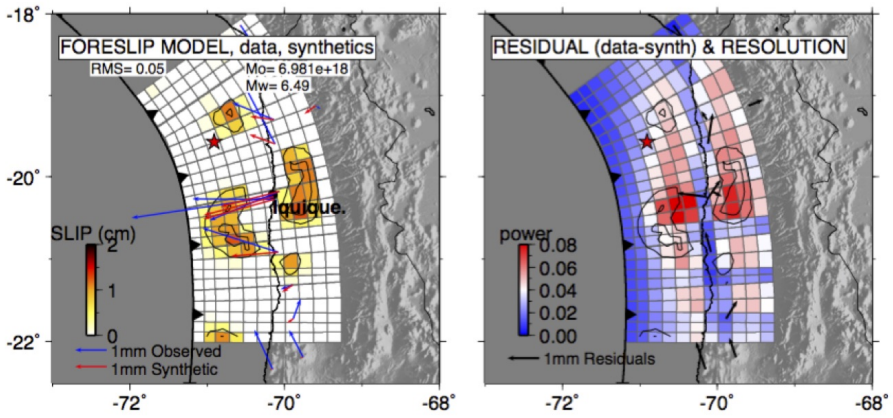

Figure S6 : Left: Displacements (observed: blue, modeled: red) during preseismic period 1 (July 6th 2013 to March 13th 2014) and preseismic slip distribution for the two weeks preceding the main shock inverted from surface displacements, Right: residuals and resolution. Five-mm contours are drawn.

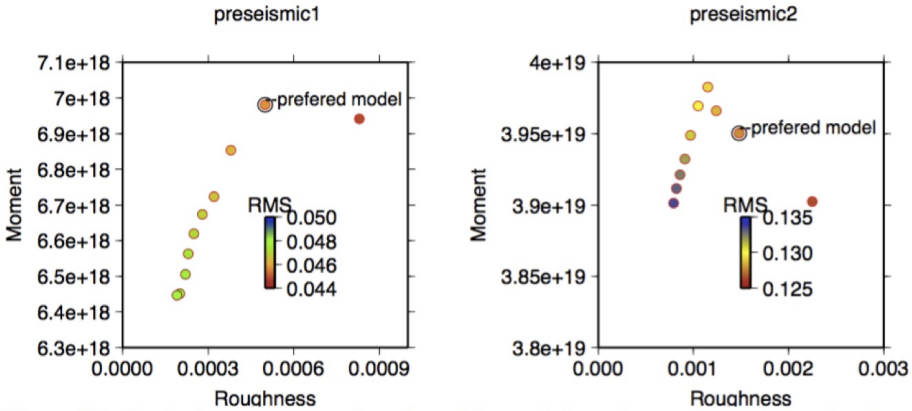

Figure S7: Geodetic moment as a function of the model roughness, for both preseismic models. Dots are color coded with the model – data misfit. The preferred model is chosen as a compromise between smoothness and RMS.

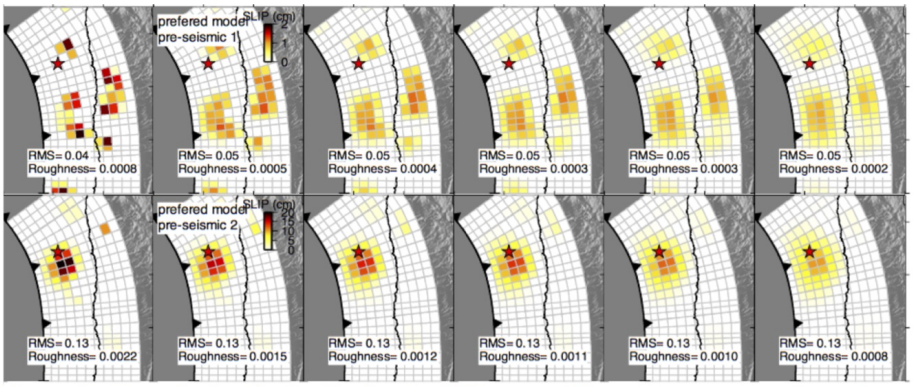

Figure S8: Pre-seismic slip distribution for different model roughnesses. Top: 8 months preseismic (july 2013 – mid-March 2014), Bottom: 15-day pre-seismic (Mid-March to End March 2014).

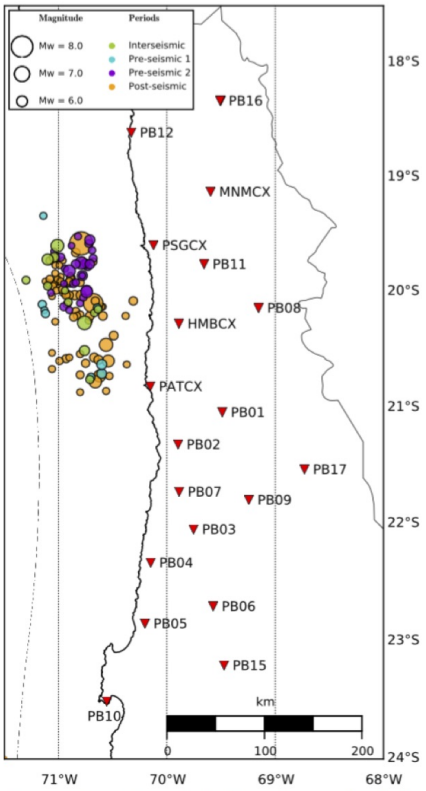

Figure S9: Map of the interface seismicity data set (dots colored as a function of the 4 periods defined in the paper), and network of IPOC accelerometric stations (red inverted triangles) used to perform earthquakes frequency content analysis. All these stations are installed on bedrock. Most of them are also colocated with GPS stations used in this paper.

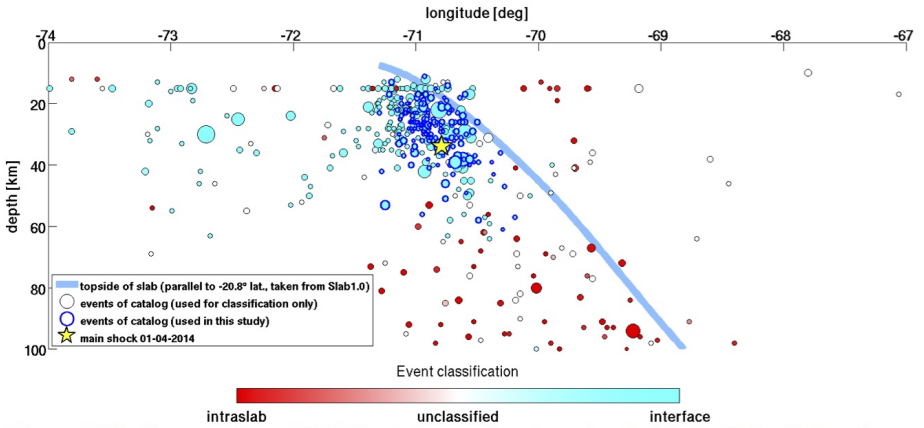

Figure S10: Cross section of IPOC catalogue of earthquakes in North Chile. Colored dots represents the classification of earthquakes (interface, unclassified or intraplate) as a function of their focal mechanism. The blue line represents the Slab1.0 subduction interface. The events used in this study (contoured in blue) have been selected as being interface events that occurred between January 2008 and June 2014.

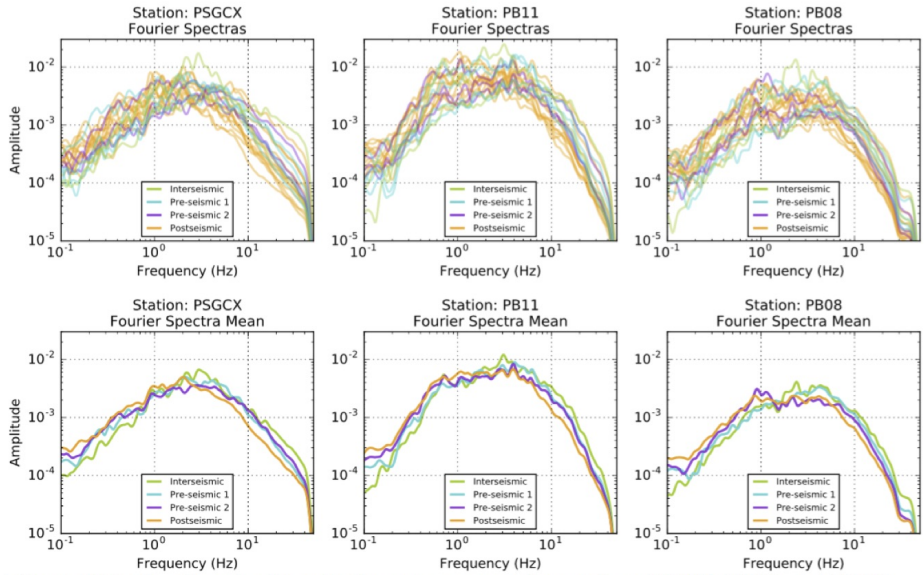

Figure S11: Acceleration Fourier Spectra computed at stations PSGX, PB11 and PB08 (see **Figure S9** for location) for interface earthquake within 5.1-5.2 Magnitude range. Spectra are color-coded as function of the period when occured the earthquake (interseismic in green, pre-seismic 1 in cyan, pre-seismic 2 in purple, post-seismic in orange). Top line shows all individual spectra while bottom line shows the mean spectrum for each time period.

315

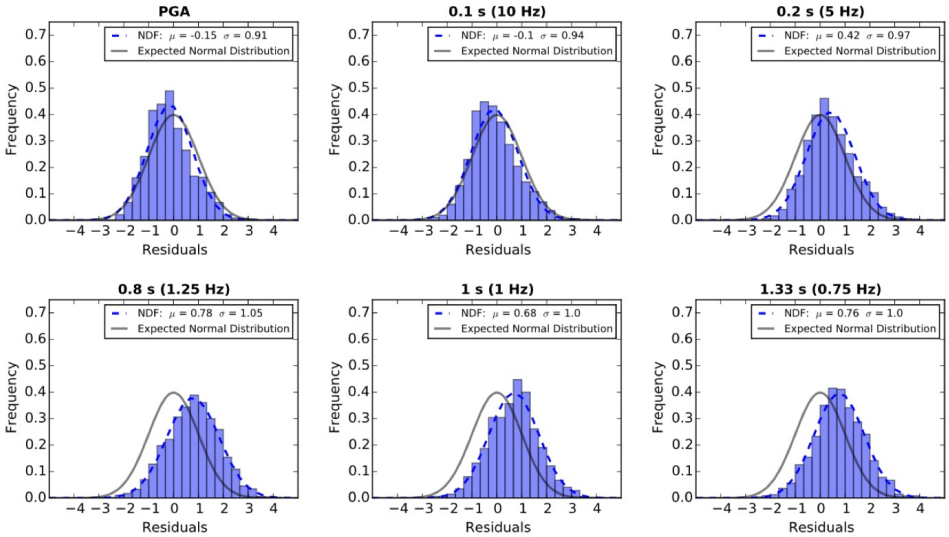

316

317 **Figure S12:** Histograms of ground motion absolute residuals normalized with respect to
318 the total standard deviation of the GMPE model [Abrahamson et al., 2015]. The Normal
319 Density Function (NDF) of the residuals is shown by the dashed lines and the expected
320 normal distribution is represented by the gray lines.

321

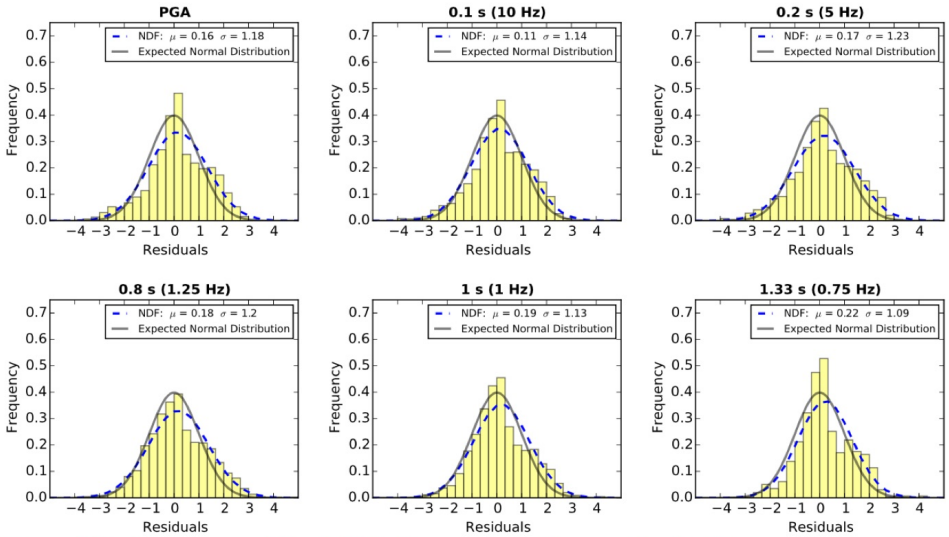

322
323 **Figure S13:** Histograms of the Within-Events residuals normalized with respect to the
324 Within-Event standard deviation of the model. The Normal Density Function (NDF) of
325 the residuals is shown by dashed lines and the expected normal distribution by gray lines.
326

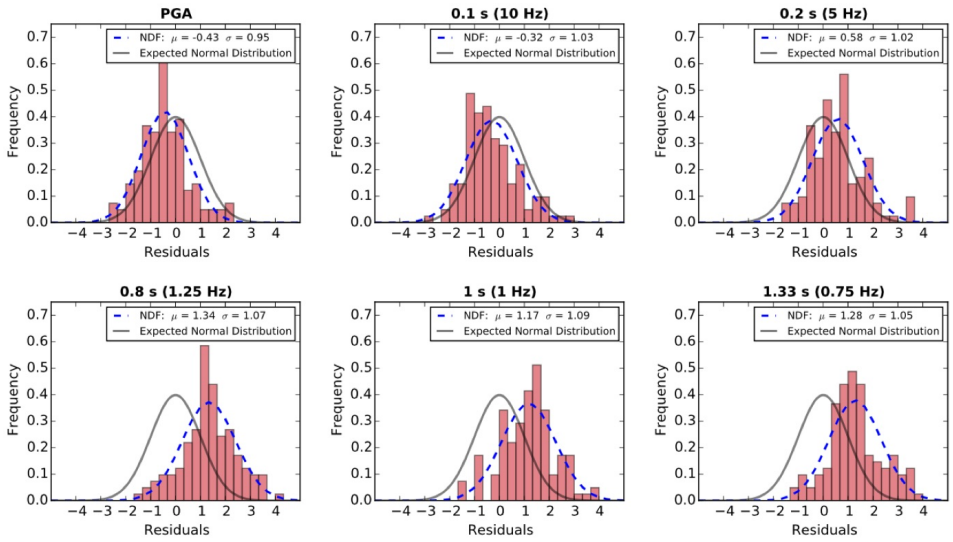

Figure S14: Histograms of the Between-Event residuals normalized with respect to the Between-Event standard deviation of the model. The Normal Density Function (NDF) of the residuals is shown by dashed lines and the expected normal distribution by gray lines.

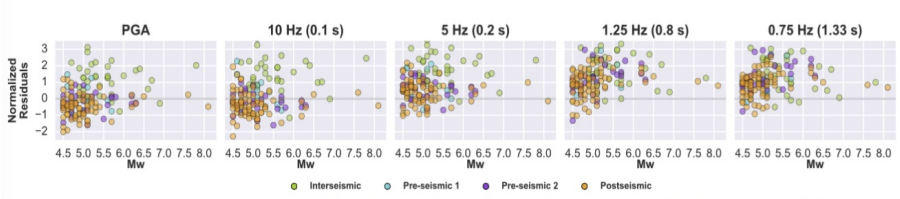

Figure S15: Between-event residuals as a function of event magnitude at the different frequency values shown in figure 1 (mid-panel). At frequencies above 5Hz, earthquakes occurring during the interseismic period exhibit significantly larger residuals than earthquakes belonging to preseismic and postseismic sequences. Instead, values of residuals are similar for all considered time periods at frequencies below 1.25Hz.

References

Abercrombie, R. E., M. Antolik, K. Felzer, and G. Ekström (2001), The 1994 Java tsunami earthquake: Slip over a subducting seamount, *J. Geophys. Res. Solid Earth*, *106*(B4), 6595–6607.

Abrahamson, N., G. Atkinson, D. Boore, Y. Bozorgnia, K. Campbell, B. Chiou, I. Idriss, W. Silva, and R. Youngs (2008), Comparisons of the NGA ground-motion relations, *Earthq. Spectra*, *24*(1), 45–66.

Abrahamson, N., N. Gregor, and K. Addo (2016), BC Hydro Ground Motion Prediction Equations for Subduction Earthquakes, *Earthq. Spectra*, *32*(1), 23–44, doi:10.1193/051712EQS188MR.

Abrahamson, N. A., and R. R. Youngs (1992), A stable algorithm for regression analyses using the random effects model, *Bull. Seismol. Soc. Am.*, *82*(1), 505–510.

Aki, K. (1967), Scaling law of seismic spectrum, *J. Geophys. Res.*, *72*(4), 1217–1231.

Aki, K. (1972), Scaling law of earthquake source time-function, *Geophys. J. Int.*, *31*(1–3), 3–25.

Aki, K. (1979), Characterization of barriers on an earthquake fault, *J. Geophys. Res. Solid Earth*, *84*(B11), 6140–6148.

Aki, K. (1984), Asperities, barriers, characteristic earthquakes and strong motion prediction, *J. Geophys. Res. Solid Earth*, *89*(B7), 5867–5872.

Aki, K. (1993), Local site effects on weak and strong ground motion, *Tectonophysics*, *218*(1–3), 93–111.

Aki, K., and P. G. Richards (2002), *Quantitative seismology*.

Akkar, S. et al. (2014), Reference database for seismic ground-motion in Europe (RESORCE), *Bull. Earthq. Eng.*, *12*(1), 311–339, doi:10.1007/s10518-013-9506-8.

Al Atik, L., N. Abrahamson, J. J. Bommer, F. Scherbaum, F. Cotton, and N. Kuehn (2010), The Variability of Ground-Motion Prediction Models and Its Components, *Seismol. Res. Lett.*, *81*(5), 794–801, doi:10.1785/gssrl.81.5.794.

Ambraseys, N., P. Smit, J. Douglas, B. Margaris, R. Sigbjörnsson, S. Olafsson, P. Suhadolc, and G. Costa (2004), Internet site for European strong-motion data, *Boll. Geofis. Teor. Ed Appl.*, *45*(3), 113–129.

Ando, M. (1975), Source mechanisms and tectonic significance of historical earthquakes along the Nankai Trough, Japan, *Tectonophysics*, *27*(2), 119–140.

Aoi, S., T. Kunugi, and H. Fujiwara (2004), Strong-motion seismograph network operated by NIED: K-NET and KiK-net, *J. Jpn. Assoc. Earthq. Eng.*, *4*(3), 65–74.

Arango, M., F. Strasser, J. Bommer, J. Cepeda, R. Boroschek, D. Hernandez, and H. Tavera (2012), An evaluation of the applicability of current ground-motion models to the South and Central American Subduction Zones, *Bull. Seismol. Soc. Am.*, *102*(1), 143–168.

Arango, M. C., F. O. Strasser, J. J. Bommer, R. Boroschek, D. Comte, and H. Tavera (2011), A strong-motion database from the Peru–Chile subduction zone, *J. Seismol.*, *15*(1), 19–41, doi:10.1007/s10950-010-9203-x.

Archuleta, R. J., and S. H. Hartzell (1981), Effects of fault finiteness on near-source ground motion, *Bull. Seismol. Soc. Am.*, *71*(4), 939–957.

Argus, D. F., Gordon, R. G., & DeMets, C. (2011). Geologically current motion of 56 plates relative to the no-net-rotation reference frame. Geochemistry, Geophysics, Geosystems, 12(11), 1525-2027.

Arias, A. (1970). MEASURE OF EARTHQUAKE INTENSITY. Massachusetts Inst. of Tech., Cambridge. Univ. of Chile, Santiago de Chile.

Asano, Y., K. Obara, and Y. Ito (2008), Spatiotemporal distribution of very-low frequency earthquakes in Tokachi-oki near the junction of the Kuril and Japan

trenches revealed by using array signal processing, *Earth Planets Space*, *60*(8), 871–875.

Astiz, L., T. Lay, and H. Kanamori (1988), Large intermediate-depth earthquakes and the subduction process, *Phys. Earth Planet. Inter.*, *53*(1), 80–166.

Atkinson, G. M., and D. M. Boore (2003), Empirical ground-motion relations for subduction-zone earthquakes and their application to Cascadia and other regions, *Bull. Seismol. Soc. Am.*, *93*(4), 1703–1729.

Bastías, N., and G. A. Montalva (2016), Chile Strong Ground Motion Flatfile, *Earthq. Spectra*, *32*(4), 2549–2566, doi:10.1193/102715eqs158dp.

Béjar-Pizarro, M. et al. (2010), Asperities and barriers on the seismogenic zone in North Chile: state-of-the-art after the 2007 Mw 7.7 Tocopilla earthquake inferred by GPS and InSAR data, *Geophys. J. Int.*, *183*(1), 390–406, doi:10.1111/j.1365-246X.2010.04748.x.

Béjar-Pizarro, M., A. Socquet, R. Armijo, D. Carrizo, J. Genrich, and M. Simons (2013), Andean structural control on interseismic coupling in the North Chile subduction zone, *Nat. Geosci.*, *6*(6), 462–467.

Bilek, S. L., and T. Lay (2002), Tsunami earthquakes possibly widespread manifestations of frictional conditional stability, *Geophys. Res. Lett.*, *29*(14).

Bindi, D., S. Parolai, H. Grosser, C. Milkereit, and E. Durukal (2007), Empirical ground-motion prediction equations for northwestern Turkey using the aftershocks of the 1999 Kocaeli earthquake, *Geophys. Res. Lett.*, *34*(8).

Bindi, D., D. Spallarossa, and F. Pacor (2017), Between-event and between-station variability observed in the Fourier and response spectra domains: comparison with seismological models, *Geophys. J. Int.*, *210*(2), 1092–1104.

Bird, P. (2003), An updated digital model of plate boundaries, *Geochem. Geophys. Geosystems*, *4*(3).

Bonilla, L. F., J. H. Steidl, G. T. Lindley, A. G. Tumarkin, and R. J. Archuleta (1997), Site amplification in the San Fernando Valley, California: Variability of site-effect estimation using the S-wave, coda, and H/V methods, *Bull. Seismol. Soc. Am.*, *87*(3), 710–730.

Boore, D. M. (1972), A note on the effect of simple topography on seismic SH waves, *Bull. Seismol. Soc. Am.*, *62*(1), 275–284.

Boore, D. M. (1983), Stochastic simulation of high-frequency ground motions based on seismological models of the radiated spectra, *Bull. Seismol. Soc. Am.*, *73*(6A), 1865–1894.

Boore, D. M., and J. J. Bommer (2005), Processing of strong-motion accelerograms: needs, options and consequences, *Soil Dyn. Earthq. Eng.*, *25*(2), 93–115, doi:10.1016/j.soildyn.2004.10.007.

Bouchon, M., C. A. Schultz, and M. N. Toksöz (1996), Effect of three-dimensional topography on seismic motion, *J. Geophys. Res. Solid Earth*, *101*(B3), 5835–5846.

Bouchon, M., V. Durand, D. Marsan, H. Karabulut, and J. Schmittbuhl (2013), The long precursory phase of most large interplate earthquakes, *Nat. Geosci.*, *6*(4), 299–302.

Bouchon, M., D. Marsan, V. Durand, M. Campillo, H. Perfettini, R. Madariaga, and B. Gardonio (2016), Potential slab deformation and plunge prior to the Tohoku, Iquique and Maule earthquakes, *Nat. Geosci.*, *9*(5), 380–383.

Bozorgnia, Y., and K. W. Campbell (2004), The vertical-to-horizontal response spectral ratio and tentative procedures for developing simplified V/H and vertical design spectra, *J. Earthq. Eng.*, *8*(02), 175–207.

Brace, W. F., and J. D. Byerlee (1966), Stick-slip as a mechanism for earthquakes, *Science*, *153*(3739), 990–992.

Brune, J. N. (1970), Tectonic stress and the spectra of seismic shear waves from earthquakes, *J. Geophys. Res.*, *75*(26), 4997–5009.

Bürgmann, R., M. G. Kogan, V. E. Levin, C. H. Scholz, R. W. King, and G. M. Steblov (2001), Rapid aseismic moment release following the 5 December, 1997 Kronotsky, Kamchatka, earthquake, *Geophys. Res. Lett.*, *28*(7), 1331–1334.

Byerlee, J. D. (1970), The mechanics of stick-slip, *Tectonophysics*, *9*(5), 475–486.

Byrne, D. E., D. M. Davis, and L. R. Sykes (1988), Loci and maximum size of thrust earthquakes and the mechanics of the shallow region of subduction zones, *Tectonics*, *7*(4), 833–857.

Cadet, J.-P. et al. (1987), The Japan Trench and its juncture with the Kuril Trench: cruise results of the Kaiko project, Leg 3, *Earth Planet. Sci. Lett.*, *83*(1–4), 267–284.

Campbell, K. W. (1981), Near-source attenuation of peak horizontal acceleration, *Bull. Seismol. Soc. Am.*, *71*(6), 2039–2070.

Cesca, S., F. Grigoli, S. Heimann, T. Dahm, M. Kriegerowski, M. Sobiesiak, C. Tassara, and M. Olcay (2016), The Mw 8.1 2014 Iquique, Chile, seismic sequence: a tale of foreshocks and aftershocks, *Geophys. J. Int.*, *204*(3), 1766–1780, doi:10.1093/gji/ggv544.

Chiou, B.-J., and R. R. Youngs (2008), An NGA Model for the Average Horizontal Component of Peak Ground Motion and Response Spectra, *Earthq. Spectra*, *24*(1), 173–215, doi:10.1193/1.2894832.

Chlieh, M. et al. (2014), Distribution of discrete seismic asperities and aseismic slip along the Ecuadorian megathrust, *Earth Planet. Sci. Lett.*, *400*, 292–301.

Clift, P., and P. Vannucchi (2004), Controls on tectonic accretion versus erosion in subduction zones: Implications for the origin and recycling of the continental crust, *Rev. Geophys.*, *42*(2).

Collot, J.-Y., B. Marcaillou, F. Sage, F. Michaud, W. Agudelo, P. Charvis, D. Graindorge, M.-A. Gutscher, and G. Spence (2004), Are rupture zone limits of great subduction earthquakes controlled by upper plate structures? Evidence from multichannel seismic reflection data acquired across the northern Ecuador–southwest Colombia margin, *J. Geophys. Res. Solid Earth*, *109*(B11).

Contreras-Reyes, E., E. R. Flueh, and I. Grevemeyer (2010), Tectonic control on sediment accretion and subduction off south central Chile: Implications for coseismic rupture processes of the 1960 and 2010 megathrust earthquakes, *Tectonics*, *29*, TC6018, doi:10.1029/2010TC002734.

Contreras-Reyes, E., J. Jara, I. Grevemeyer, S. Ruiz, and D. Carrizo (2012), Abrupt change in the dip of the subducting plate beneath north Chile, *Nat. Geosci.*, *5*(5), 342–345.

Cotton, F., R. Archuleta, and M. Causse (2013), What is Sigma of the Stress Drop?, *Seismol. Res. Lett.*, *84*(1), 42–48, doi:10.1785/0220120087.

Cummins, P. R., T. Baba, S. Kodaira, and Y. Kaneda (2002), The 1946 Nankai earthquake and segmentation of the Nankai Trough, *Phys. Earth Planet. Inter.*, *132*(1), 75–87.

Dawood, H. M., A. Rodriguez-Marek, J. Bayless, C. A. Goulet, and E. Thompson (2016), A Flatfile for the KiK-net Database Processed Using an Automated Protocol,

Delouis, B., M. Pardo, D. Legrand, and T. Monfret (2009), The Mw 7.7 Tocopilla Earthquake of 14 November 2007 at the Southern Edge of the Northern Chile Seismic Gap: Rupture in the Deep Part of the Coupled Plate Interface, *Bull. Seismol. Soc. Am.*, *99*(1), 87–94, doi:10.1785/0120080192.

Delouis, B., J.-M. Nocquet, and M. Vallée (2010), Slip distribution of the February 27, 2010 Mw= 8.8 Maule earthquake, central Chile, from static and high-rate GPS, InSAR, and broadband teleseismic data, *Geophys. Res. Lett.*, *37*(17).

DeMets, C. (1992), Oblique convergence and deformation along the Kuril and Japan trenches, *J. Geophys. Res. Solid Earth*, *97*(B12), 17615–17625.

DeMets, C., R. G. Gordon, D. F. Argus, and S. Stein (1990), Current plate motions, *Geophys. J. Int.*, *101*(2), 425–478.

Derras, B., P.-Y. Bard, and F. Cotton (2016), Site-Condition Proxies, Ground Motion Variability, and Data-Driven GMPEs: Insights from the NGA-West2 and RESORCE Data Sets, *Earthq. Spectra*, *32*(4), 2027–2056.

Dieterich, J. H. (1972), Time-dependent friction in rocks, *J. Geophys. Res.*, *77*(20), 3690–3697.

Dieterich, J. H. (1981), Constitutive properties of faults with simulated gouge, *Mech. Behav. Crustal Rocks Handin Vol.*, 103–120.

Edwards, B., and D. Fäh (2014), *Ground motion prediction equations*, Report, ETH Zurich.

Fuenzalida, A., B. Schurr, M. Lancieri, M. Sobiesiak, and R. Madariaga (2013), High-resolution relocation and mechanism of aftershocks of the 2007 Tocopilla (Chile) earthquake, *Geophys. J. Int.*, *194*(2), 1216–1228, doi:10.1093/gji/ggt163.

Fujiwara, H., S. Aoi, T. Kunugi, and S. Adachi (2004), Strong-motion Observation Networks of NIED: K-NET and KiK-net, *Cosm. Rep.*

Gusman, A. R., S. Murotani, K. Satake, M. Heidarzadeh, E. Gunawan, S. Watada, and B. Schurr (2015), Fault slip distribution of the 2014 Iquique, Chile,

earthquake estimated from ocean-wide tsunami waveforms and GPS data, *Geophys. Res. Lett.*, *42*(4), 1053–1060.

Haendel, A., S. Specht, N. M. Kuehn, and F. Scherbaum (2014), Mixtures of ground-motion prediction equations as backbone models for a logic tree: an application to the subduction zone in Northern Chile, *Bull. Earthq. Eng.*, *13*(2), 483–501, doi:10.1007/s10518-014-9636-7.

Hanks, T. C. (1979), b values and $ømega$- γ seismic source models: Implications for tectonic stress variations along active crustal fault zones and the estimation of high-frequency strong ground motion, *J. Geophys. Res. Solid Earth*, *84*(B5), 2235–2242.

Hartzell, S. H., and T. H. Heaton (1983), Inversion of strong ground motion and teleseismic waveform data for the fault rupture history of the 1979 Imperial Valley, California, earthquake, *Bull. Seismol. Soc. Am.*, *73*(6A), 1553–1583.

Hashimoto, C., A. Noda, T. Sagiya, and M. Matsu'Ura (2009), Interplate seismogenic zones along the Kuril-Japan trench inferred from GPS data inversion, *Nat. Geosci.*, *2*(2), 141.

Hayes, G. P., M. W. Herman, W. D. Barnhart, K. P. Furlong, S. Riquelme, H. M. Benz, E. Bergman, S. Barrientos, P. S. Earle, and S. Samsonov (2014), Continuing megathrust earthquake potential in Chile after the 2014 Iquique earthquake, *Nature*, *512*(7514), 295–298.

Heaton, T. H. (1990), Evidence for and implications of self-healing pulses of slip in earthquake rupture, *Phys. Earth Planet. Inter.*, *64*(1), 1–20.

Hetland, E., and M. Simons (2010), Post-seismic and interseismic fault creep II: transient creep and interseismic stress shadows on megathrusts, *Geophys. J. Int.*, *181*(1), 99–112.

Heuret, A., S. Lallemand, F. Funiciello, C. Piromallo, and C. Faccenna (2011), Physical characteristics of subduction interface type seismogenic zones revisited, *Geochem. Geophys. Geosystems*, *12*(1).

Heuret, A., C. Conrad, F. Funiciello, S. Lallemand, and L. Sandri (2012), Relation between subduction megathrust earthquakes, trench sediment thickness and upper plate strain, *Geophys. Res. Lett.*, *39*(5).

Hirose, H., T. Matsuzawa, T. Kimura, and H. Kimura (2014), The Boso slow slip events in 2007 and 2011 as a driving process for the accompanying earthquake swarm, *Geophys. Res. Lett.*, *41*(8), 2778–2785.

Hoechner, A., A. Y. Babeyko, and S. V. Sobolev (2008), Enhanced GPS inversion technique applied to the 2004 Sumatra earthquake and tsunami, *Geophys. Res. Lett.*, *35*(8).

Hoffmann-Rothe, A., N. Kukowski, G. Dresen, H. Echtler, O. Oncken, J. Klotz, E. Scheuber, and A. Kellner (2006), Oblique Convergence along the Chilean Margin: Partitioning, Margin-Parallel Faulting and Force Interaction at the Plate Interface, in *The Andes: Active Subduction Orogeny*, edited by O. Oncken, G. Chong, G. Franz, P. Giese, H.-J. Götze, V. A. Ramos, M. R. Strecker, and P. Wigger, pp. 125–146, Springer Berlin Heidelberg, Berlin, Heidelberg.

Hooper, A., D. Bekaert, K. Spaans, and M. Arıkan (2012), Recent advances in SAR interferometry time series analysis for measuring crustal deformation, *Tectonophysics*, *514*, 1–13.

Hooper, A., J. Pietrzak, W. Simons, H. Cui, R. Riva, M. Naeije, A. T. van Scheltinga, E. Schrama, G. Stelling, and A. Socquet (2013), Importance of horizontal seafloor motion on tsunami height for the 2011 M w= 9.0 Tohoku-Oki earthquake, *Earth Planet. Sci. Lett.*, *361*, 469–479.

Hu, Y., and K. Wang (2008), Coseismic strengthening of the shallow portion of the subduction fault and its effects on wedge taper, *J. Geophys. Res. Solid Earth*, *113*(B12).

Hyndman, R. D., and K. Wang (1993), Thermal constraints on the zone of major thrust earthquake failure: The Cascadia subduction zone, *J. Geophys. Res. Solid Earth*, *98*(B2), 2039–2060.

Hyndman, R. D., K. Wang, and M. Yamano (1995), Thermal constraints on the seismogenic portion of the southwestern Japan subduction thrust, *J. Geophys. Res. Solid Earth*, *100*(B8), 15373–15392.

Hyndman, R. D., M. Yamano, and D. A. Oleskevich (1997), The seismogenic zone of subduction thrust faults, *Isl. Arc*, *6*(3), 244–260.

Ide, S., A. Baltay, and G. C. Beroza (2011), Shallow dynamic overshoot and energetic deep rupture in the 2011 Mw 9.0 Tohoku-Oki earthquake, *Science*, *332*(6036), 1426–1429.

Irikura, K. (1986), Prediction of strong acceleration motion using empirical Green's function, in *Proc. 7th Japan Earthq. Eng. Symp*, vol. 1986, pp. 151–156.

Irikura, K., and S. Kurahashi (2011), Source Model for Generating Strong Ground Motions during the 2011 off the Pacific coast of Tohoku Earthquake, in *AGU Fall Meeting Abstracts*.

Ito, Y., K. Obara, K. Shiomi, S. Sekine, and H. Hirose (2007), Slow earthquakes coincident with episodic tremors and slow slip events, *Science*, *315*(5811), 503–506.

Jackson, D. D., and D. L. Anderson (1970), Physical mechanisms of seismic-wave attenuation, *Rev. Geophys.*, *8*(1), 1–63.

Jara-Munoz, J., D. Melnick, D. Brill, and M. R. Strecker (2015), Segmentation of the 2010 Maule Chile earthquake rupture from a joint analysis of uplifted marine terraces and seismic-cycle deformation patterns, *Quat. Sci. Rev.*, *113*, 171–192.

Jonsson, S., P. Segall, R. Pedersen, and G. Bjornsson (2003), Post-earthquake ground movements correlated to pore-pressure transients, *Nature*, *424*(6945), 179.

Joyner, W. B., and D. M. Boore (1988), Measurement, Characterization, and Prediction of Strong Ground Motion, pp. 43–102, ASCE.

Kale, Ö., and S. Akkar (2013), A new procedure for selecting and ranking ground-motion prediction equations (GMPEs): The Euclidean distance-based ranking (EDR) method, *Bull. Seismol. Soc. Am.*, *103*(2A), 1069–1084.

Kanamori, H. (1972), Mechanism of tsunami earthquakes, *Phys. Earth Planet. Inter.*, *6*(5), 346–359.

Kanamori, H. (1977), The energy release in great earthquakes, *J. Geophys. Res.*, *82*(20), 2981–2987.

Kanamori, H. (1986), Rupture process of suduction-zone earthquakes, *Annu. Rev. Earth Planet. Sci.*, *14*, 293.

Kanamori, H., and E. E. Brodsky (2004), The physics of earthquakes, *Rep. Prog. Phys.*, *67*(8), 1429.

Kaneko, Y., J.-P. Avouac, and N. Lapusta (2010), Towards inferring earthquake patterns from geodetic observations of interseismic coupling, *Nat. Geosci.*, *3*(5), 363.

Kato, A., and S. Nakagawa (2014), Multiple slow-slip events during a foreshock sequence of the 2014 Iquique, Chile Mw 8.1 earthquake, *Geophys. Res. Lett.*, *41*(15), 5420–5427.

Kato, A., K. Obara, T. Igarashi, H. Tsuruoka, S. Nakagawa, and N. Hirata (2012), Propagation of slow slip leading up to the 2011 Mw 9.0 Tohoku-Oki earthquake, *Science*, *335*(6069), 705–708.

Kato, A., J. Fukuda, T. Kumazawa, and S. Nakagawa (2016), Accelerated nucleation of the 2014 Iquique, Chile Mw 8.2 Earthquake, *Sci. Rep.*, *6*.

Kawasaki, I., Y. Asai, and Y. Tamura (2001), Space–time distribution of interplate moment release including slow earthquakes and the seismo-geodetic coupling in the Sanriku-oki region along the Japan trench, *Tectonophysics*, *330*(3), 267–283.

Kiser, E., and M. Ishii (2012), The March 11, 2011 Tohoku-oki earthquake and cascading failure of the plate interface, *Geophys. Res. Lett.*, *39*(7).

Klein, E., L. Fleitout, C. Vigny, and J. D. Garaud (2016), Afterslip and viscoelastic relaxation model inferred from the large-scale post-seismic deformation following the 2010 M w 8.8 Maule earthquake (Chile), *Geophys. J. Int.*, *205*(3), 1455–1472.

Kodaira, S., E. Kurashimo, J.-O. Park, N. Takahashi, A. Nakanishi, S. Miura, T. Iwasaki, N. Hirata, K. Ito, and Y. Kaneda (2002), Structural factors controlling the rupture process of a megathrust earthquake at the Nankai trough seismogenic zone, *Geophys. J. Int.*, *149*(3), 815–835.

Kodaira, S., T. Hori, A. Ito, S. Miura, G. Fujie, J.-O. Park, T. Baba, H. Sakaguchi, and Y. Kaneda (2006), A cause of rupture segmentation and synchronization in the Nankai trough revealed by seismic imaging and numerical simulation, *J. Geophys. Res. Solid Earth*, *111*(B9).

Konca, A. O. et al. (2008), Partial rupture of a locked patch of the Sumatra megathrust during the 2007 earthquake sequence, *Nature*, *456*(7222), 631.

Konno, K., and T. Ohmachi (1998), Ground-motion characteristics estimated from spectral ratio between horizontal and vertical components of microtremor, *Bull. Seismol. Soc. Am.*, *88*(1), 228–241.

Koper, K. D., A. R. Hutko, T. Lay, C. J. Ammon, and H. Kanamori (2011), Frequency-dependent rupture process of the 2011 Mw 9.0 Tohoku Earthquake: Comparison of short-period P wave backprojection images and broadband seismic rupture models, *Earth Planets Space*, *63*(7), 16.

Koper, K. D., A. R. Hutko, T. Lay, and O. Sufri (2012), Imaging short-period seismic radiation from the 27 February 2010 Chile (Mw 8.8) earthquake by back-projection of P, PP, and PKIKP waves, *J. Geophys. Res. Solid Earth*, *117*(B2).

Kopp, H. (2013), Invited review paper: The control of subduction zone structural complexity and geometry on margin segmentation and seismicity, *Tectonophysics*, *589*, 1–16.

Ktenidou, O.-J., Z. Roumelioti, N. Abrahamson, F. Cotton, K. Pitilakis, and F. Hollender (2017), Understanding single-station ground motion variability and uncertainty (sigma): lessons learnt from EUROSEISTEST, *Bull. Earthq. Eng.*, 1–26, doi:10.1007/s10518-017-0098-6.

Kumar, A., H. Mittal, R. Sachdeva, and A. Kumar (2012), Indian strong motion instrumentation network, *Seismol. Res. Lett.*, *83*(1), 59–66.

Kurahashi, S., and K. Irikura (2011), Source model for generating strong ground motions during the 2011 off the Pacific coast of Tohoku Earthquake, *Earth Planets Space*, *63*(7), 11.

Lallemand, S., and X. Le Pichon (1987), Coulomb wedge model applied to the subduction of seamounts in the Japan Trench, *Geology*, *15*(11), 1065–1069.

Lay, T. (2015), The surge of great earthquakes from 2004 to 2014, *Earth Planet. Sci. Lett.*, *409*, 133–146.

Lay, T., and S. Bilek (2007), Anomalous earthquake ruptures at shallow depths on subduction zone megathrusts, *Seism. Zone Subduction Thrust Faults*, 476–511.

Lay, T., and T. C. Wallace (1995), *Modern global seismology*, Academic press.

Lay, T., H. Kanamori, C. J. Ammon, K. D. Koper, A. R. Hutko, L. Ye, H. Yue, and T. M. Rushing (2012), Depth-varying rupture properties of subduction zone megathrust faults, *J. Geophys. Res. Solid Earth*, *117*(B4).

Leyton, F., C. Pastén, G. Montalva, G. Hurtado, A. Leopold, S. Ruiz, and E. Saéz (2017), Towards a geophysical characterization of the Chilean seismological stations.

Li, S., M. Moreno, J. Bedford, M. Rosenau, and O. Oncken (2015), Revisiting viscoelastic effects on interseismic deformation and locking degree: A case study of the Peru-North Chile subduction zone, *J. Geophys. Res. Solid Earth*, *120*(6), 4522–4538.

Lomnitz, C. (2004), Major earthquakes of Chile: a historical survey, 1535-1960, *Seismol. Res. Lett.*, *75*(3), 368–378.

Loveless, J. P., and B. J. Meade (2010), Geodetic imaging of plate motions, slip rates, and partitioning of deformation in Japan, *J. Geophys. Res. Solid Earth*, *115*(B2).

Loveless, J. P., and B. J. Meade (2011), Spatial correlation of interseismic coupling and coseismic rupture extent of the 2011 MW= 9.0 Tohoku-oki earthquake, *Geophys. Res. Lett.*, *38*(17).

Loveless, J. P., and B. J. Meade (2016), Two decades of spatiotemporal variations in subduction zone coupling offshore Japan, *Earth Planet. Sci. Lett.*, *436*, 19–30, doi:10.1016/j.epsl.2015.12.033.

Madariaga, R. (1976), Dynamics of an expanding circular fault, *Bull. Seismol. Soc. Am.*, *66*(3), 639–666.

Madariaga, R., and S. Ruiz (2016), Earthquake dynamics on circular faults: a review 1970–2015, *J. Seismol.*, *20*(4), 1235–1252.

Marone, C., and C. H. Scholz (1988), The depth of seismic faulting and the upper transition from stable to unstable slip regimes, *Geophys. Res. Lett.*, *15*(6), 621–624.

Marsan, D., M. Bouchon, B. Gardonio, H. Perfettini, A. Socquet, and B. Enescu (2017), Change in seismicity along the Japan trench, 1990-2011, and its relationship with seismic coupling, *J. Geophys. Res. Solid Earth*.

Mavrommatis, A. P., P. Segall, and K. M. Johnson (2014), A decadal-scale deformation transient prior to the 2011 Mw 9.0 Tohoku-oki earthquake, *Geophys. Res. Lett.*, *41*(13), 4486–4494.

Mavrommatis, A. P., P. Segall, N. Uchida, and K. M. Johnson (2015), Long-term acceleration of aseismic slip preceding the Mw 9 Tohoku-oki earthquake: Constraints from repeating earthquakes, *Geophys. Res. Lett.*, *42*(22), 9717–9725.

McCaffrey, R. (2007), The next great earthquake, *Sci.-N. Y. THEN Wash.-*, *315*(5819), 1675.

Melnick, D., B. Bookhagen, M. R. Strecker, and H. P. Echtler (2009), Segmentation of megathrust rupture zones from fore-arc deformation patterns over hundreds to millions of years, Arauco peninsula, Chile, *J. Geophys. Res. Solid Earth*, *114*(B1).

Métois, M., A. Socquet, and C. Vigny (2012), Interseismic coupling, segmentation and mechanical behavior of the central Chile subduction zone, *J. Geophys. Res. Solid Earth*, *117*(B3).

Métois, M., A. Socquet, C. Vigny, D. Carrizo, S. Peyrat, A. Delorme, E. Maureira, M.-C. Valderas-Bermejo, and I. Ortega (2013), Revisiting the North Chile seismic gap segmentation using GPS-derived interseismic coupling, *Geophys. J. Int.*, *194*(3), 1283–1294.

Métois, M., C. Vigny, and A. Socquet (2016), Interseismic Coupling, Megathrust Earthquakes and Seismic Swarms Along the Chilean Subduction Zone (38°–18°S), *Pure Appl. Geophys.*, *173*(5), 1431–1449, doi:10.1007/s00024-016-1280-5.

Montalva, G., N. Bastias, and A. Rodriguez-Marek, Ground Motion Prediction Equation for the Chilean Subduction Zone, *Bull. Seismol. Soc. Am.*, (In press).

Montalva, G. A., N. Bastías, and A. Rodriguez-Marek (2017), Ground-Motion Prediction Equation for the Chilean Subduction Zone, *Bull. Seismol. Soc. Am.*, doi:10.1785/0120160221.

Moreno, M. et al. (2011), Heterogeneous plate locking in the South–Central Chile subduction zone: Building up the next great earthquake, *Earth Planet. Sci. Lett.*, *305*(3), 413–424.

Moreno, M., D. Melnick, M. Rosenau, J. Baez, J. Klotz, O. Oncken, A. Tassara, J. Chen, K. Bataille, and M. Bevis (2012), Toward understanding tectonic control on the M w 8.8 2010 Maule Chile earthquake, *Earth Planet. Sci. Lett.*, *321*, 152–165.

Motagh, M., B. Schurr, J. Anderssohn, B. Cailleau, T. R. Walter, R. Wang, and J.-P. Villotte (2010), Subduction earthquake deformation associated with 14 November 2007, Mw 7.8 Tocopilla earthquake in Chile: Results from InSAR and aftershocks, *Tectonophysics*, *490*(1), 60–68.

Naeim, F. (Ed.) (2001), *The seismic design handbook*.

Nigam, N. C., and P. C. Jennings (1969), Calculation of response spectra from strong-motion earthquake records, *Bull. Seismol. Soc. Am.*, *59*(2), 909–922.

Obara, K. (2002), Nonvolcanic deep tremor associated with subduction in southwest Japan, *Science*, *296*(5573), 1679–1681.

Obara, K., Y. Haryu, Y. Ito, and K. Shiomi (2004), Low frequency events occurred during the sequence of aftershock activity of the 2003 Tokachi-Oki earthquake; a dynamic process of the tectonic erosion by subducted seamount, *Earth Planets Space*, *56*(3), 347–351.

Okada, Y., K. Kasahara, S. Hori, K. Obara, S. Sekiguchi, H. Fujiwara, and A. Yamamoto (2004), Recent progress of seismic observation networks in Japan —Hi-net, F-net, K-NET and KiK-net—, *Earth Planets Space*, *56*(8), xv–xxviii.

Oleskevich, D., R. Hyndman, and K. Wang (1999), The updip and downdip limits to great subduction earthquakes: Thermal and structural models of Cascadia, south Alaska, SW Japan, and Chile, *J. Geophys. Res. Solid Earth*, *104*(B7), 14965–14991.

Ozawa, S. (2014), Shortening of recurrence interval of Boso slow slip events in Japan, *Geophys. Res. Lett.*, *41*(8), 2762–2768.

Ozawa, S., S. Miyazaki, Y. Hatanaka, T. Imakiire, M. Kaidzu, and M. Murakami (2003), Characteristic silent earthquakes in the eastern part of the Boso peninsula, Central Japan, *Geophys. Res. Lett.*, *30*(6).

Ozawa, S., H. Suito, and M. Tobita (2007), Occurrence of quasi-periodic slow-slip off the east coast of the Boso peninsula, Central Japan, *Earth Planets Space*, *59*(12), 1241–1245.

Ozawa, S., T. Nishimura, H. Munekane, H. Suito, T. Kobayashi, M. Tobita, and T. Imakiire (2012), Preceding, coseismic, and postseismic slips of the 2011 Tohoku earthquake, Japan, *J. Geophys. Res. Solid Earth*, *117*(B7).

Pacheco, J. F., L. R. Sykes, and C. H. Scholz (1993), Nature of seismic coupling along simple plate boundaries of the subduction type, *J. Geophys. Res. Solid Earth*, *98*(B8), 14133–14159.

Patzwahl, R., J. Mechie, A. Schulze, and P. Giese (1999), Two-dimensional velocity models of the Nazca plate subduction zone between 19.5 S and 25 S from wide-angle seismic measurements during the CINCA95 project, *J. Geophys. Res. Solid Earth*, *104*(B4), 7293–7317.

Peacock, S. M., and R. D. Hyndman (1999), Hydrous minerals in the mantle wedge and the maximum depth of subduction thrust earthquakes, *Geophys. Res. Lett.*, *26*(16), 2517–2520.

Perfettini, H., J.-P. Avouac, and J.-C. Ruegg (2005), Geodetic displacements and aftershocks following the 2001 Mw= 8.4 Peru earthquake: Implications for the mechanics of the earthquake cycle along subduction zones, *J. Geophys. Res. Solid Earth*, *110*(B9).

Perfettini, H. et al. (2010), Seismic and aseismic slip on the Central Peru megathrust, *Nature*, *465*(7294), 78.

Peyrat, S., R. Madariaga, E. Buforn, J. Campos, G. Asch, and J. Vilotte (2010), Kinematic rupture process of the 2007 Tocopilla earthquake and its main aftershocks from teleseismic and strong-motion data, *Geophys. J. Int.*, *182*(3), 1411–1430.

Piña-Valdés, J., F. Cotton, A. Socquet, and S. Specht (submmited 2017), Spatio-temporal variations of ground motion in northern Chile before and after the 2014 MW 8.1 Iquique megathrust event, *Bull. Seismol. Soc. Am.*

Rathje, E. M., N. A. Abrahamson, and J. D. Bray (1998), Simplified frequency content estimates of earthquake ground motions, *J. Geotech. Geoenvironmental Eng.*, *124*(2), 150–159.

Rathje, E. M., F. Faraj, S. Russell, and J. D. Bray (2004), Empirical relationships for frequency content parameters of earthquake ground motions, *Earthq. Spectra*, *20*(1), 119–144.

Reverso, T., D. Marsan, A. Helmstetter, and B. Enescu (2016), Background seismicity in Boso Peninsula, Japan: Long-term acceleration, and relationship with slow slip events, *Geophys. Res. Lett.*, *43*(11), 5671–5679.

Rice, J. R. (1983), Constitutive relations for fault slip and earthquake instabilities, *Pure Appl. Geophys.*, *121*(3), 443–475.

Ross, Z. E., and Y. Ben-Zion (2016), Toward reliable automated estimates of earthquake source properties from body wave spectra, *J. Geophys. Res. Solid Earth*, *121*(6), 4390–4407.

Ruegg, J., M. Olcay, and D. Lazo (2001), Co-, post-and pre (?)-seismic displacements associated with the Mw 8.4 Southern Peru earthquake of 23 June 2001 from continuous GPS measurements, *Seismol. Res. Lett.*, *72*(6), 673–678.

Ruegg, J. C. et al. (1996), The Mw= 8.1 Antofagasta (North Chile) earthquake of July 30, 1995: first results from teleseismic and geodetic data, *Geophys. Res. Lett.*, *23*(9), 917–920.

Ruff, L., and H. Kanamori (1983), Seismic coupling and uncoupling at subduction zones, *Tectonophysics*, *99*(2–4), 99–117.

Ruff, L. J. (1992), Asperity distributions and large earthquake occurrence in subduction zones, *Tectonophysics*, *211*(1–4), 61–83.

Ruina, A. (1983), Slip instability and state variable friction laws, *J. Geophys. Res. Solid Earth*, *88*(B12), 10359–10370.

Ruiz, S., M. Metois, A. Fuenzalida, J. Ruiz, F. Leyton, R. Grandin, C. Vigny, R. Madariaga, and J. Campos (2014), Intense foreshocks and a slow slip event preceded the 2014 Iquique Mw 8.1 earthquake, *Science*, *345*(6201), 1165–1169, doi:10.1126/science.1256074.

Sanchez-Sesma, F. J. (1987), Site effects on strong ground motion, *Soil Dyn. Earthq. Eng.*, *6*(2), 124–132.

Sandwell, D., E. Garcia, K. Soofi, P. Wessel, M. Chandler, and W. H. Smith (2013), Toward 1-mGal accuracy in global marine gravity from CryoSat-2, Envisat, and Jason-1, *Lead. Edge*, *32*(8), 892–899.

Sandwell, D. T., and W. H. Smith (1997), Marine gravity anomaly from Geosat and ERS 1 satellite altimetry, *J. Geophys. Res. Solid Earth*, *102*(B5), 10039–10054.

Satriano, C., V. Dionicio, H. Miyake, N. Uchida, J.-P. Vilotte, and P. Bernard (2014), Structural and thermal control of seismic activity and megathrust rupture dynamics in subduction zones: Lessons from the Mw 9.0, 2011 Tohoku earthquake, *Earth Planet. Sci. Lett.*, *403*, 287–298.

Scherbaum, F., F. Cotton, and P. Smit (2004), On the use of response spectral-reference data for the selection and ranking of ground-motion models for seismic-hazard analysis in regions of moderate seismicity: The case of rock motion, *Bull. Seismol. Soc. Am.*, *94*(6), 2164–2185.

Scholz, C., P. Molnar, and T. Johnson (1972), Detailed studies of frictional sliding of granite and implications for the earthquake mechanism, *J. Geophys. Res.*, *77*(32), 6392–6406.

Scholz, C. H. (1988), The brittle-plastic transition and the depth of seismic faulting, *Geol. Rundsch.*, *77*(1), 319–328.

Scholz, C. H. (1998), Earthquakes and friction laws, *Nature*, *391*(6662), 37.

Scholz, C. H., and J. Campos (2012), The seismic coupling of subduction zones revisited, *J. Geophys. Res. Solid Earth*, *117*(B5).

Schurr, B., G. Asch, M. Rosenau, R. Wang, O. Oncken, S. Barrientos, P. Salazar, and J. Vilotte (2012), The 2007 M7. 7 Tocopilla northern Chile earthquake sequence: Implications for along-strike and downdip rupture segmentation and megathrust frictional behavior, *J. Geophys. Res. Solid Earth*, *117*(B5).

Schurr, B. et al. (2014), Gradual unlocking of plate boundary controlled initiation of the 2014 Iquique earthquake, *Nature*, *512*(7514), 299–302, doi:10.1038/nature13681.

Sibson, R. H. (1977), Fault rocks and fault mechanisms, *J. Geol. Soc.*, *133*(3), 191–213.

Simons, M. et al. (2011), The 2011 magnitude 9.0 Tohoku-Oki earthquake: Mosaicking the megathrust from seconds to centuries, *science*, *332*(6036), 1421–1425.

Socquet, A., J. Piña-Valdes, J. Jara, F. Cotton, A. Walpersdorf, N. Cotte, S. Specht, F. Ortega-Culaciati, D. Carrizo, and E. Norabuena (2017), An 8 month slow slip event triggers progressive nucleation of the 2014 Chile megathrust, *Geophys. Res. Lett.*

Somerville, P. G. (2003), Magnitude scaling of the near fault rupture directivity pulse, *Phys. Earth Planet. Inter.*, *137*(1), 201–212, doi:10.1016/S0031-9201(03)00015-3.

Song, T.-R. A., and M. Simons (2003), Large trench-parallel gravity variations predict seismogenic behavior in subduction zones, *Science*, *301*(5633), 630–633.

Specht, S., O. Heidbach, F. Cotton, and A. Zang (2017), *Data-driven earthquake focal mechanism cluster analysis, (Scientific Technical Report STR; 17/01)*, GFZ German Research Centre for Geosciences, Postdam.

Stein, S., and M. Wysession (2009), *An introduction to seismology, earthquakes, and earth structure*, John Wiley & Sons.

Stern, R. J. (2002), Subduction Zones, *Rev. Geophys.*, *40*(4), 1012, doi:10.1029/2001RG000108.

Strasser, F. O., N. A. Abrahamson, and J. J. Bommer (2009), Sigma: Issues, Insights, and Challenges, *Seismol. Res. Lett.*, *80*(1), 40–56, doi:10.1785/gssrl.80.1.40.

Strasser, F. O., M. Arango, and J. J. Bommer (2010), Scaling of the source dimensions of interface and intraslab subduction-zone earthquakes with moment magnitude, *Seismol. Res. Lett.*, *81*(6), 941–950.

Suwa, Y., S. Miura, A. Hasegawa, T. Sato, and K. Tachibana (2006), Interplate coupling beneath NE Japan inferred from three-dimensional displacement field, *J. Geophys. Res. Solid Earth*, *111*(B4).

Tanioka, Y., L. Ruff, and K. Satake (1997), What controls the lateral variation of large earthquake occurrence along the Japan Trench?, *Isl. Arc*, *6*(3), 261–266.

Tassara, A., and A. Echaurren (2012), Anatomy of the Andean subduction zone: three-dimensional density model upgraded and compared against global-scale models, *Geophys. J. Int.*, *189*(1), 161–168, doi:10.1111/j.1365-246X.2012.05397.x.

Tichelaar, B. W., and L. J. Ruff (1993), Depth of seismic coupling along subduction zones, *J. Geophys. Res. Solid Earth*, *98*(B2), 2017–2037.

Trubienko, O., L. Fleitout, J.-D. Garaud, and C. Vigny (2013), Interpretation of interseismic deformations and the seismic cycle associated with large subduction earthquakes, *Tectonophysics*, *589*, 126–141.

Udías, A. (1991), Source mechanism of earthquakes, *Adv. Geophys.*, *33*, 81–140.

Udías, A., R. Madariaga, and E. Buforn (2014), *Source mechanisms of earthquakes: Theory and practice*, Cambridge University Press.

Wang, K. (2007), Elastic and viscoelastic models of crustal deformation in subduction earthquake cycles, *Seism. Zone Subduction Thrust Faults*, 540–575.

Wang, K., and J. He (2008), Effects of frictional behavior and geometry of subduction fault on coseismic seafloor deformation, *Bull. Seismol. Soc. Am.*, *98*(2), 571–579.

Wells, R. E., R. J. Blakely, Y. Sugiyama, D. W. Scholl, and P. A. Dinterman (2003), Basin-centered asperities in great subduction zone earthquakes: A link between slip, subsidence, and subduction erosion?, *J. Geophys. Res. Solid Earth*, *108*(B10).

Wilson, M. (1993), Plate-moving mechanisms: constraints and controversies, *J. Geol. Soc.*, *150*(5), 923–926.

Yagi, Y. (2004), Source rupture process of the 2003 Tokachi-oki earthquake determined by joint inversion of teleseismic body wave and strong ground motion data, *Earth Planets Space*, *56*(3), 311–316.

Yamanaka, Y., and M. Kikuchi (2004), Asperity map along the subduction zone in northeastern Japan inferred from regional seismic data, *J. Geophys. Res. Solid Earth*, *109*(B7).

Yang, W., and Y. Ben-Zion (2016), Corner frequency ratios of P and S waves and strain drops of earthquakes recorded by a tight network around the Karadere segment of the North Anatolian Fault Zone: evidence for non-classical source processes, *Geophys. Suppl. Mon. Not. R. Astron. Soc.*, *205*(1), 220–235.

Yokota, Y., and K. Koketsu (2015), A very long-term transient event preceding the 2011 Tohoku earthquake, *Nat. Commun.*, *6*.

Yomogida, K., K. Yoshizawa, J. Koyama, and M. Tsuzuki (2011), Along-dip segmentation of the 2011 off the Pacific coast of Tohoku Earthquake and

comparison with other megathrust earthquakes, *Earth Planets Space*, *63*(7), 34.

Youngs, R. R., N. Abrahamson, F. I. Makdisi, and K. Sadigh (1995), Magnitude-dependent variance of peak ground acceleration, *Bull. Seismol. Soc. Am.*, *85*(4), 1161–1176.

Youngs, R. R., S.-J. Chiou, W. J. Silva, and J. R. Humphrey (1997), Strong Ground Motion Attenuation Relationships for Subduction Zone Earthquakes, *Seismol. Res. Lett.*, *68*(1), 58–73, doi:10.1785/gssrl.68.1.58.

Zhao, J. X. et al. (2006), Attenuation Relations of Strong Ground Motion in Japan Using Site Classification Based on Predominant Period, *Bull. Seismol. Soc. Am.*, *96*(3), 898–913, doi:10.1785/0120050122.

Zhao, Z., Z. Zhao, J. Xu, R. Kubota, and L. Liu (2007), Strong ground motion simulation for seismic hazard assessment in an urban area, *J. Geophys. Eng.*, *4*(3), 308.